STABILITY OF HAPTIC DISPLAY IN TIME-DELAYED NETWORKED VIRTUAL ENVIRONMENTS

YANG HONG

A Thesis

In

The Department

of

Electrical and Computer Engineering

Presented in Partial Fulfillment of the Requirements
for the Degree of Master of Applied Science (Electrical Engineering) at
Concordia University
Montreal, Quebec, Canada

May 2005

Your file Votre référence
ISBN: 0-494-04376-8
Our file Notre référence
ISBN: 0-494-04376-8

ABSTRACT

Stability of Haptic Displays in Time-delayed Networked Virtual Environments

Yang Hong

With the development of Distributed Virtual Environment, haptic simulation is becoming a popular research field. However, time delay issue is always an obstacle in haptic simulation because this lag over the network-based haptic display violates the stability and performance of haptic display. In the research of teleoperations, some delay prediction methods have been introduced already; however, the performance requirements have been decreased to obtain the stability reducing the total loop gain. The design of virtual coupling, an artificial link between the haptic display and virtual environment, has been introduced into haptic interaction. However, in the traditional design, virtual coupling is always coupled with the virtual environment; as a result, stability condition for the haptic simulation becomes too tight because zero order hold has the phase lag over frequency. To guarantee the stability in the presence of unpredictable time delays new control design strategies are required.

In this thesis, two-port network theory is introduced to design the virtual coupling to guarantee stability of haptic display in time-delayed Distributed Virtual Environments. By decoupling the hatpic display control problem from the design of virtual environments, the use of a virtual coupling network frees the developer of haptic-enabled virtual reality models from the issues of mechanical stability. Passivity criteria in two-port networks are introduced to guarantee stability of haptic interface with a unit time delay. Furthermore, two kinds of virtual environments models – "spring" and "spring-damping" have been simulated. Steady state error and transient

response for the interaction between haptic displays and above virtual environments models are investigated. This technique overcomes the influence of time delay to violate the stability of the system and reduces the human risk involved.

Acknowledgements

I am indebted to my parents, who have always encouraged me to follow my research whenever I met any difficulty or any problem in my study. I am very grateful of their supports.

I would like to express gratitude and appreciation my advisor Dr. K. Khorasani for all his thoughtful guidance and invaluable assistance throughout my graduate research at Concordia University. Especially, in this program, with his supervision, I not only make a lot of progress on my academic area, but also I set up a series of serious attitudes in the research. I totally trust I would get rewards from these benefits in my later career.

Table of Contents

List of Figure

List of Table

Nomenclature

VE	Virtual Environment
VR	Virtual Reality
DVE	Distributed Virtual Environment
NVE	Networked Virtual Environment
A/D	Analog-to-Digital
D/A	Digital-to-Analog
LTI	Linear Time-Invariant
ZOH	Zero Order Holder
DOF	Degree Of Freedom
PC	Passivity Controller
PO	Passivity Observer
DTC	Dead-time Compensator
SISO	Single Input Single Output

Chapter 1

Introduction

Haptic is a sense of touch and also a sense of body position and motion (kinesthesia). A haptic interface is a device that conveys a kinesthetic sense of presence to a human operator interacting with a computer-generated (virtual) environment. This haptic interface can be viewed as a generator of mechanical impedances or admittances.

Currently, virtual reality (VR) and environment is an active research topic. In this research area, a number of other areas such as in 3-D graphic generation, audio transmission and protocols, network and communication architectures are utilized. However, an operator interacting with a virtual environment needs to know what the reaction of VR will be when that operator applies a force to it. Vision and audio from VR are usually not able to provide enough information to determine the true reaction of VR. The feedback virtual force generated by VR would be significant for the operator to take the next action. In other words, human neuromuscular and decision responses close the information communication between the VR and the operator. For example, when an operator tries to grasp a virtual object, the operator has to ensure he/she has held that virtual object well before he/she takes the next action. However, vision and audio from VR could not offer this information to the operator efficiently. Therefore, it is necessary that a virtual sense could be generated by VR after a virtual object is touched. This virtual sense would help the operator know the properties of this virtual object which he/she has held, such as the shape, stiffness, and the roughness characteristics and properties.

Presently, a typical haptic interface involves a manipulator capable of force reflection (often called a manipulandum). The PHANToM, developed by SensAble Technologies, Inc., is one example of a commercial haptic interface used in many research labs. Other examples include a force-feedback joystick and mouse (e.g., Logitech iFeel mouse, Logitech WingMan Force Feedback Mouse, Nostromo n30 Game mouse, and Gravis Destroyer Joystick), which are capable of providing a more interactive interface between a computer and its human operator. There are numerous applications of a haptic system, which are involved in entertainment, education/training, and industrial applications, etc.

1.1 What is "Distributed VR"

With recent increases in network bandwidth and graphics performance in desktop computers, there is a growing interest in distributed visual simulation systems that allow multiple users to interact in a shared 3D virtual environment. Also we can state that the simulated world runs not on one computer, but on several. Further the users using those computers connected over a network (possibly the global Internet) are able to interact in real time, sharing the same virtual world. This shared information includes 3D graphic vision, stereo audio, and the feeling of touching virtual objects. As each user is represented in the shared virtual environment by an entity (avatar) whose state is controlled by user input and kept up-to-date on participating workstations via messages, these systems support visual interactions between multiple users in a shared 3D virtual environment. Applications for this technology include distributed training simulations, collaborative design, virtual meeting, and multiplayer games [1].

It is clear that there are a number of obstacles to be overcome in achieving this goal. The fact that we want people to be able to access from their homes means that we have to be able to turn over relatively limited-bandwidth links, such as 28.8k modems. The fact that we want to run over the Internet means that we have to tolerate certain amount of latency in the delivery of update information. Finally, the fact that people are running on different computer systems with different hardware and different software means that we must design the system for portability [2].

A distributed virtual environment (DVE) provides a graphical representation of a virtual world that may be navigated by geographically dispersed users. Mechanisms are provided to enable users to interact with the world, and each other, in real-time. Sound and tactile feedback may be used in the presentation of a world to enhance user interaction. DVE applications have been used successfully for collaborative work [3] [7], training individuals via military simulations [4] [8] [9], and social play via multiplayer games [5] [6].

1.2 Terminology

Before we start the discussion about haptic display, it is better for us to define the terminology of this new field because we found terms are intermixed and may lead to confusion in the technical community.

In human haptic system, we classify it into two subsystems, which is tactile system and kinesthetic system. The tactile system refers to the sense of contact with an object, receives information mediated by the response of mechanoreceptors in the skin within and around the contact area, while the kinesthetic system refers to the position and motion of limbs along with the associated forces, receives information from sensory receptors in the skin around the joints, joint capsules, tendons, and

muscles, as well as from motor-command signals [10]. Actually, tactile and kinesthetic systems play different roles in situations when the human touches the object. Based on this understanding, the scientists also set two kinds of sense (tactile feedback and force feedback) in the human simulation research. In the book [11], authors described that tactile feedback is sensed by receptors placed close to the skin, with the highest density being found in the hand, while force feedback is sensed by low-bandwidth receptors placed deeper in the body, typically on muscle tendon attachments to bones and joints. These terms differ also in functionality, namely the ability to oppose actively the user volitional hand movement [12]. Force feedback (at large levels) can stop the user's motion, whereas tactile feedback cannot. It therefore cannot prevent virtual or robotics hands from possibly destroying remotely grasped objects [11].

Haptic feedback. From the Greek *haptesthai*, meaning to touch, is synonymous with tactile feedback [13]. The author in [13] and others extend its meaning to that of force feedback [11].

Kinesthetic feedback. Synonymous with proprioception, it refers to *kinesthesia*, a sense mediated by end organs located in muscles, tendons, and joints and stimulated by bodily movements and tensions [13]. Some authors use kinesthetic feedback to group both tactile and force feedback in single definition, but this is somewhat incorrect [11].

Proprioceptive feedback. Relates to stimuli arising within the organism. It provides information related to body posture and is based on receptors located at the skeletal joints, in the inner ear, and on impulses from the central nervous system (memory effect) [11].

Haptic Display. A mechanical device configured to convey kinaesthetic cues to a human operator. They vary greatly in kinematic structure, workspace, and force output [16].

Haptic Interface. It includes everything that comes between the human operator and the virtual environment [16].

1.3 Types of Haptic Display

In recent years, haptic interfaces have been developed for an impressive array of applications. In general, two main types for a haptic system are categorized: impedance type and admittance type. The impedance display type will sense the position from the manipulator and a computer simulation will calculate the force output to the manipulator, in other words, it measures motion and display force. Most haptic interfaces use impedance displays, such as the well-known Phantom [15] family of haptic displays, the McGill University Pantograph [14], and the University of Washington Pen-Based Force Display [17]. This is the simplest and least expensive choice because it requires only an actuator and position or velocity sensor. This kind of haptic display has low inertia and is highly back drivable. The admittance display type will sense the force from the manipulator and a computer simulation will calculate the position output to the manipulator, which means it measures force and displays motion. This kind of haptic display includes Carnegie Mellon University's WYSIWYF Display [18] and the Iowa State/Boeing virtual aircraft control column [19], both of which are based upon PUMA 560 industrial robots. This type of display usually is used in a heavy industrial robot, since it is non-back drivable; furthermore, admittance display is often high-inertia. Because of the force input, an expensive force sensor is needed for the admittance type of haptic system.

1.4 Review of Applications

Before virtual reality was introduced into our research area, researchers used force/tactile feedback control in the teleoperator systems and the remote control robotic systems. In these systems, the operator controls a "master" arm that transmits his commands to the remote slave. Sheridan [20] defines the master-slave teleoperator as following:

In a teleoperation sense, a master-slave teleoperator system has two subsystems: (1) the master device, which typically is a multi-degree-of-freedom, more-or-less anthropomorphic (having a serial-kinematic form like a human arm) mechanical device, positioned directly by a human operator; and (2) a slave device, which typically is isomorphic to (having the same form as) the master. The latter is often equipped with an end effector (a hand for grasping, or a specialized tool to perform some specialized task).

The slave follows the master input and interacts with a (usually) harmful environment (such as nuclear, outer-space, or underwater sites) [11]. The first teleoperator systems had purely mechanical linkages so that the slave was in close proximity to the master arm [11]. A newer electrical servomechanism was developed in 1954 by Goertz and Thompson [21] at Argonne National Laboratory. In this system, the electrical servoactuators in the master arm received feedback signal from the slave sensors and applied forces to the user's hand grasping the master. As a result, the user felt as if he/she was manipulating the remote environment directly. Later, Frederick Brooks, Jr. and his colleagues at the University of North Carolina at Chapel Hill developed the longest research project in virtual force feedback. They hoped to challenge the real-time simulation of three-dimensional molecular docking forces. Within 20 years, they continually designed GROPE (1967), GROPE I (1971) and

GROPE II (1976) to try the simulation of three-dimensional virtual forces. Finally, in 1990, after introducing much faster computing hardware into their systems, they reached their original goal of a three-dimensional molecular docking simulation [20].

Jones and Thousand, who in 1966 patented one of the first dextrous master manipulators, developed a much simpler and safer design using pneumatic bladders. In his concept, the user's hand position was measured by a sensing glove and transmitted to a slave robot gripper. Errors between user and robot hands could appear when the robot grasped objects. A pressure proportional to the measured position error was used to inflate pneumatic bladder actuators placed in the palm of the master. Thus the user received a very natural sensation, as if he/she was grasping the object directly [11].

However, all of above masters were developed originally for telerobotic applications and not to serve as I/O devices for Virtual Reality (VR), a field that appeared in the late 1970s. The "Sandpaper" system developed at the Massachusetts Institute of Technology Media Laboratory [22] was one of the first prototypes to provide tactile feedback from a graphics simulation. This design consisted of a two-degree-of-freedom (2-DOF) joystick with large electrical actuators in an enclosure placed by the computer.

In 1992, Salcudean [23] designed the UBC magnetically levitated (maglev) joystick, which has a high frequency response, frictionless, back-drivable device with limited 6-DOF ranges. Its assembly sketch is shown in Figure 1-1 and its characteristics are given in Table 1-1.

The device has six Lorentz actuators, arranged in a start configuration with 120° symmetry. Each actuator consists of a flat coil immersed in the magnetic field of four rectangular magnets attached to permeable plates that contain the flux, and produces a

force proportional to the current passing through it. In keeping with the terminology of Hollis et al. [24], the actively levitated joystick handle is referred to as the "flotor." The location of the flotor with respect to the stator is detected by sensing the projections of three narrow beam LEDs on the surfaces of three dimensional Position Sensing Diodes, as described in Hollis et al. [24]. The actuator coils are driven by current drivers each having a maximum continuous current of 10 A.

The maglev joystick flotor is kept in controlled "flight" by a VME-based *SPARC™* processor running the *VxWorks™* real-time operating system, and associated input-output cards. A Silicon Graphics workstation is used for graphical display and communicates with the haptic interface control processor via a serial link [25].

Table 1-1 Summary of the UBC maglev joystick characteristics

Dimensions	Cylinder with $r = 66mm$ $h = 110mm$
Stator mass	2 kg
Flotor mass	0.65 kg
Payload (continuous)	2kg (along the z-axis)
Translation range	$\pm 4.5mm$ from center
Rotation range	$\pm 6\deg$ from center
Resolution	$< 5\mu m$ (trans.) $< 10\mu rad$ (rot.)
Force/torque freq. resp.	$> 3kHz$
Close-loop position freq. resp.	$> 30Hz$ (trans.) $> 15Hz$ (rot.)
Actuator force constant	2 N/A
Max. continuous current	3 A/coil
Peak current	10 A/coil

Although the UBC wrist can produce the same forces and only slightly reduced torques, it is substantially smaller. It can be modeled as a single controlled rigid mass,

of mass $m = 0.7kg$. With the present current amplifier, the maximum force along vertical axis is $60N$.

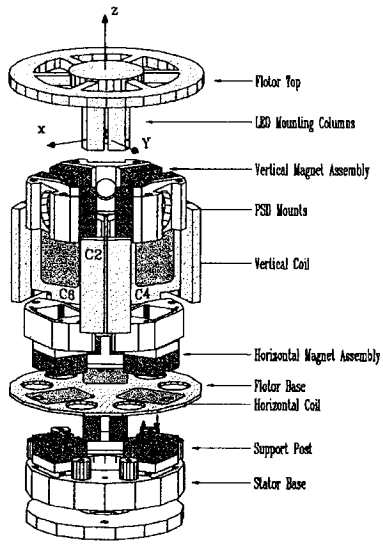

Figure 1-1 The UBC maglev joystick assembly sketch [25]

Another kind of haptic device is based on pen-based masters. It allows interaction with the virtual environment through familiar tools such as a pen (or pointer) or a scalpel (in the case of surgical simulators). These desktop devices are compact, typically have a workspace larger than spherical and magnetically levitated haptic joysticks and have between three and six degrees of freedom. Since the tool (pen) is geometrically constant, regardless of the user's hand size, there is no need for complex calibrations associated with sensing gloves [11]. University of Washington Pen-based Force Display and The PHANToM Master are the two famous cases of this kind of haptic interface.

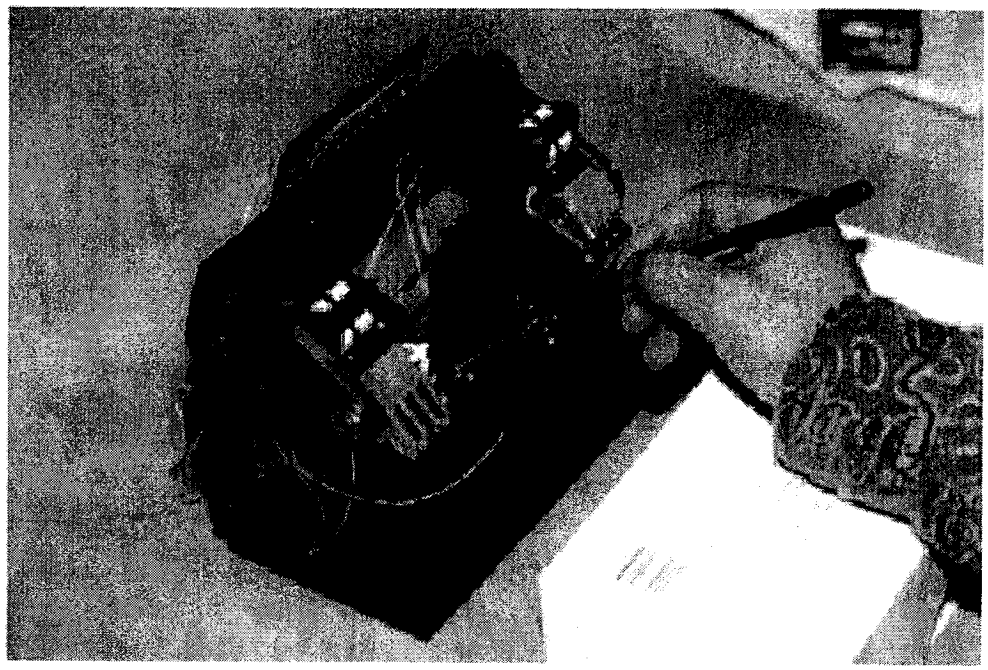

Figure 1-2 The pen-based forced display [26]

Let us now look through the design of the University of Washington pen-based force display. Its structure is shown in Figure 1-2. In Buttolo and Hannaford's research [26], they believe that in the application of manipulator with very low inertia and friction the operator doesn't feel a burden while the scalpel is in free motion, and he/she can feel the high frequency force components generated by the interaction of the scalpel with different kinds of tissues. At the same time, they find that geared manipulators couldn't satisfy the design requirements of low inertia and friction manipulators because they don't have very high bandwidth, and they couldn't reproduce the force information with high frequency components, and further addition of backlash and friction phenomena always occurs. On the contrary, direct drive manipulators are characterized by very high force generation bandwidth, low friction and no backlash [26]. Of course, the drawback of this manipulator is that a higher mass/torque ratio exists in the application compared to the geared manipulators. This is a reason why serial direct drive manipulators are characterized by a very high

inertia. Based on above analysis, in 1995, Buttolo and Hannaford designed a 2-DOF manipulator in the horizontal cartesian space using a parallel structure. As a result, they conclude that the evaluation of a parallel manipulator dynamic behavior could be an extremely complex mathematical problem. Because the robot is not an open chain, it is impossible to use directly the Newton-Euler approach, and quite a complex to derive the Hamiltonian. To simplify the above problem, they use three serial 2 links manipulator, which are connected together at the end-effector, instead of a 2-DOF parallel structure. Figure 1-3 shows the structure of 2-DOF parallel, and Figure 1-4 is the schematic representation of the pen-based force display. In Figure 1-4, between the two links there is no actuator; however, it is possible to introduce a fictitious actuator with null mass and null output torque.

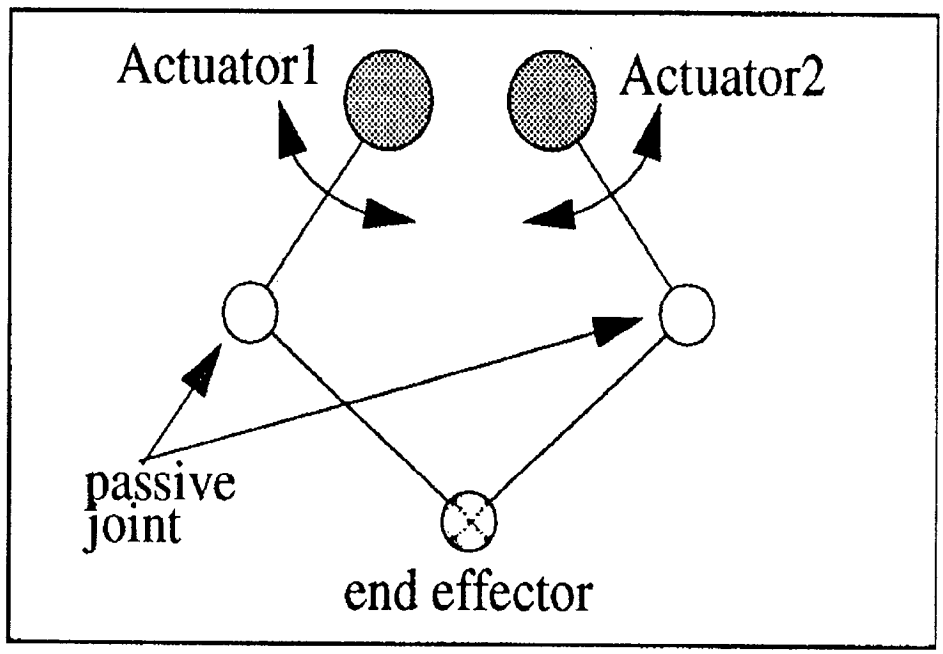

Figure 1-3 Schematic representation of a typical 2DOF parallel manipulator [26]

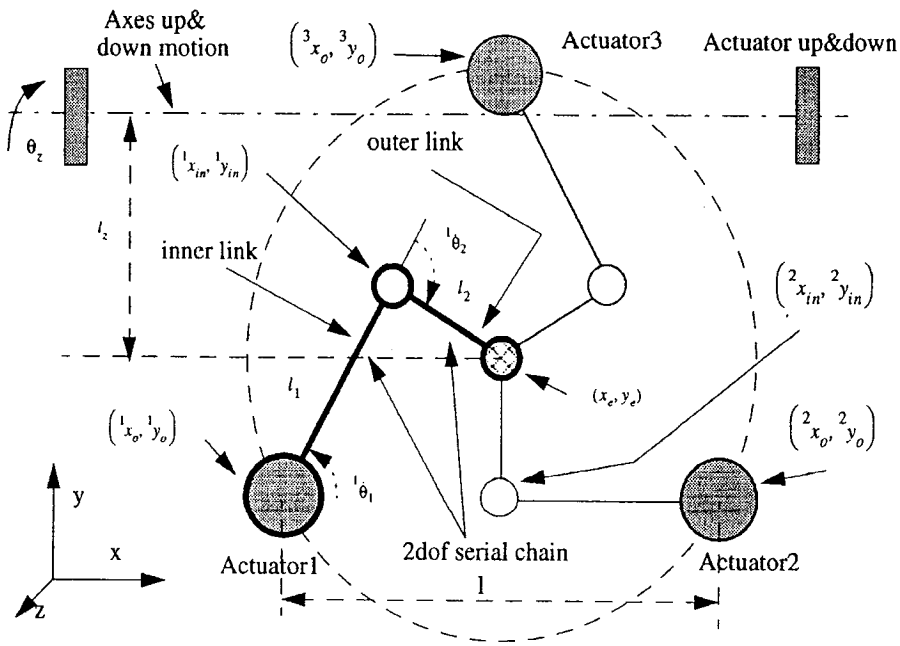

Figure 1-4 Schematic representation of the pen-based force display [26]

According to their design, Buttolo and Hannaford [26] conclude that the pen-based force display could be an effective tool for precision manipulation in virtual environment or for scaled telemanipulation. The human operator interacts with the force display in a very familiar way, using a pencil or a scalpel. This configuration can be very effective for microsurgery. A drawback of the design of a parallel redundant structure is the high computational requirement needed to solve the dynamic equations and to choose a torque configuration among the infinite possible choices. On the other hand, their parallel manipulator has a very low inertia, no backlash, almost zero friction, and the actuator redundancy can provide a homogenous force capability. They tried to measure the static friction and it was less than the resolution of their measuring devices. As an additional advantage of their design, multiple closed chains provide an easy way to self-calibrate the mechanical devices [27]. In their case the presence of a redundant close loop allowed them to self-

calibrate all the parameters of the parallel planar device, such as the position of each actuator and the length of the links. They also built a simulation virtual reality test-bed, where an operator can see virtual objects on a video display and touch them using the force display. The feeling coming from touching the virtual object confirmed them that their device is capable of high-frequency force reflection [28].

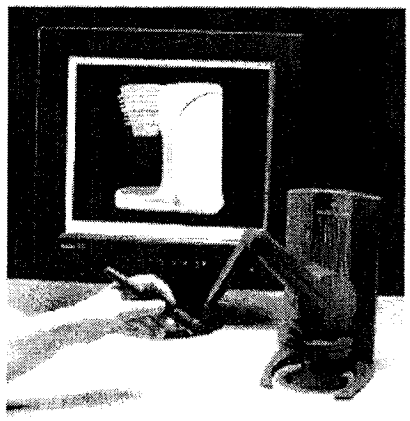

Figure 1-5 PHANTOM desktop from sensAble technologies [28]

The Personal Haptic Interface Mechanism (PHANToM) is another desk-grounded pen-based mechanism designed for virtual force feedback [15]. Their characteristic is shown in Figure 1-5. Its main interface component is a serial – feedback arm that ends with a fingertip thimble-gimbals support. Alternately the thimble can be replaced by a stylus. In chapter 2 of the thesis, we are going to describe the detail information about the PHANToM system.

1.5 Impedance Control Theory

In telerobotic systems, dynamic interaction between the robot and its environment has been always one of the hardest research topics. Similarly, in virtual environment, haptic display between human beings and virtual environment is also one of the hardest problems as well. Actually, haptic display is a kind of dynamic

interaction between human beings and virtual environments. Dynamic interaction can cause severe problems. The by-now-familiar phenomenon of contact instability [32] is a clear example. Teleoperated systems are a level more difficult than applying robots to contact tasks because there are at least three distinct systems that interact — the human operator, the robot and its environment [33]. Dynamic interaction between systems may be quantified by their impedances that are used here in the sense of a generalized dynamic relation between force and motion.

In Faye's thesis, an experimental facility for investigating human-machine interaction has been developed [38]. It is a computer-controlled manipulandum with programmable mechanical impedance. The mechanical system is a "direct drive" motorized open-chain planar mechanism [33].

Understanding the performance of a human interaction requires a characterization of human impedance. Lanman [34] reported an incremental stiffness ranging from a minimum below 2 N-m/rad to a maximum as high as 400 N-m/rad. Hayes and Hatze [35] reported a minimum stiffness between 1 and 1.4 N-m/rad. Cannon and Zahalak [36] reported a maximum stiffness greater than 350 N-m/rad mechanical impedance.

In research in the literature, impedance control theory is employed in robot control to get the stable execution of contact tasks. Contact tasks are considerably more difficult. Dynamic interaction is a complex nonlinear procedure between robot and environment, and current model of robot is not sufficient for different environments, furthermore, the human operator is extremely complex and difficult to characterize [33]. In the traditional control system design, motion-based control design is eminently reasonable and quite successful for non-contact tasks because only the robot's motion needs to be controlled, while this approach to contact tasks

has been less successful because it ignores the fundamental mechanics of interaction in a contact task. An alternative is to recognize that the dynamic interactions are not a source of disturbances to be rejected, but an integral part of the task. This is the idea behind the impedance control. Neville Hogan detailed the impedance control approach for manipulation [37]. This approach defines a unified and general framework to control of manipulation [37]. It includes the simple positioning or transporting tasks typically performed by robots and/or prostheses. It also builds on this capability, extending it to facilitate the application of robots and/or prostheses to tasks involving static and dynamic interactions between the manipulator and its environment [37].

Similarly, in the stability of haptic display, we also introduce impedance control. Colgate [39] thought of a haptic interface as a device that generates mechanical impedances. Impedance represents a dynamic (history-dependent) relationship between velocity and force [49]. For instance, if the haptic interface is intended to represent manipulation of a point mass, it must exert on the user's hand a force proportional to acceleration, whereas if it is to represent squeezing of a spring, it must generate a force proportional to displacement [39]. Actually, physical systems come in only two types: admittance, which accepts effort (e.g., force) inputs and yields flow (e.g., motion) outputs; and impedance, which accepts flow (e.g., motion) inputs and yields effort (e.g., force) outputs. Thus we are able to describe the dynamic display of virtual contact or touch in the virtual environment easily through impedance control. Some applications have used impedance or admittance control methods in haptic displays [16] [41] [42] [43].

1.6 The Stability of Haptic Display Systems

An important issue in the haptic display of virtual environments is stability. Often, unintended oscillations of the human/display system are found to occur. Stability of the haptic device and ultimately safety of the user is very important. In order to guarantee the stability of the system, scientists have made different attempts in the structure.

Passivity is a powerful tool for the analysis of coupled stability problems arising in robotics and related disciplines. For example, passivity methods have been used to establish conditions for the stability of a robot contacting an uncertain dynamic environment [29], to investigate the robustness of force feedback controllers [30], and to study the stability of telemanipulation with a time delay [31]. Furthermore, passivity techniques have been used in the design of "haptic interfaces" to virtual environments [39]. An hpatic interface is a device that lets human operators touch, feel, and manipulate virtual (computer-generated) environments [40]. Colgate and Schenkel [44] thought if a necessary and sufficient condition for the passivity of a class of sampled-data systems would be derived, the stability of haptic interface could be guaranteed.

In their research, they build a sampled-data system model with continuous time plant and discrete-time controller. Amplifier and sensor dynamics, nonlinearity, and noise are ignored. Colgate and Schenkel [44] have derived the necessary and sufficient conditions for passivity for the linear case with one degree of freedom. The model is shown in Figure 1-6. The element, the unilateral constraint, is ubiquitous in the physical world. Unilateral constraints are needed to account for collisions and contact. The element $H(z)$ represents virtual environment and is a stable linear, shift-invariant transfer function. The parameter m is a rigid body. The parameter b is some

viscous friction. They concluded that if the haptic display behaved passively, the energy input to the haptic display from the operator must be positive for all admissible force histories $f(t)$ and all times greater than zero:

$$\int_0^t f(\tau)v(\tau)d\tau > 0, \quad \forall\, t > 0, \, admissible\ f(t) \tag{1-1}$$

A system that does not satisfy (1-1) is said to be "active".

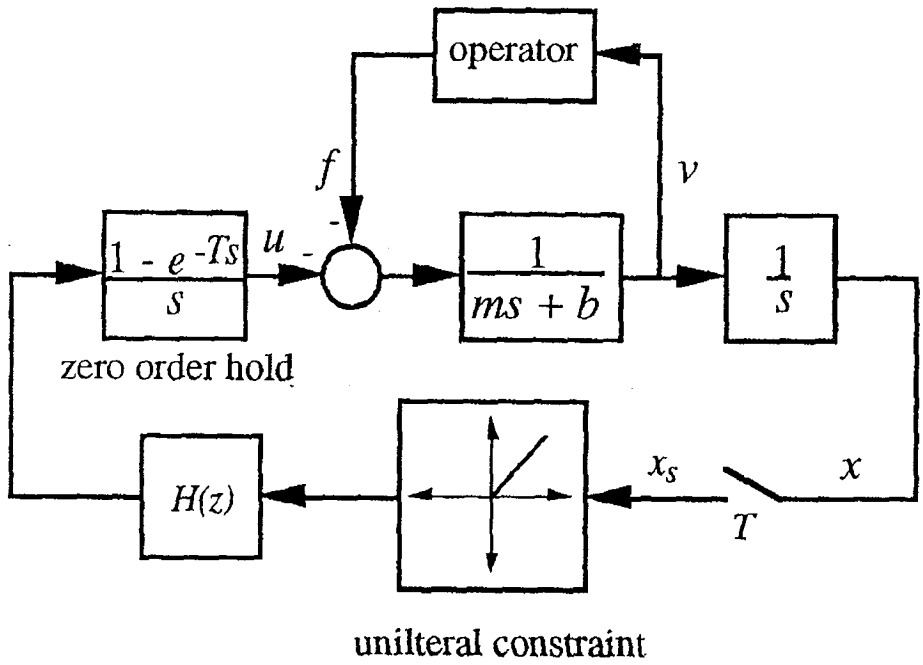

Figure 1-6 Model of a one degree-of-freedom haptic interface [44]

Colgate and Schenkel [44] proved a necessary and sufficient condition for passivity of the sampled data system in Figure 1-6 is:

$$b > \frac{T}{2}\frac{1}{1-\cos(\omega)}\mathrm{Re}\{(1-e^{-j\omega T})H(e^{j\omega T})\} \qquad 0 \le \omega \le \omega_N \tag{1-2}$$

where $\omega_N = \pi/T$ is the Nyquist frequency and T is the sampling period.

The detail procedure for the proof for this theorem has been described in [44]. They also employ this theorem into a common implementation of a "virtual wall", composed of a virtual spring and damper in mechanical parallel, together with a unilateral constraint operator [39]. A velocity estimate is obtained via backward difference of position, giving the following transfer function within the wall:

$$H(z) = K_e + b_e \frac{z-1}{Tz} \tag{1-3}$$

where $K_e > 0$ is virtual stiffness, and $b_e > 0$ is a virtual damping coefficient. From (1-2), the condition for passivity is:

$$b > \frac{T}{2}\frac{1}{1-\cos(\omega)}\mathrm{Re}\{(1-e^{-j\omega T})(K_e + b_e \frac{e^{j\omega T}-1}{Te^{j\omega T}})\},\ 0 \le \omega \le \omega_N \tag{1-4}$$

By algebraic manipulation the above expression leads to

$$b > \frac{TK_e}{2} - B\cos(\omega T),\quad 0 \le \omega \le \omega_N \tag{1-5}$$

The right hand side is maximized at $\omega = \omega_N$, leading to the condition:

$$b > \frac{TK_e}{2} + b_e \tag{1-6}$$

Based on the above results, it is concluded that (a) some physical dissipation is essential to achieve passivity; (b) given fixed physical and virtual damping, the maximum achievable virtual stiffness is proportional to the sampling rate; and (c) the achievable virtual damping is independent of the sampling rate [44]. Actually, these findings are useful for the implementations for the haptic interface design. When our implementation needs very stiff, dissipative constraints (high K_e, b_e), to maximize b and to minimize T are excusable. Fast sampling is a standard objective, but maximizing damping goes against conventional wisdom [44]. It is generally argued that the dynamics of a haptic interface should be dominated by the virtual

environment (which is the programmed behavior we wish to display) rather than any inherent dynamics (which is considered parasitic). In other words, the interface hardware should be "transparent." Unfortunately, the notion of transparency places focus on mimicking the governing equations (e.g., state equations) of physical systems, but not on obeying underlying physical laws (such as conservation of energy). The addition of physical damping helps the sampled-data system to behave as physical law would dictate [45]. Unfortunately, this ignores the effect of sampling. Sampling ensures a certain disparity between the actual and intended behaviors of the virtual environment which will result in active behavior and the potential for coupled instability unless accompanied by a sufficient degree of inherent damping (b) [44]. It is interesting to note, however, that the passivity condition doesn't rule out the use of negative virtual damping. For instance, if $B < 0$ is permitted, passivity condition 1-6 changes to:

$$b > \frac{TK_e}{2} + |\dot{b}_e| \tag{1-7}$$

Thus, negative virtual damping is permissible as much as positive virtual damping. In the case of $K_e = 0$, it should be possible to eliminate almost completely the effect of inherent damping [44].

Blake Hannaford and Jee-Hwan Ryu [46] have developed another analysis and control of instability in complex systems such as haptic interfaces using the time-domain definition of passivity. They define the "Passivity Observer" and the "Passivity Controller" and apply them to haptic interfaces in place of fixed-parameter virtual couplings. Their experimental evaluation and simulation is based on Excalibur system [47], [48].

The conjugate variables which define power flow in such computer systems are discrete-time values, further, they confine their analysis to systems having sampling rate substantially faster than the dynamics of the haptic device, human operator, and virtual environment so that the change in force and velocity with each sample is small. Many haptic interface systems have sampling rates of 1000 Hz, more than ten times the highest significant mode in their system [46]. The passivity observer (PO) for one-port network may be defined as following:

$$E_{obsv}(n) = \Delta T \sum_{k=0}^{n} f(k)v(k) \tag{1- 8}$$

where ΔT is the sampling period. For an M-port network with zero initial energy storage, the definition of passivity observer (PO) becomes:

$$E_{obsv}(n) = \Delta T \sum_{k=0}^{n} [f_1(k)v_1(k) + \cdots + f_M(k)v_M(k)] \tag{1- 9}$$

If $E_{obsv}(n) \geq 0$ for every n, this means the system dissipates energy. If there is an instance that $E_{obsv}(n) < 0$, this means the system generates energy and the amount of generated energy is $-E_{obsv}(n)$ [46]. When there are multiple interconnected elements, researchers might want to observe each one separately in order to determine which ones are active and which are passive.

For one-port system, if it is negative at any time, the one-port may then be contributing to instability. Moreover, we know the exact amount of energy generated. Hannaford and Ryu [46] design a time-varying element to dissipate only the required amount of energy and define this element a passivity controller (PC). The PC takes the form of a dissipative element in a series or parallel configuration, such as in Figure 1-7. A series PC has the impedance causality; while a parallel PC has the

admittance causality. The PO and PC can both be implemented with simple software in existing haptic interface systems. The stability can be proven, yet it is not a fixed parameter design based on a worst-case analysis. Secondly, energy storage elements in the system do not have to be modeled, only dissipation. Dissipation in the elements outside the PO needs to be identified for optimum performance. However, the added performance due to modeling external dissipation appears to be small. Thus, the PC can be very useful without any parameter estimation at all. Nevertheless, this method has some limitations. First, there are important cases in which virtual environments have very different behavior in different locations. The second issue is the performance of the system with limits imposed on the PC and sensitivity to low values of velocity [46].

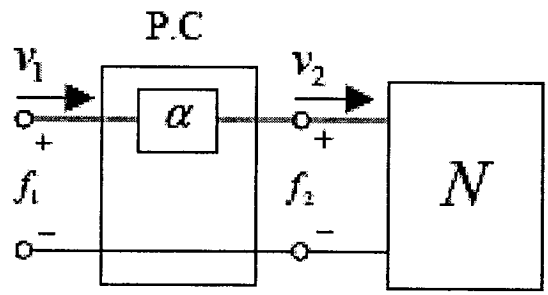

(a) Series or velocity conserving Passivity Controller

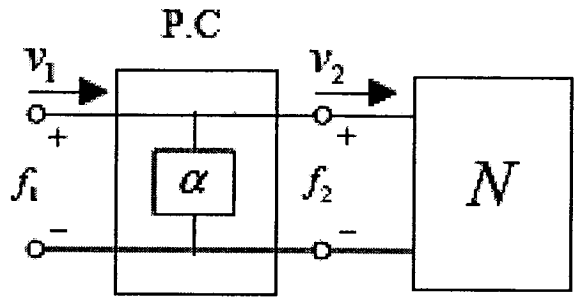

(b) Parallel or force conserving Passivity Controller.

Figure 1-7 Configuration of passivity controller for one-port network [46]

1.7 The Performance of Haptic Display Systems

As we described before, a haptic interface is a device that generates mechanical impedances [39] [49]. In the physical world, impedances vary widely. For instance, while holding a pencil, the perceived impedance is that of a low mass rigid body, but when pressing a pencil against a writing surface, the perceived impedance is that of a stiff viscoelastic body. In one case, the pencil provides almost no resistance to motion, in the other case almost complete resistance to motion (at least in the direction normal to the surface). The challenge of designing a haptic interface is to build a single programmable device that can exhibit a comparably broad *dynamic range* of impedances (or at least a "Z-Width" which is perceived to be comparably broad) [49]. Rosenberg and Adelstein address the analysis and construction of virtual surfaces from a perceptual, rather than solely a dynamics and controls point of view [50]; however, they don't state that dynamic range of haptic display is one important factor of affecting the performance of a haptic display. Colgate and Brown [49] address this problem. They are concerned with achievable dynamic range in theoretical and experimental research. They detail how to build a haptic interface capable of exhibiting a wide range of mechanical impedances while preserving a robust stability property. Through their research, they find physical damping could play a pivotal role in increasing the Z-width, regardless of the configuration. In all cases, the addition of physical damping increased both the maximum stiffness and the maximum damping. Further, high update rate is needed to achieve high stiffness; however, high update rates exacerbate noise due to differentiation of the position signal, making large damping coefficients difficult to achieve [49]. To achieve higher damping, the update rate can be slowed down (at the expense of stiffness) or digital filter can be used to attenuate high frequency noise. With the proper digital filter, the velocity signal can

be smoothed out to allow large damping in addition to high stiffness [49]. However, they didn't address high frequency oscillations and performed psychophysical experiments to match the virtual environment to the desired physical one.

The performance of a haptic interface can be described in terms of transparency, the quality in which velocities and forces are passed between human operator and the virtual environment. A haptic interface with perfect transparency has the hybrid mapping [51]

$$\begin{bmatrix} F_h \\ -v_e^* \end{bmatrix} = \begin{bmatrix} 0 & 1 \\ -1 & 0 \end{bmatrix} \begin{bmatrix} v_h \\ F_e^* \end{bmatrix} \tag{1-10}$$

The range of Z-width may be used as a method that evaluates the transparency. This range is delimited by frequency dependent lower and upper bounds, $Z_{\min}$ and $Z_{\max}$. The ideal haptic interface could simulate free motion without inertia or friction, as well as infinitely rigid and massive objects [16]. Hannaford [16] looks at the virtual coupling as a bridge that connects a haptic display and virtual environment. However, virtual coupling affects the transparency as well as the stability. In impedance display, high virtual stiffness and virtual damping cause a large conductance of the virtual coupling. As a result, the performance of transparency will close the perfect one and the range of Z-width is large as well. In admittance display, in order to gain the good performance, we need the low virtual damping to get the small conductance of the admittance display. In passive haptic interface, there is always critical trade off between sampling rate, virtual wall stiffness, and viscosity of haptic device [52]. In [53], researchers also discuss the relationship between stability and transparency when virtual coupling factors are designed. In [53], admittance haptic display is applied. Admittance display means that an operator commands force to virtual reality and velocity of virtual reality returns through a haptic device. Through computation, a

haptic interface is affected by admittance of virtual reality, sampling time as well as virtual coupling factors. They conclude there are limits of expressible admittance and increasing sampling time doesn't mean better performance without exception [53]. Sampling time and virtual coupling factors should be changed according to passive inequalities [16] [53] to express desired admittance [53].

1.8 Update Rate of Haptic Display Systems

Obviously, a complete haptic display system is a hybrid system because a virtual environment is generated by computer and a haptic device includes the servomotor. It is inevitable to use digital-to-analog and analog-to-digital technologies to send command signals or get the resulting signals. As a result, update rate of system is necessary. Actually, according to [54], hatpic device vibration is an important factor in the success of a haptic technology. This problem is caused by two critical designed factors, force magnitude and update rate, that can cause vibration and measures the effect of these factors on an operator's ability to detect small features on a simulated hard surface [54].

In order to fix the above problem, at first, the researchers have attempted to apply control theory. Kazerooni and Her [103] developed a sophisticated analysis that accounts for the dynamics of the human arm and its relationship with the haptic devices. Their model requires that the haptic device measure the force exerted by the operator on the device, but many force-feedback joysticks are manufactured without a force transducer to provide this information. Colgate et al. [45] present a control theory model that requires the device to sense only position information and apply a linear function response force as the cursor intrudes into the wall. They conclude that this approach can provide walls that feel "stiff" if the following conditions are met:

(1) the position is sampled quickly and (2) the haptic device has a large amount of inherent damping. Since programmers are often not in a position to change the damping coefficient of the haptic device, they must concentrate on sampling period quickly. Chen and Marcus [56] report that "The common rule of thumb for stable, smooth, and crisp force-feedback control loops dictates that the servo rate should be at 1000 Hz or above". Chang and Colgate [57] report that their unpublished experiments indicate that haptic devices require an update rate of 500 Hz - 1kHz. Several other approaches to dealing with haptic interactions with solid objects, including Zilles and Salisbury's object model [90] and Adams, Moreyra and Hannaford's [16] virtual coupling network, also require high update rates on the order of 1kHz. Practical implementation requires designers to balance update rate and the stiffness of the virtual surface. Fast update rates require simple servo algorithms, particularly when other processes run on the same computer that runs the servo functions.

Steven, Thomas and Johnson [54] report the effects of gain and update rate on an operator's ability to perceive small step-like features along a smooth, hard edge. In their experiments, six participants (male, mean age of 25.8) slid the haptic device along the virtual edge at a prescribed pace and indicated whether they detected a small, upward step on the surface. The update rate and magnitude of the resistive force were varied according to a full-factorial design. Through the analysis of experimental results, they make the following conclusions. The trial type that presented the largest force and the slow update rate resulted in the poorest performance, while the trial with a large force and a fast update did quite well. If the difference in update rate is the only discriminating factor, then one would expect the same performance gap between the two small force trials, which differed only in update rate. Data from individual trials tells more of the story. As expected, the

position graphs of the big force/slow update and big force/fast update trials indicate that the slow update causes larger vibrations. These large vibrations leave the user uncertain about the position of the virtual wall, hiding the presence of small details, so the performance is poor. Turning to the trials with smaller output force, the participants receive two clues about the presence of a small step: kinesthetic movement of the hand, and a momentary lapse of vibration. For the small forces, the user enters the step from the side and does not feel vibration until they move back up to the surface. They also hypothesize that the participants used both cues, the momentary gap in the vibration and the change in kinesthetic positioning of the hand, to detect the edge. For the trials with big forces and slow update rate, there is no gap in vibration, so the clues about the presence of a step comes solely from discerning the change in position of the virtual wall [54]. Thus, before setting the force and update rate, haptic interface designers should consider to level of touch detail needed. Also if the sense of touch is more important than the graphics, performance of the system can be improved by displaying simple graphics. Another recommendation is to implement control theory by considering the user's force input as the adjustment variable [54].

In another research, Murat [58] concentrates on the difference between the sampling rate requirements of haptic interfaces and the significantly lower update rates of the physical models being manipulated. They propose a multirate simulation approach that uses a local linear approximation. This approach is also shown to improve the stability of the haptic interaction. In their discussion, the models are limited to lumped element models, which are also referred to as mass-spring-damper models in the literature, but the arguments can easily be extended to deformable models based on finite element analysis.

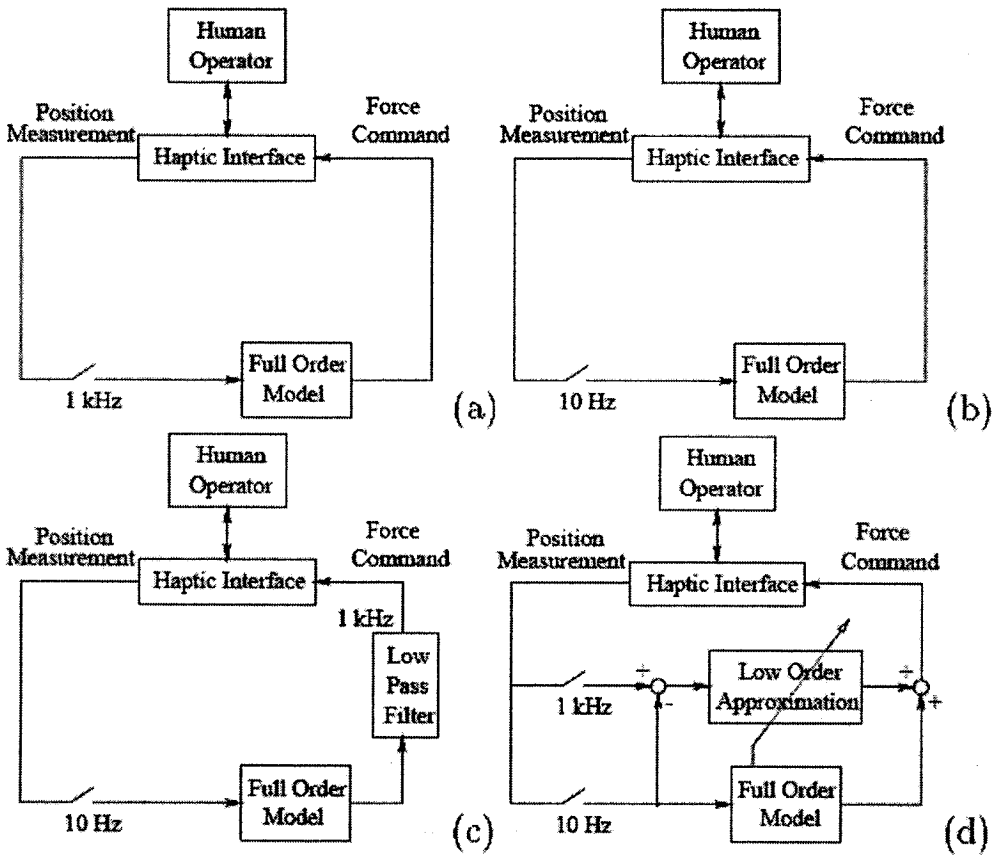

Figure 1-8 Simulation paradigms [58]

They build four different simulation models with 1 kHz haptic update rate, shown in Figure 1-8, in order to introduce their research results. They also consider an hpatic interface interacting with a simulated nonlinear spring in one dimension. Through compared demonstrations based on Figure 1-8, they find that although the use of a low-pass filter to improves the performance of the constant output method seems to help by reducing contaminating noise at the harmonics of the model update rate, however, this approach has two main limitations. First, low pass filtering may eliminate useful high frequency force information. Second, the lag introduced by the low pass filter tends to destabilize the haptic interaction, or introduce oscillation.

When the instrument interacts with the deformable model in a VE simulator, the haptic interface will displace the node(s) it is touching and display the reaction force.

However, the underlying dynamical system has a very high order as it includes the deformation of the whole body. It is impossible to simulate that high order dynamic system in real time because of the limitations of hardware and software. As a result, a low order approximation for real time haptic performance is needed to replace it. In the construction of the low order approximation, linearization is a basic step. The linearized model gives the tangential behavior of the full model. Because the order of the linearized model is equal to the full order, improvement may be processed on the linear model. Model reduction is the critical step of this research. A balanced model reduction [59] is implemented in this model to approximate the system's input-output response with a 10^{th} order system, with the infinity norm of the error resulting from the approximation being less than 1.6×10^{-3}, less than 1% of the full order model. The states of the new low order model show that it is a local approximation. This result is actually expected, because stress decays inversely proportional to the square of the distance from the load in a semi-infinite linear elastic body under a point load [60].

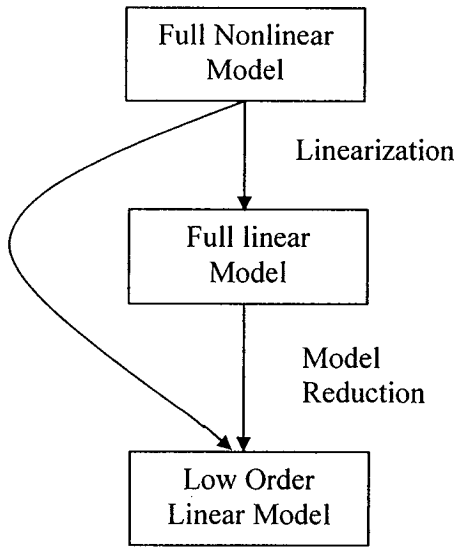

Figure 1-9 Construction of the low order model [58]

Real time response is necessarily needed in the implementation of haptic systems. A balanced model reduction prevents the use of order reduction as a part of the on-line computation because it costs calculations. In order to simplify the approximation construction with less computation, Murat [58] constructs a local linear model directly from the full order model as shown in Figure 1-9.

It is important to note that the local linear approximation used here is not necessarily the best choice. Local approximations are explored in detail in [39]. The major limit of this method is that the local states must be the dominant ones. This could be violated if the material was inhomogeneous, for example if the deep tissue were significantly more compliant than at the surface so that most of the deformation occurred in states far from the interaction [58]. In this case, Astley and Hayward's method [61] would be useful, if the model was linear. Other effects that could violate the dominance of local modes include significant geometric nonlinearities or discontinuities in the tissue that produced large local stresses away from the instrument contact [58].

1.9 Time Delay of Haptic Display Systems

A haptic display system is a kind of application of force reflection or force feedback. Haptic display applications sharing one VE in the network with several users are becoming very popular. It is well known from physiological and psychological data of the haptic modality and from the haptic control theory that the haptic loop requires a high bandwidth of around 1 kHz to guarantee the stability of the haptic interaction, and more importantly, to make a coherent feedback between the visual and the haptic scenes. Developing a network protocol that can provide sufficient bandwidth with minimum latency to a group of distant users is a

challenging problem [64] and physics-based models that simulate haptic interactions among users have begun to be developed [65]. Yet one of the important problems of haptic feedback, even if only one user interacts with the VE engine, is time delay [63]. It is obvious that time delay during the transfer and processing of the data may easily result in unstable forces and can be harmful to the user.

Up-to-now, time delay is still known to be one of the most severe problems in force reflecting teleoperators. Many solutions have been proposed to deal with this problem. Some of the most attractive ones are based on passivity derived from scattering network theory [66] [67] [68] and [69]. Others are based on a passive transformation of power parameters (namely velocity and force) into waves. Other techniques use known classical control theory to derive stable controller from Lyapunov criteria [72], [73], and we can state other works as [74] using μ-synthesis and [85] with notion of virtual time delay, etc. In [71], a simple buffering technique to deal with time-varying delay was also developed.

In teleoperation technologies, force feedback renders a system very sensitive to delays. Small amounts of lag can drive a force feedback loop unstable and the levels of delay encountered in networked teleoperation systems make force feedback impossible without compensation for the delay [76]. Niemeyer and Slotine [75] [67] proposed a passivity-based controller known as a "wave variable" formulation of the problem derived from network theory. A wave variable architecture uses a transformation of variables to encode the control information in a manner that enables the communication link to remain passive in the presence of delay [67]. The complimentary pair of wave variables (u, v) are defined as

$$u = \frac{b\dot{x} + F}{\sqrt{2b}} \qquad v = \frac{b\dot{x} - F}{\sqrt{2b}} \tag{1-11}$$

where u is forward moving wave from master to slave while v is the returning wave from slave to master as depicted in Figure 1-10. Through this substitution, the power flow at any point in the system can be redefined as

$$P = \dot{x}^T F = \frac{1}{2} u^T u + \frac{1}{2} v^T v \tag{1- 12}$$

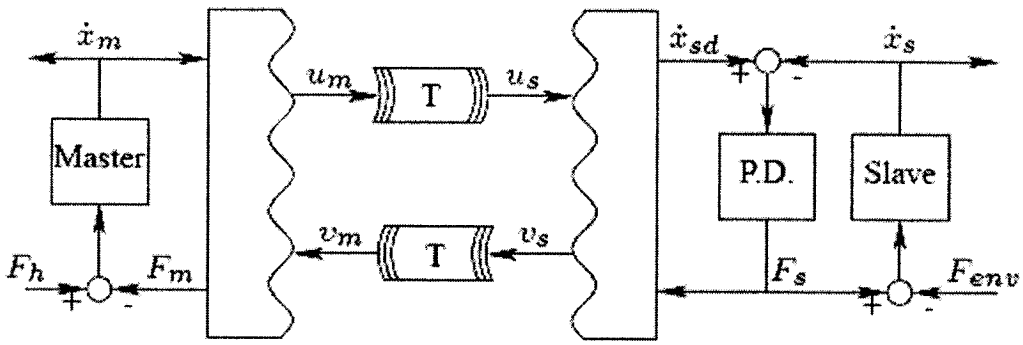

Figure 1-10 A basic configuration for a wave variable based teleoperator system[67]

Under this construction, the power flow has been separated into independent flows in the forward and reverse directions. By transmitting wave variables rather than traditional effort and flow variables across the communication delay, passivity of the communication link can be guaranteed for arbitrary delays. For a formal treatment of wave variables and passivity, see [78], [79]. Notice that using wave variables for transmitting control data across a delay ensures that the communication link is a passive element, but does nothing to guarantee the passivity of the other elements in the system [76]. In Niemeyer' research, their implementation of the wave filter is a fundamentally asymmetric controller [76]. This is useful because the bandwidth of any meaningful input from the operator is below the achievable bandwidth for their system, but higher frequencies have been shown to be very valuable feedback to the operator. By only filtering the forward wave path, we have ensured the passivity of the system while still allowing high frequency feedback from the slave to reach the

master. In addition, the simplicity of the criterion for passivity in wave space lends itself to wide variety of compensator options [76]. However, there are two practical limitations in wave controllers: a maximum wave impedance and maximum wave bandwidth.

Time delay is an old problem in remote control operation. Besides above wave variable method, Smith prediction [81] is another approach to adapt on delayed haptic feedback interaction. This proposed controller requires only the master model space [80]. This solution is proven to be stable and also robust to master device parameters estimation. In the work of [63], the principle of Smith prediction has been adapted for the synthesis of a stable haptic feedback controller to be used with constant and varying time delay.

The Smith Predictor is an effective Dead-time Compensator (DTC) for a stable process with a large dead-time [81]. The classical configuration of a Smith Predictor [83] is shows in Figure 1-11. In the figure, r represents the reference signal, $P(s)$ is the transfer function of the process with large dead-time, $\hat{P}(s)$ and $\hat{P}_0(s)$ are process models with and without dead time respectively. The shaded area $C(s)$ is the Smith predictor or Dead-time compensators (DTS). The presence of a large dead-time (e.g. $n\tau$) in the process $P(s)$ causes the feedback to be delayed and forces conventional controllers to operate with a low gain. The Smith Predictor improves the closed-loop performance by introducing a minor feedback loop around the primary controller to produce $v(t)$, which is an estimation of the variation $y(t)$ during the last n units of time. This variation $v(t)$ added to the delayed measurement constitutes an estimate of the current value of y, which will become available at the later measurement $y(t+n\tau)$. This is subtracted form the requested value r to produce the error that is fed

into the controller. This eliminates the sluggish responses or over-correction that is associated with conventional controllers [82].

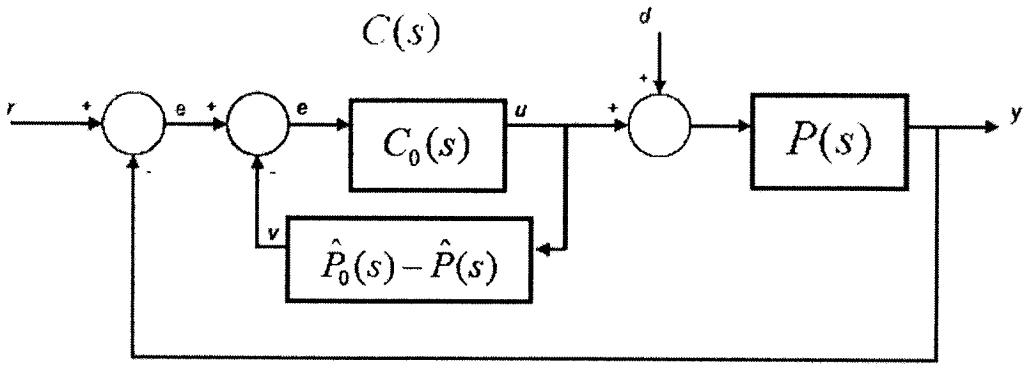

Figure 1-11 A classical diagram of a control system incorporating a Smith Predictor [83]

Mammmar [84] design a model-based controller for interactive delayed force feedback virtual environment lying in an astute adaptation and implementation of the Smith prediction scheme. Their controller is also implemented in commercial haptic libraries and interface build-in controllers. The estimation of both (upwards and downwards) delays is not needed. Their simulation results confirmed a stable virtual environment haptic interaction in the presence of both constant and time-varying delays. A robustness analysis of the proposed controller was also conducted. The error margins that guarantee the stability of the haptic interaction are found to be large enough to state robustness of the approach [84].

Comparing to wave-based methods, Smith prediction scheme is more transparent to the user, since there is no additional corrupting damping. The price to be paid is in the position discrepancy between the haptic device and the virtual probe when the contact is made. Many experiments have showen the validity of the proposed theory.

1.10 Thesis Objectives

Haptic display is one of most active topics in Virtual Environments (VE), which involves use of different kinds of technologies, such as software engineering, network architectures, communication protocols and real time control laws. In prior works, virtual coupling, passivity observer and passivity controller have been introduced into the stability and passivity of haptic interfaces; however, because of the limitation, such as time delay, mathematical models of the plant and data transformation from Analog-to-Digital (A/D) and from Digital-to-Analog (D/A) should be investigated. Furthermore, in networked haptic display system, the above limitations would become even more complex and vague. Thus in this thesis, our main objective is in development of conditions for the guaranteed stability of a networked haptic in distributed VE. We also hope to find a set of parameters for the virtual coupling to guarantee the passivity and stability of the haptic interface when a delay is introduced into a networked haptic in distributed VE. The two-port network will be introduced into the design of our VR system with the PHANToM Premium 1.5 haptic device to find the condition of stability for our VR system.

1.11 Thesis Contributions

In this thesis, a procedure of designing the parameters for the virtual coupling in a distributed virtual environment with two users interacting simultaneously with force feedback device and one unit time delay is presented. The feasibility of passivity criterion to ensure the stability condition of the haptic interface to ensure the stability condition of the closed-loop system is presented for the two different interactions scenarios. The main contributions of this thesis are as follows: (1) The analysis of the

mathematical models of the PHANToM Premium 1.5 has been done; (2) The parameters of the virtual coupling to guarantee the stability of haptic interface have been designed; (3) The closed-loop pseuocontrol ratios for output versus reference input in a multi-user networked VR system with a unit delay has been derived; (4) The closed-loop stability conditions of the interactions with two kinds of the virtual environment models have been obtained. (5) The complete response results of the closed-loop system with different parameters of the virtual environment model have been simulated.

The outline of this thesis is as follows: In Chapter 2 mathematical models of Phantom 1.5 are presented. In Chapter 3 network theory and passivity criterion are introduced into the design of virtual coupling for networked haptic displays based on Phantom 1.5. Furthermore, the stability conditions for the haptic interface are also obtained. In Chapter 4 the stability condition for the closed loop system was derived from the opened-loop stability condition for the haptic interface through Jury stability test. Chapter 5 describes implementation and results of passivity condition utilized to guarantee the stability of the haptic display in the distributed VE. Finally, Chapter 6 concludes the thesis with suggestions for future work and possible improvements.

Chapter 2

Mathematical Model of the Phantom Haptic Interface

2.1 Introduction

In chapter 1, we briefly described the PHANToM system. In this chapter, we are going to introduce it in detail.

The first PHANToM haptic device was designed and built in the early 1990s by Thomas Massie and Dr. Kenneth Salisbury. In 1993, SensAble Technologies, Inc. was founded to commercialize PHANToM haptic device. Presently, PHANToM haptic device has become one of the most popular haptic devices because it has a large workspace, low inertia, low friction, and high position precision characteristics.

Currently, PHANToM haptic devices have four models for different customers and requirements. The PHANTOM Premium models are high-precision instruments and, within the PHANTOM product line, provide the largest workspaces and highest forces, and some offer 6DOF capabilities. The PHANTOM® Desktop™ device and PHANTOM® Omni™ device offer affordable desktop solutions. Of the two devices, the PHANTOM Desktop delivers higher fidelity, stronger forces, and lower friction, while the PHANTOM Omni is the most cost-effective haptic device available today. In this thesis, we use PHANToM Premium 1.5.

The Premium 1.5 device provides a range of motion approximating lower arm movement pivoting at the elbow. The Premium 1.5 device includes a passive stylus and thimble gimbal and provides 3 degrees of freedom positional sensing and 3

degrees of freedom force feedback. An encoder stylus gimbal that may be purchased separately enables the measurement of an additional 3 degrees of positional sensing (pitch, roll & yaw). The Premium 1.5 device connects to the PC via the parallel port (EPP) interface. Supported OS platforms include Windows® 2000/XP/NT, RedHat® Linux® 7.2, RedHat Linux 9, RedHat Fedora™, and SUSE 9.0.

In haptic interface applications, researchers hope to satisfy the common requirements of low noise/granularity/latency measurements, an accurate system model, high bandwidth, the need for an open architecture, and the ability to operate for long periods without interruption while exerting significant forces. To satisfy these requirements, it is necessary to study the kinematics, dynamics, high frequency dynamic response, and velocity estimation of the PHANToM system.

In this thesis, we try to derive the mathematical model for the PHANToM Premium 1.5 based on dynamic equations of the physical system. We then linearize this mathematical model to get the linear transfer function.

In this thesis, we follow the notation of Murray, Li, and Sastry [70] in representing rigid body transformations, and kinematics and dynamics calculations. Results of the calculations are also related to the notation of Craig [87] and Murat and David [88].

2.2 Kinematics

In this section we perform the kinematic analysis of the PHANToM premium 1.5 manipulator. In SensAble's GHOST and Basic I/O libraries, they have offered some of the kinematic analysis; however, it is not enough for the researchers to have a more open architecture, and to use in tasks and functions not supported in these libraries.

In the following subsections, solutions of forward and inverse kinematics are presented, followed by the calculation of the manipulator Jacobian and a basic analysis of the workspace.

2.2.1 Forward Kinematics

In robotics, the forward kinematics problem is that the given joint variables of the robot may determine the position and orientation of the end-effector through mathematical expressions. The joint variables are the angles between the links in the case of revolute or rotational joints, and the link extension in the case of prismatic or sliding joints.

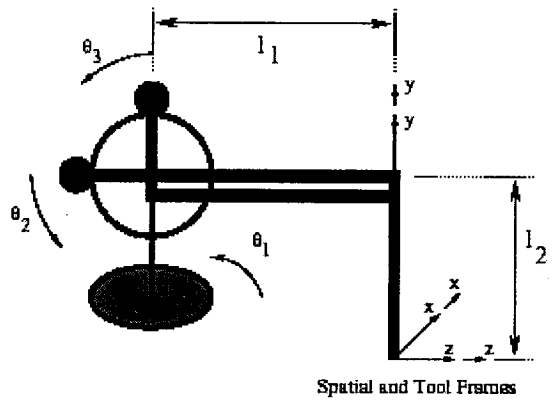

Figure 2-1 Zero configuration of the manipulator [88]

Figure 2-1 shows the zero configuration and the conventions. To make the computations as easy, we characterize the kinematic configuration of the manipulator with the following vectors and points:

$$\omega_1 = [0 \quad 1 \quad 0]^T \tag{2-1}$$

$$\omega_2 = \omega_3 = [-1 \quad 0 \quad 0]^T \tag{2-2}$$

$$q_1 = [0 \quad 0 \quad -l_1]^T \tag{2-3}$$

$$q_2 = q_3 = [0 \quad l_2 \quad -l_1]^T \tag{2-4}$$

$$\xi_i = \begin{bmatrix} -\omega_i \times q_i \\ \omega_i \end{bmatrix}, \; i = 1,2,3. \tag{2-5}$$

The definitions for l_1 and l_2 for the PHANToM model 1.5 are given in Figure 2-1.

From the side and top view illustration in Figure 2-2, the forward kinematic map is derived by:

$$g_{st}(\theta) = \begin{bmatrix} R(\theta) & \\ 0 \quad 0 \quad 0 & p(\theta) \end{bmatrix} \tag{2-6}$$

where

$$R(\theta) = e^{\hat{\omega}_1\theta_1} e^{\hat{\omega}_3\theta_3} I_{3\times 3} = \begin{bmatrix} \cos(\theta_1) & -\sin(\theta_1)\sin(\theta_3) & \cos(\theta_3)\sin(\theta_1) \\ 0 & \cos(\theta_3) & \sin(\theta_3) \\ -\sin(\theta_1) & -\cos(\theta_1)\sin(\theta_3) & \cos(\theta_1)\cos(\theta_3) \end{bmatrix} \tag{2-7}$$

and

$$p(\theta) = e^{\hat{\xi}_1\theta_1} e^{\hat{\xi}_2\theta_2} \begin{bmatrix} & & & 0 \\ & I_{3\times 3} & & l_2 \\ & & & 0 \\ 0 & 0 & 0 & 1 \end{bmatrix} \begin{bmatrix} 0 \\ 0 \\ 0 \\ 1 \end{bmatrix} + \begin{bmatrix} R(\theta) \begin{bmatrix} 0 \\ -l_2 \\ 0 \end{bmatrix} \\ 0 \end{bmatrix} \tag{2-8}$$

In closed form,

$$g_{st}(\theta) = \begin{bmatrix} \cos(\theta_1) & -\sin(\theta_1)\sin(\theta_3) & \cos(\theta_3)\sin(\theta_1) & \sin(\theta_1)(l_1\cos(\theta_2) + l_2\sin(\theta_3)) \\ 0 & \cos(\theta_3) & \sin(\theta_3) & l_2 - l_2\cos(\theta_3) + l_1\sin(\theta_2) \\ -\sin(\theta_1) & -\cos(\theta_1)\sin(\theta_3) & \cos(\theta_1)\cos(\theta_3) & -l_1 + \cos(\theta_1)(l_1\cos(\theta_2) + l_2\sin(\theta_3)) \\ 0 & 0 & 0 & 1 \end{bmatrix} \tag{2-9}$$

In the notation of Craig [87], ${}^S_T T = g_{st}(\theta)$ as described above.

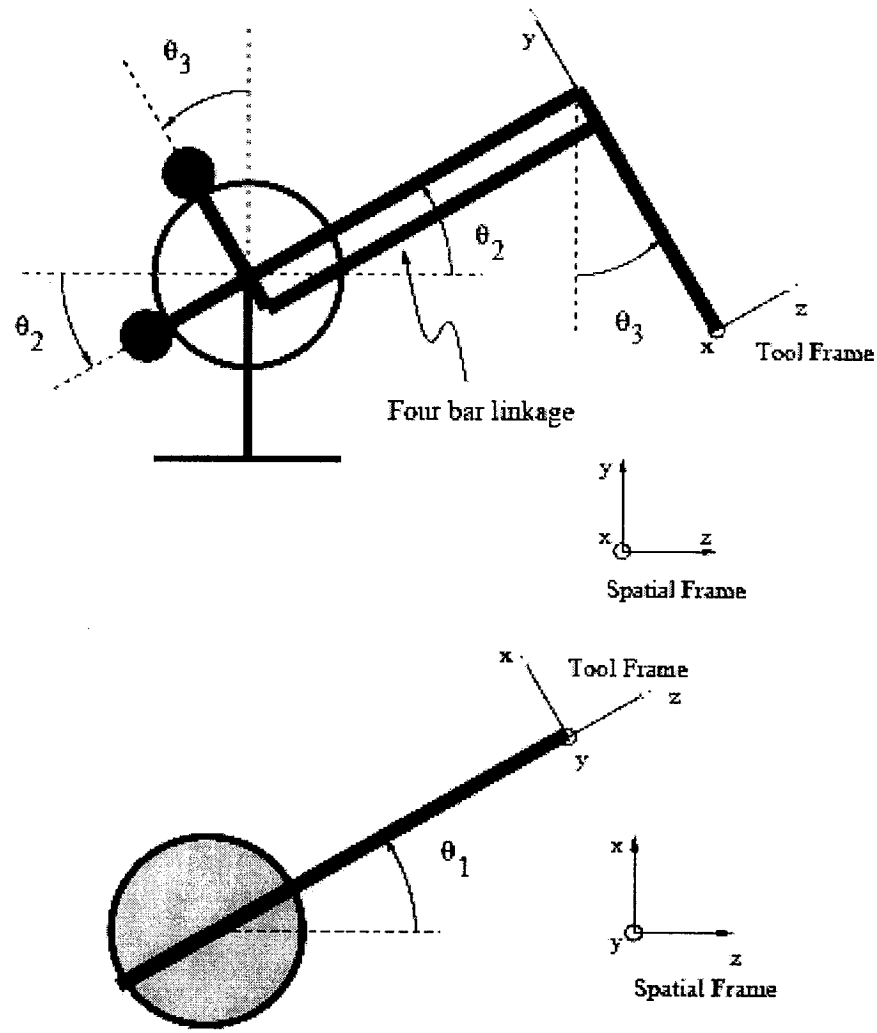

Figure 2-2 Side and top views [84]

2.2.2 Inverse Kinematics

Inverse kinematics problem is concerned with finding a set of joint variables to achieve the desired position and orientation when a desired position and orientation for the end-effector of the robot is given.

PHANToM Premium 1.5 is a 3 DOF manipulator. The inverse kinematics helps us to find the relationship between the set of $(\theta_1,\theta_2,\theta_3)$ and a desired end-effector

position $p_o = [p_{ox} \quad p_{oy} \quad p_{oz}]^T$, where θ_1, θ_2, θ_3 is shown in Figure 2-2. The resulting angles are given by:

$$\theta_1 = a\tan 2(p_{ox}, p_{oz} + l_1) \tag{2- 10}$$

$$d = \sqrt{p_{ox}^2 + (p_{oz} + l_1)^2} \tag{2- 11}$$

$$r = \sqrt{p_{ox}^2 + (p_{oy} - l_2)^2 + (p_{oz} + l_1)^2} \tag{2- 12}$$

$$\theta_2 = \cos^{-1}\left(\frac{l_1^2 + r^2 - l_2^2}{2l_1 r}\right) + a\tan 2(p_{oy} - l_2, d) \tag{2- 13}$$

$$\theta_3 = \theta_2 + \cos^{-1}\left(\frac{l_1^2 + l_2^2 - r^2}{2l_1 l_2}\right) - \frac{\pi}{2} \tag{2- 14}$$

where d and r are intermediate variables.

2.2.3 Manipulator Jacobian

In the notation of Craig [87], mathematically the forward kinematic equations define a function between the space of cartesian positions and orientations and the space of joint positions. The velocity relationships are then determined by the Jacobian of this function. The Jacobian is a matrix-valued function and can be thought of as the vector version of the ordinary derivative of a scalar function. This Jacobian or Jacobian matrix is one of the most important quantities in the analysis and control of robot motion. It arises in virtually every aspect of robotic manipulation: in the planning and execution of smooth trajectories, in the determination of singular configurations, in the execution of coordinated anthropomorphic motion, in the derivation of the dynamic equations of motion, and in the transformation of forces and torques from the end-effecter to the manipulator joints.

The body Jacobian of the manipulator is expressed as followed:

$$J^b(\theta) = \left[\cdots \left(g_{st}^{-1} \frac{\partial g_{st}}{\partial \theta_i} \right)^{\vee} \cdots \right], \quad i = 1,2,3. \tag{2- 15}$$

Through (2-9) and (2-15), we compute the Jacobian matrix for the PHANToM Premium 1.5 as following:

$$J^b(\theta) = \begin{bmatrix} l_1 \cos(\theta_2) + l_2 \sin(\theta_3) & 0 & 0 \\ 0 & l_1 \cos(\theta_2 - \theta_3) & 0 \\ 0 & -l_1 \sin(\theta_2 - \theta_3) & l_2 \\ 0 & 0 & -1 \\ \cos(\theta_3) & 0 & 0 \\ \sin(\theta_3) & 0 & 0 \end{bmatrix} \tag{2- 16}$$

Using (2-16), we can get the hybrid velocity matrix of the tool frame (the translational and angular velocity of the tool frame around the origin of the tool frame expressed in spatial coordinates) is calculated as

$$V^h = \begin{bmatrix} R(\theta) & 0 \\ 0 & R(\theta) \end{bmatrix} J^b(\theta)\dot{\theta} \tag{2- 17}$$

where $R(\theta)$ is given by (2-7). In the Craig's book [87], ${}^S V = V^h$. The motor torques required to counteract the hybrid wrench F^h applied to the manipulator are given by

$$\tau = J^{bT}(\theta) \begin{bmatrix} R^T(\theta) & 0 \\ 0 & R^T(\theta) \end{bmatrix} F^h \tag{2- 18}$$

The hybrid wrench is the force/torque combination applied to the origin of the tool frame expressed in the spatial coordinates. In the Craig's book [87], ${}^S F = F^h$.

2.2.4 Inertial Parameters of the PHANToM Premium 1.5

In Cavusoglu and Feygin's report [89], they derived dynamic equations and inertia parameters for the PHANToM Premium 1.5 in detail. In this chapter, we will use their result directly.

Firstly, the physical parts of PHANToM Premium 1.5 is consisted of seven segments, shown in Figure 2-3. The units are in MKS (meter-kilogram-second) system unless otherwise noted.

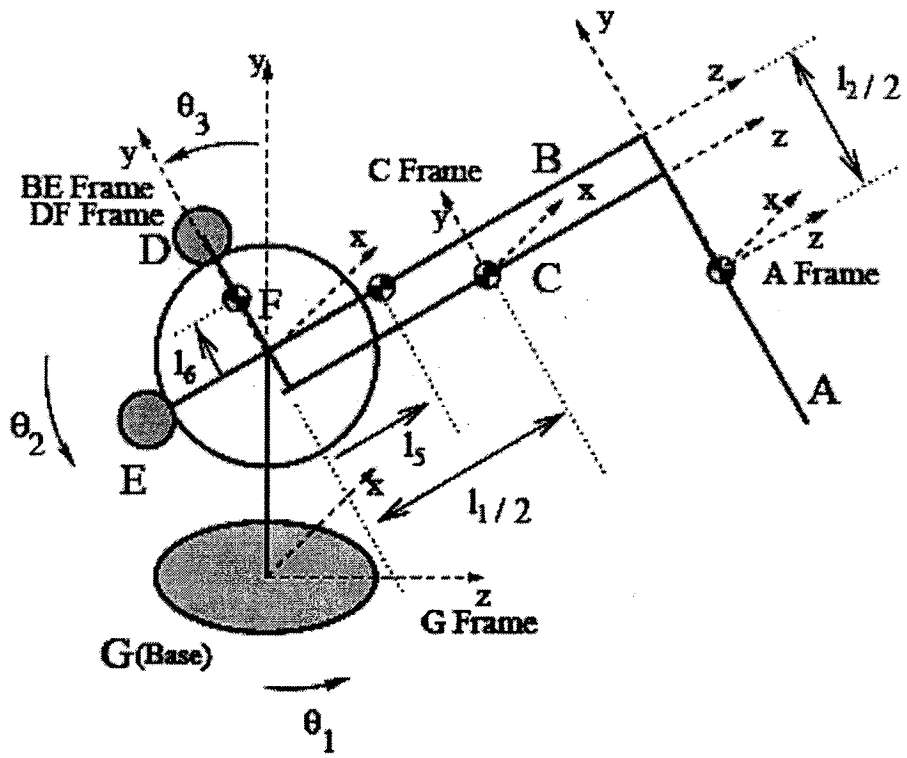

Figure 2-3 Segments used in dynamics analysis [89]

Secondly, to calculate the inertial parameters, we assume the manipulator to be mainly made of aluminium, with a density of 1750 kg/m^3. The motors are assumed to be Maxon RE-025-055035. Thus, according to Cavusoglu and Feygin's work [89], the following results are obtained.

The following parameters of the manipulator are measured as:

$$l_1 = 0.215 \tag{2-19}$$

$$l_2 = 0.170 \tag{2-20}$$

$$l_3 = 0.0325 \tag{2-21}$$

The inertial parameters of segment A, the mass of segment A and its rotational inertia matrix are estimated to be:

$$m_a = 0.0202 \tag{2-22}$$

$$I_a = \begin{bmatrix} I_{axx} & 0 & 0 \\ 0 & I_{ayy} & 0 \\ 0 & 0 & I_{azz} \end{bmatrix} \tag{2-23}$$

$$I_{axx} = 0.4864 \times 10^{-4} \tag{2-24}$$

$$I_{ayy} = 0.001843 \times 10^{-4} \tag{2-25}$$

$$I_{azz} = 0.4864 \times 10^{-4} \tag{2-26}$$

For segment C, the parameters are estimated as:

$$m_c = 0.0249 \tag{2-27}$$

$$I_c = \begin{bmatrix} I_{cxx} & 0 & 0 \\ 0 & I_{cyy} & 0 \\ 0 & 0 & I_{czz} \end{bmatrix} \tag{2-28}$$

$$I_{cxx} = 0.959 \times 10^{-4} \tag{2-29}$$

$$I_{cyy} = 0.959 \times 10^{-4} \tag{2-30}$$

$$I_{czz} = 0.0051 \times 10^{-4} \tag{2-31}$$

For segment BE combined by segment B and segment E, the parameters are estimated as:

$$m_{be} = 0.2359 \tag{2-32}$$

$$I_{be} = \begin{bmatrix} I_{bexx} & 0 & 0 \\ 0 & I_{beyy} & 0 \\ 0 & 0 & I_{bezz} \end{bmatrix} \tag{2-33}$$

$$I_{bexx} = 11.09 \times 10^{-4} \tag{2-34}$$

$$I_{beyy} = 10.06 \times 10^{-4} \tag{2-35}$$

$$I_{bezz} = 0.591 \times 10^{-4} \tag{2-36}$$

The location of the center of mass of the segment BE is calculated as

$$l_5 = -36.8 \tag{2-37}$$

For segment DF combined by segment D and segment F, the parameters are estimated as:

$$m_{df} = 0.1906 \tag{2-38}$$

$$I_{df} = \begin{bmatrix} I_{dfxx} & 0 & 0 \\ 0 & I_{dfyy} & 0 \\ 0 & 0 & I_{dfzz} \end{bmatrix} \tag{2-39}$$

$$I_{dfxx} = 7.11 \times 10^{-4} \tag{2-40}$$

$$I_{dfyy} = 0.629 \times 10^{-4} \tag{2-41}$$

$$I_{dfzz} = 6.246 \times 10^{-4} \tag{2-42}$$

The location of the center of mass of the segment DF is calculated as

$$l_6 = -52.7 \tag{2-43}$$

The rotation inertia matrix of the base that is of interest is calculated as

$$I_{baseyy} = 11.87 \times 10^{-4} \tag{2-44}$$

We also note that the motor inertia has been added to the inertia around the x-axis with a transmission ratio of 11.6:1.0.

2.2.5 Dynamics

Lagrangian formulation is a powerful mathematic tool for the analysis of dynamics of physical systems. It helps us to build the dynamic equations of the

manipulator. Thus based on the analysis and computation of Cavusoglu and Feygin [89], we get the dynamic equations for the PHANToM manipulator as given below:

$$\begin{bmatrix} M_{11} & 0 & 0 \\ 0 & M_{22} & M_{23} \\ 0 & M_{32} & M_{33} \end{bmatrix} \begin{bmatrix} \ddot{\theta}_1 \\ \ddot{\theta}_2 \\ \ddot{\theta}_3 \end{bmatrix} + \begin{bmatrix} C_{11} & C_{12} & C_{13} \\ C_{21} & 0 & C_{23} \\ C_{31} & C_{32} & 0 \end{bmatrix} \begin{bmatrix} \dot{\theta}_1 \\ \dot{\theta}_2 \\ \dot{\theta}_3 \end{bmatrix} + \begin{bmatrix} 0 \\ N_2 \\ N_3 \end{bmatrix} = \begin{bmatrix} \tau_1 \\ \tau_2 \\ \tau_3 \end{bmatrix} \qquad (2\text{-}45)$$

where

$$\begin{aligned} M_{11} = & (\frac{1}{8}(4I_{ayy} + 4I_{azz} + 8I_{baseyy} + 4I_{beyy} + 4I_{bezz} + 4I_{cyy} + 4I_{czz} + 4I_{dfyy} + 4I_{dfzz} + 4l_1^2 m_a + l_2^2 m_a + l_1^2 m_c + 4l_3^2 m_c) \\ & + \frac{1}{8}(4I_{beyy} - 4I_{bezz} + 4I_{cyy} - 4I_{czz} + l_1^2(4m_a + m_c))\cos(2\theta_2) \\ & + \frac{1}{8}(4I_{ayy} - 4I_{azz} + 4I_{dfyy} - 4I_{dfzz} - l_2^2 m_a - 4l_3^2 m_c)\cos(2\theta_3) + l_1(l_2 m_a + l_3 m_c)\cos(\theta_2)\sin(\theta_3)) \end{aligned} \qquad (2\text{-}46)$$

$$M_{22} = \frac{1}{4}(4(I_{bexx} + I_{cxx} + l_1^2 m_a) + l_1^2 m_c) \qquad (2\text{-}47)$$

$$M_{23} = -\frac{1}{2} l_1 (l_2 m_a + l_3 m_c)\sin(\theta_2 - \theta_3) \qquad (2\text{-}48)$$

$$M_{32} = M_{23} \qquad (2\text{-}49)$$

$$M_{33} = \frac{1}{4}(4I_{axx} + 4I_{dfxx} + l_2^2 m_a + 4l_3^2 m_c) \qquad (2\text{-}50)$$

$$\begin{aligned} C_{11} = & \frac{1}{8}(-2\sin(\theta_2)((4I_{beyy} - 4I_{bezz} + 4I_{cyy} - 4I_{czz} + 4l_1^2 m_a + l_1^2 m_c)\cos(\theta_2) + 2l_1(l_2 m_a + l_3 m_c)\sin(\theta_3))\dot{\theta}_2 \\ & + 2\cos(\theta_3)(2l_1(l_2 m_a + l_3 m_c)\cos(\theta_2) + (-4I_{ayy} + 4I_{azz} - 4I_{dfyy} + 4I_{dfzz} + l_2^2 m_a + 4l_3^2 m_c)\sin(\theta_3))\dot{\theta}_3) \end{aligned} \qquad (2\text{-}51)$$

$$C_{12} = -\frac{1}{8}((4I_{beyy} - 4I_{bezz} + 4I_{cyy} - 4I_{czz} + l_1^2(4m_a + m_c))\sin(2\theta_2) + 4l_1(l_2 m_a + l_3 m_c)\sin(\theta_2)\sin(\theta_3))\dot{\theta}_1 \qquad (2\text{-}52)$$

$$C_{13} = -\frac{1}{8}(-4l_1(l_2 m_a + l_3 m_c)\cos(\theta_2)\cos(\theta_3) - (-4I_{ayy} + 4I_{azz} - 4I_{dfyy} + 4I_{dfzz} + l_2^2 m_a + 4l_3^2 m_c)\sin(2\theta_3))\dot{\theta}_1 \qquad (2\text{-}53)$$

$$C_{21} = -C_{12} \qquad (2\text{-}54)$$

$$C_{23} = \frac{1}{2} l_1 (l_2 m_a + l_3 m_c)\cos(\theta_2 - \theta_3)\dot{\theta}_3 \qquad (2\text{-}55)$$

$$C_{31} = -C_{13} \qquad (2\text{-}56)$$

$$C_{32} = \frac{1}{2} l_1 (l_2 m_a + l_3 m_c)\cos(\theta_2 - \theta_3)\dot{\theta}_2 \qquad (2\text{-}57)$$

$$N_2 = \frac{1}{2} g(2l_1 m_a + 2l_5 m_{be} + l_1 m_c)\cos(\theta_2) \qquad (2\text{-}58)$$

$$N_3 = \frac{1}{2} g(2l_2 m_a + 2l_3 m_c - 2l_6 m_{df}) \sin(\theta_3) \tag{2-59}$$

In above dynamic equations, τ_1, τ_2 and τ_3 are the separate motor torques at each axis (x, y and z); θ_1, θ_2 and θ_3 are separately shown in Figure 2-3; furthermore, $\dot{\theta}_1$, $\dot{\theta}_2$ and $\dot{\theta}_3$ are the differentials of the angular displacements. The above dynamic equation assumes that the gravity vector is in the –y direction.

2.3 Control Design

We rewrite (2-45) into another expression as shown below:

$$\begin{bmatrix} \ddot{\theta}_1 \\ \ddot{\theta}_2 \\ \ddot{\theta}_3 \end{bmatrix} = \begin{bmatrix} M_{11} & 0 & 0 \\ 0 & M_{22} & M_{23} \\ 0 & M_{32} & M_{33} \end{bmatrix}^{-1} \left(\begin{bmatrix} \tau_1 \\ \tau_2 \\ \tau_3 \end{bmatrix} - \begin{bmatrix} 0 \\ N_2 \\ N_3 \end{bmatrix} - \begin{bmatrix} C_{11} & C_{12} & C_{13} \\ C_{21} & 0 & C_{23} \\ C_{31} & C_{32} & 0 \end{bmatrix} \begin{bmatrix} \dot{\theta}_1 \\ \dot{\theta}_2 \\ \dot{\theta}_3 \end{bmatrix} \right) \tag{2-60}$$

From the above equation, we note that the dynamics of the PHANToM Premium 1.5 is unstable. For the purpose of future efforts, we now use negative feedback control law to make the physical plant stable.

2.3.1 States Feedback Design

In order to achieve acceptable performance behavior, we propose a new relationship among τ, θ and $\dot{\theta}$, such that:

For $\tau_1 : \tau_1^{new} = \tau_1 + k_1 \dot{\theta}_1 + \gamma_1 \theta_1$ (2-61)

For $\tau_2 : \tau_2^{new} = \tau_2 + k_2 \dot{\theta}_2 + \gamma_2 \theta_2$ (2-62)

For $\tau_3 : \tau_3^{new} = \tau_3 + k_3 \dot{\theta}_3 + \gamma_3 \theta_3$ (2-63)

where k_1, k_2 and k_3 are real parameters and γ_1, γ_2 and γ_3 are parameters to be designed to meet certain specifications as well.

2.3.2 Closed Loop Dynamic Equations

After we substitute (2-61), (2-62) and (2-63) into (2-60), we get the closed loop dynamic equations:

$$\begin{bmatrix}\ddot{\theta}_1\\ \ddot{\theta}_2\\ \ddot{\theta}_3\end{bmatrix}=\begin{bmatrix}M_{11} & 0 & 0\\ 0 & M_{22} & M_{23}\\ 0 & M_{32} & M_{33}\end{bmatrix}^{-1}\left(\begin{bmatrix}\tau_1^{new}\\ \tau_2^{new}\\ \tau_3^{new}\end{bmatrix}-\begin{bmatrix}0\\ N_2\\ N_3\end{bmatrix}-\begin{bmatrix}C_{11}+k_1 & C_{12} & C_{13}\\ C_{21} & k_2 & C_{23}\\ C_{31} & C_{32} & k_3\end{bmatrix}\begin{bmatrix}\dot{\theta}_1\\ \dot{\theta}_2\\ \dot{\theta}_3\end{bmatrix}-\begin{bmatrix}\gamma_1 & 0 & 0\\ 0 & \gamma_2 & 0\\ 0 & 0 & \gamma_3\end{bmatrix}\begin{bmatrix}\theta_1\\ \theta_2\\ \theta_3\end{bmatrix}\right) \tag{2-64}$$

We now establish a set of state variables to express (2-64) into a state space representation. Firstly, we assume that the variables θ_1, θ_2, θ_3, $\dot{\theta}_1$, $\dot{\theta}_2$ and $\dot{\theta}_3$ are the state variables, so we get $x_1=\theta_1; x_2=\theta_2; x_3=\theta_3; x_4=\dot{\theta}_1; x_5=\dot{\theta}_2; x_6=\dot{\theta}_3;$ where $x_i(i=1,2,3,4,5,6)$ is the state variable. We can now rewrite (2-64) into the state equations $f(x_1,x_2,x_3,x_4,x_5,x_6,\tau_1^{new},\tau_2^{new},\tau_3^{new})$ as shown below:

$$\begin{bmatrix}f_1\\ f_2\\ f_3\\ f_4\\ f_5\\ f_6\end{bmatrix}=\begin{bmatrix}\dot{x}_1\\ \dot{x}_2\\ \dot{x}_3\\ \dot{x}_4\\ \dot{x}_5\\ \dot{x}_6\end{bmatrix}=\begin{bmatrix}1&0&0&0&0&0\\ 0&1&0&0&0&0\\ 0&0&1&0&0&0\\ 0&0&0&\multicolumn{3}{c}{\multirow{3}{*}{$\begin{bmatrix}M_{11} & 0 & 0\\ 0 & M_{22} & M_{23}\\ 0 & M_{32} & M_{33}\end{bmatrix}^{-1}$}}\\ 0&0&0&&&\\ 0&0&0&&&\end{bmatrix}\left(\begin{bmatrix}0\\ 0\\ 0\\ \tau_1^{new}\\ \tau_2^{new}\\ \tau_3^{new}\end{bmatrix}-\begin{bmatrix}0\\ 0\\ 0\\ 0\\ N_2\\ N_3\end{bmatrix}-\begin{bmatrix}0&0&0&1&0&0\\ 0&0&0&0&1&0\\ 0&0&0&0&0&1\\ \gamma_1&0&0&C_{11}+k_1&C_{12}&C_{13}\\ 0&\gamma_2&0&C_{21}&k_2&C_{23}\\ 0&0&\gamma_3&C_{31}&C_{32}&k_3\end{bmatrix}\begin{bmatrix}x_1\\ x_2\\ x_3\\ x_4\\ x_5\\ x_6\end{bmatrix}\right) \tag{2-65}$$

2.3.3 Equilibrium Points

Before we linearize the dynamic equations, we need to find the equilibrium points for our dynamic equations. Let $f(x_1,x_2,x_3,x_4,x_5,x_6,\tau_1^{new},\tau_2^{new},\tau_3^{new})=0$, (2-65) becomes:

$$\begin{cases}f_1=\dot{x}_1=x_4=0\\ f_2=\dot{x}_2=x_5=0\\ f_3=\dot{x}_3=x_6=0\\ f_4=\tau_1^{new}-\gamma_1x_1=0\\ f_5=\tau_2^{new}-N_2-\gamma_2x_2=0\\ f_6=\tau_3^{new}-N_3-\gamma_3x_3=0\end{cases} \tag{2-66}$$

From (2-66), we find

$$x_4 = 0; x_5 = 0; x_6 = 0 \tag{2- 67}$$

As a result,

$$x_1 = \text{constant}; x_2 = \text{constant}; x_3 = \text{constant} \tag{2- 68}$$

so that,

$$\tau_1^{new} = \gamma_1 x_1; \tau_2^{new} = N_2 + \gamma_2 x_2; \tau_3^{new} = N_3 + \gamma_3 x_3 \tag{2- 69}$$

Therefore, the equilibrium points are equilibrium set, but this set should satisfy (2-67), (2-68) and (2-69).

2.3.4 Jacobian Matrix

A nonlinear system can behave in the small neighbourhood about an equilibrium point like a linear system. If we expand the state equations into a Taylor series about an equilibrium point and assume we only operate within a small neighbourhood of the equilibrium point, the higher-order terms in the Taylor series may be neglected. Thus, the Jacobian matrix is derived as following:

$$A = \left[\frac{\partial f_i}{\partial x_j}\right], \text{ where } i = [1,6]; j = [1,6] \tag{2- 70}$$

$$B = \left[\frac{\partial f_i}{\partial \tau_j}\right], \text{ where } i = [1,6]; j = [1,3] \tag{2- 71}$$

2.3.5 Linearization at an Equilibrium Point Set

Now we set $x_1 = 0$, $x_2 = \pi/4$ and $x_3 = \pi/4$ as an equilibrium point according to (2-68), therefore, we substitute them into (2-58), (2-59) and (2-66), to get:

$$x_4 = 0; x_5 = 0; x_6 = 0 \tag{2- 72}$$

and

$$\tau_1^{new} = 0 \tag{2- 73}$$

$$\tau_2^{new} = -0.0115 + 0.7854\gamma_2 \tag{2- 74}$$

$$\tau_3^{new} = -0.0521 + 0.7854\gamma_3 \tag{2- 75}$$

First, we substitute (2-72), (2-73), (2-74), (2-75) and (2-19) – (2-44) into (2-46) – (2-59); next, we substitute above the results into (2-65); and finally, we employ (2-70) and (2-71) in (2-65); so that the matrices A and B for the linearized model are obtained as following:

$$A = \begin{bmatrix} 0 & 0 & 0 & 1 & 0 & 0 \\ 0 & 0 & 0 & 0 & 1 & 0 \\ -304.05\gamma_1 & 0 & 0 & 0 & 0 & 1 \\ 0 & 0 & 0 & -304.05k_1 & 0 & 0 \\ 0 & a_{52} & 0 & 0 & -412.13k_2 & 0 \\ 0 & 0 & a_{63} & 0 & 0 & -1073.1k_3 \end{bmatrix} \tag{2- 76}$$

where,

$a_{52} = -4.748 - 412.13\gamma_2$; $a_{63} = 55.945 - 1073.1\gamma_3$;

$$B = \begin{bmatrix} 0 & 0 & 0 \\ 0 & 0 & 0 \\ 0 & 0 & 0 \\ 304.05 & 0 & 0 \\ 0 & 412.13 & 0 \\ 0 & 0 & 1073.1 \end{bmatrix} \tag{2- 77}$$

We also express the output equation as $Y = Cx$, where

$$C=\begin{bmatrix} C_1 & 0 & 0 & 0 & 0 & 0 \\ 0 & C_2 & 0 & 0 & 0 & 0 \\ 0 & 0 & C_3 & 0 & 0 & 0 \\ 0 & 0 & 0 & C_4 & 0 & 0 \\ 0 & 0 & 0 & 0 & C_5 & 0 \\ 0 & 0 & 0 & 0 & 0 & C_6 \end{bmatrix},\ C_i = 1\,(i = 1,2,3,4,5,6) \qquad (2\text{-}78)$$

According to (2-76), (2-77) and (2-78), we can write the linearized state space equations about an equilibrium point for the dynamics of the PHANToM Premium 1.5 as following:

$$\begin{cases} \dot{X} = AX + BU \\ Y = CX + DU \end{cases} \qquad (2\text{-}79)$$

where, U is the vector $\Gamma = \begin{pmatrix} \tau_1 & \tau_2 & \tau_3 \end{pmatrix}^T$, and $D = 0$.

2.3.6 Transfer Functions

From the dynamic equation (2-60) and the linearization results, we know this system has coupling affects. In order to simplify our design, we first omit these coupling affects and later we only consider single input and single output representation. Thus, based on the SISO method, we try to find transfer functions between angular displacements and input torques. The block diagram of a typical closed-loop system is shown in Figure 2-4.

In Figure 2-4, we are interested in finding the relationship between τ^{new} and θ. For linear systems, the mathematical expression for the transfer function is given by.

$$H = \frac{Y}{U} = CB(sI - A)^{-1} \qquad (2\text{-}80)$$

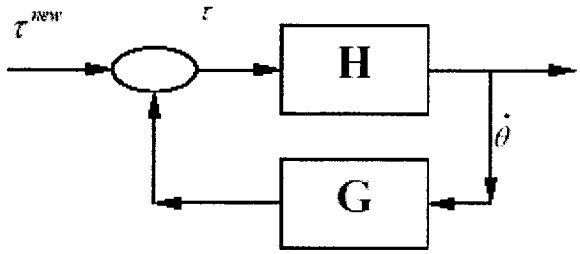

Figure 2-4 Closed-loop transfer function

We can employ (2-76), (2-77) and (2-78) into (2-80), so to get the relationship between the angular displacements and torques and between the angular velocity and the torques. The results are shown below:

For the angular displacement/torque expressions we have:

$$H_1 = \frac{\theta_1}{\tau_1^{new}} = \frac{30.745}{(0.10112s^2 + 30.745k_1 s + 30.745\gamma_1)} \tag{2-81}$$

$$H_2 = \frac{\theta_2}{\tau_2^{new}} = \frac{N_2}{D_2} \tag{2-82}$$

where,

$$N_2 = 25.806(8.0148s^2 + 8600k_3 s - 448.39 + 8600.6\gamma_3)$$

$$\begin{aligned} D_2 = {} & 0.50185s^4 + (206.83k_2 + 538.53k_3)s^3 \\ & + (0.22195\times 10^6 k_2 k_3 + 206.83\gamma_2 + 538.53\gamma_3 - 25.694)s^2 \\ & + (-0.11571\times 10^5 k_2 + 2557.0k_3 + 0.22195\times 10^6 (k_3\gamma_2 + k_2\gamma_3))s \\ & + (-0.1157\times 10^5 \gamma_2 + 2557.0\gamma_3 + 0.22195\times 10^6 \gamma_2\gamma_3 - 133.31) \end{aligned}$$

and $$H_3 = \frac{\theta_3}{\tau_3^{new}} = \frac{N_3}{D_3} \tag{2-83}$$

where,

$$N_3 = 537.539(1.00185s^2 + 412.896k_2 s + 412.896\gamma_2 + 4.75676)$$

$$\begin{aligned} D_3 = {} & 0.50185s^4 + (206.83k_2 + 538.53k_3)s^3 \\ & + (0.22195\times 10^6 k_2 k_3 + 206.83\gamma_2 + 538.53\gamma_3 - 25.694)s^2 \\ & + (-0.11571\times 10^5 k_2 + 2557.0k_3 + 0.22195\times 10^6 (k_3\gamma_2 + k_2\gamma_3))s \\ & + (-0.1157\times 10^5 \gamma_2 + 2557.0\gamma_3 + 0.22195\times 10^6 \gamma_2\gamma_3 - 133.31) \end{aligned}$$

We have now obtained the relationship between the torques and angular displacements. However, in our later design algorithms, we need the angular velocity/force control schemes. Thus we have to obtain the relationship between the torques and angular velocities. Since the relationship between $\theta(s)$ and $\dot{\theta}(s)$ is $\dot{\theta}(s) = s\theta(s)$, therefore, the required transfer functions may be easily obtained. We have:

For angle velocity/torque:

$$H_4 = \frac{\dot{\theta}_1}{\tau_1^{new}} = \frac{30.745s}{(0.10112s^2 + 30.745k_1 s + 30.745\gamma_1)} \tag{2- 84}$$

$$H_5 = \frac{\dot{\theta}_2}{\tau_2^{new}} = \frac{N_2 s}{D_2} \tag{2- 85}$$

where, N_2 and D_2 are exactly as in (2-82).

and $$H_6 = \frac{\dot{\theta}_3}{\tau_3^{new}} = \frac{N_3 s}{D_3} \tag{2- 86}$$

where, N_3 and D_3 are exactly as in (2-83).

For now, we have found the transfer functions of the angular displacements vs. torques and angular velocities vs. torques. However, this torque is produced by the manipulator motors, while we need force produced by the operators in our design. Similarly, we also hope to obtain velocity and position instead of angular velocity and angular displacements. In section 2.2.3, equation (2-17) gave us the relationship between velocity and angular velocity, and (2-1) showed the relationship between torques and forces. Because PHAMToM Premium 1.5 model doesn't have rotation about any axis, we set rotation and its velocity to zero. At the same time, we linearized the dynamic system about the equilibrium point, $\theta_1 = 0$, $\theta_2 = \frac{\pi}{4}$ and

$\theta_3 = \frac{\pi}{4}$. Substituting these into (2-7), (2-17) and (2-18), the end effectors rotation and transpose matrices are:

$$R(\theta) = \begin{bmatrix} 1 & 0 & 0 \\ 0 & 0.7071 & 0.7071 \\ 0 & -0.7071 & 0.7071 \end{bmatrix} \tag{2-87}$$

$$J^b(\theta) = \begin{bmatrix} 0.2722 & 0 & 0 \\ 0 & 0.2150 & 0 \\ 0 & 0 & 0.17 \\ 0 & 0 & -1 \\ 0.7071 & 0 & 0 \\ 0.7071 & 0 & 0 \end{bmatrix} \tag{2-88}$$

$$\begin{bmatrix} R & 0 \\ 0 & R \end{bmatrix} J^b = \begin{bmatrix} 0.2722 & 0 & 0 \\ 0 & 0.1520 & 0.1202 \\ 0 & -0.1520 & 0.1202 \\ 0 & 0 & -1 \\ 1 & 0 & 0 \\ 0 & 0 & 0 \end{bmatrix} \tag{2-89}$$

$$J^{bT} \begin{bmatrix} R^T & 0 \\ 0 & R^T \end{bmatrix} = \begin{bmatrix} 0.2722 & 0 & 0 & 0 & 1 & 0 \\ 0 & 0.1520 & -0.1520 & 0 & 0 & 0 \\ 0 & 0.1202 & 0.1202 & -1 & 0 & 0 \end{bmatrix} \tag{2-90}$$

We now can find the values for the parameters k_1, k_2, k_3, γ_1, γ_2, γ_3 to make the closed-loop system stable. To ensure stability, $k_1 = 1$, $k_2 = 1$, $k_3 = 1$, $\gamma_1 = 1$, $\gamma_2 = 1$ and $\gamma_3 = 1$ is one of the selected values. When these are substituted into (2-81) – (2-86), we get the closed-loop transfer function with a stable performance. The results are given below:

For angular displacements versus torques we have:

$$H_1 = \frac{304.04}{(s+303.04)(s+1.0033)} \tag{2-91}$$

$$H_2 = \frac{19.0512(s+1072)(s+0.9487)}{(s+1072)(s+411.2)(s+1.014)(s+0.9488)} \tag{2-92}$$

$$H_3 = \frac{31.0126(s+411.2)(s+1.014)}{(s+1072)(s+411.2)(s+1.014)(s+0.9488)} \tag{2-93}$$

For the angular velocities versus torques we have:

$$H_4 = \frac{304.04s}{(s+303.04)(s+1.0033)} \tag{2-94}$$

$$H_5 = \frac{19.0512(s+1072)(s+0.9487)s}{(s+1072)(s+411.2)(s+1.014)(s+0.9488)} \tag{2-95}$$

$$H_6 = \frac{31.0126(s+411.2)(s+1.014)s}{(s+1072)(s+411.2)(s+1.014)(s+0.9488)} \tag{2-96}$$

Finally, we may use the relationship between torque/force and angular velocity/velocity as shown in (2-17) and (2-18), and substitute (2-87) to (2—96) into (2-17) and (2-18), the relationships between the velocity in a given axis direction and the force along that axis and may be expressed as shown below:

For the x axis:

Position/Force:

$$H_x = \frac{X}{F_x} = \frac{22.53}{s^2+304s+304} \tag{2-97}$$

Velocity/Force:

$$H_{v_x} = \frac{V_x}{F_x} = \frac{22.53s}{s^2+304s+304} \tag{2-98}$$

For the y axis:

Position/Force:

$$H_y = \frac{Y}{F_y} = \frac{19.05s^2 + 2.044\times10^4 s + 1.938\times10^4}{s^4 + 1485s^3 + 443690s^2 + 866560s + 424040} \quad (2\text{-}99)$$

Velocity/Force:

$$H_{v_y} = \frac{V_y}{F_y} = \frac{(19.05s^2 + 2.044\times10^4 s + 1.938\times10^4)s}{s^4 + 1485s^3 + 443690s^2 + 866560s + 424040} \quad (2\text{-}100)$$

For the z axis:

Position/Force:

$$H_z = \frac{Z}{F_z} = \frac{31.01s^2 + 1.278\times10^4 s + 1.293\times10^4}{s^4 + 1485s^3 + 443690s^2 + 866560s + 424040} \quad (2\text{-}101)$$

Velocity/Force:

$$H_{v_z} = \frac{V_z}{F_z} = \frac{(31.01s^2 + 1.278\times10^4 s + 1.293\times10^4)s}{s^4 + 1485s^3 + 443690s^2 + 866560s + 424040} \quad (2\text{-}102)$$

By investigating (2-91) – (2-96), if follows that all the zeros and poles of the transfer functions are located in the left half plane. This proves that the closed-loop system is stable. Since the relationships between angular velocity/velocity and torques/forces are through constant matrices, the transfer functions, shown in (2-97) – (2-102), are stable as well.

2.4 Conclusion

In this chapter, the analysis of dynamic models of the PHANToM Premium 1.5 has been done. The linearized models, the state spaces, and the Jacobian matrixes for the mathematical models have been derived. We have also introduced state feedback compensation methods and applied them to the open-loop unstable models to ensure that closed-loop systems are made stable. Based on a single input and single output (SISO) design procedure, the closed-loop transfer functions of different axes for

position versus force and velocity versus force are obtained. The above results will be applied into the computation in the later chapters.

Chapter 3

Background Theoretical Results

3.1 Introduction

As descried in chapter 1, stability is one important control problem in haptic display. Because we couldn't predict all virtual scenes which the virtual haptic displays touch, it is inevitable for us to decouple the relationship between haptic device control problem and virtual environments. One solution for this problem is the introduction of an artificial coupling between the haptic display and the virtual environment. Although Colgate et. al. [45], Zilles and Salisbury[90], and Ruspini et. al. [91] named this after their own designs for stability of haptic display, we still may group their designs into (a) the implementation of a virtual coupling network, and (b) a two-port interface between the haptic display and the virtual environment. In Adams and Hannaford's [16] work, they extended the concept of a virtual coupling to admittance display and attempts to treat the problem of stable haptic interaction in a more general framework that encompasses any causal combination of haptic displays and virtual environments. In this chapter, we will introduce Adams and Hannaford's method, and then try to employ this method to our multi-user haptic display. Furthermore, we derive the stability criterion and passivity for the multi-user hpatic display.

3.2 Two-Port Characterizations

Two-port models are rooted in linear circuit theory. A typical generalized two-port network is indicated in Figure 3-1. Actually, two-port models characterize the effects of different loading conditions on two terminal electrical networks. We can consider a mechanical analog to this electrical two-port, the haptic interface, which is subject to variable loading conditions both at the point of interaction with the human operator and at the point of interaction with the virtual environment [92]. In using mechanical analog, we substitute velocities for currents in representing flows and forces for voltages in representing efforts. The two-port haptic interface model characterizes the exchange of energy between the human operator and the virtual environment. Figure 3-2 shows the network model of the haptic simulation.

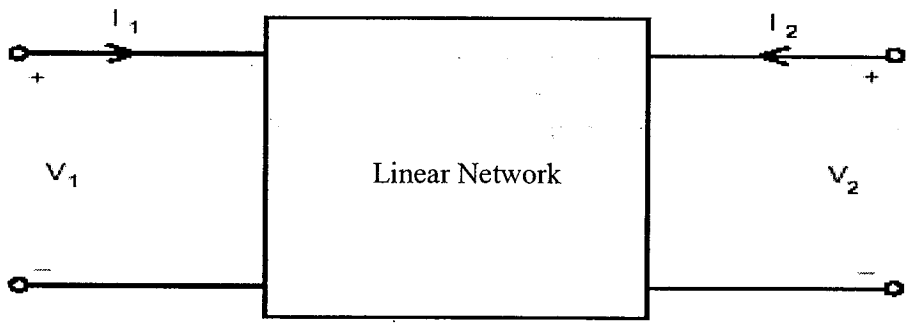

Figure 3-1 General linear network

In Figure 3-2, the force F_h and F_e^* represent efforts and v_h and $-v_e^*$ represent flows. In order to maintain consistency with the network formalism, there exists negative sign on velocity, seen here and throughout this thesis.

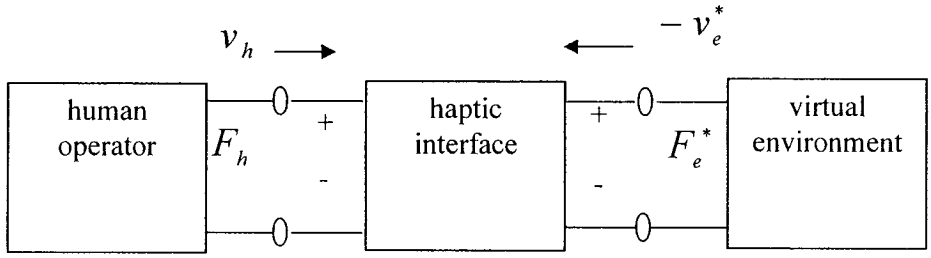

Figure 3-2 Network model of haptic simulation

In a two-port network, we use the terminology immittance matrix which describes the relationship between efforts and flows. Using two vectors, the immittance mapping can be expressed as:

$$y = Pu \tag{3-1}$$

where y and u must satisfy $y^T u = F_h v_h + F_e^*(-v_e^*)$. The matrix P is then considered as an immittance matrix.

There are four kinds of immittance matrix often used, which are the impedance matrix Z, the admittance matrix Y, the hybrid matrix H, and the alternate hybrid matrix G. At the same time, the immittance matrix and its subcomponents are frequency dependent functions, as equation (3-2) – (3-5) show their relationships:

$$\begin{bmatrix} F_h \\ F_e^* \end{bmatrix} = \begin{bmatrix} z_{11} & z_{12} \\ z_{21} & z_{22} \end{bmatrix} \begin{bmatrix} v_h \\ -v_e^* \end{bmatrix} \tag{3-2}$$

$$\begin{bmatrix} v_h \\ -v_e^* \end{bmatrix} = \begin{bmatrix} y_{11} & y_{12} \\ y_{21} & y_{22} \end{bmatrix} \begin{bmatrix} F_h \\ F_e^* \end{bmatrix} \tag{3-3}$$

$$\begin{bmatrix} F_h \\ -v_e^* \end{bmatrix} = \begin{bmatrix} h_{11} & h_{12} \\ h_{21} & h_{22} \end{bmatrix} \begin{bmatrix} v_h \\ F_e^* \end{bmatrix} \tag{3-4}$$

$$\begin{bmatrix} v_h \\ F_e^* \end{bmatrix} = \begin{bmatrix} g_{11} & g_{12} \\ g_{21} & g_{22} \end{bmatrix} \begin{bmatrix} F_h \\ -v_e^* \end{bmatrix} \tag{3-5}$$

In two-port networks, there is a special relationship between two networks. In [93], the definition of the network duality is: Two networks Ω_a and Ω_b are said to be dual if for every admissible signal pair $[F_a, v_a] \in \Omega_a$, there exists an admissible signal pair $[F_b, v_b] \in \Omega_b$, such that $F_a = v_b$ and $F_b = v_a$. Likewise, for every admissible signal pair $[F_b, v_b] \in \Omega_b$, there exists an admissible signal pair $[F_a, v_a] \in \Omega_a$, such that $F_b = v_a$ and $F_a = v_b$. This relationship could yield us have a better understanding of the dual form instead of the original form. In the analysis and design of haptic interfaces, we may make use of this concept to simplify our efforts.

3.3 Passivity and Stability

The two-port network may be looked at as the exchange of energy between two terminal loadings. Likewise, when we employ the two-port network into haptic interface, we also look at the relationship between human operators and virtual environments as the exchange of energy between the force and velocity of human operators and the force and velocity of virtual environments. This relationship may show the stability of haptic display. In Figure 3-2, the pair (F_h, v_h) represents the force and velocity of a human operator, and the pair $(F_e^*, -v_e^*)$ represents the force and velocity of the virtual environment. The star superscript indicates that a variable is in discrete-time domain, it is otherwise assumed to be in the continuous-time domain.

The stability of a two-port network depends on its terminal immittance. The immittance characteristics of the human operator can be represented either as impedance Z_h, or admittance Y_h. The immittance properties of the virtual environment can be represented either as impedance Z_e or admittance Y_e.

In the work of Adam and Hannaford [16], a definition of stability is given for a linear two-port network that states that a continuous-time (discrete-time) linear two-port network with given terminal immittances is stable if and only if the corresponding characteristic equation has no roots in the right half s-plane (outside the unit circle, z-plane) and only simple roots on the imaginary axis (unit circle).

In the notation of Pian [94], p_1 and p_2 represent input power and output power, respectively, and $p_1 - p_2 = p_{in}$ is the net power into the network. Then a linear network is passive if the net power into it is nonnegative and active if the power is negative. Adam and Hannaford [16] define:

A two-port network is passive if and only if the immittance mapping $y = Pu$ satisfies

$$\int_0^t y^T(\tau)u(\tau)d\tau \geq 0, \ \forall t \geq 0 \tag{3-6}$$

for all admissible efforts and flows. For a linear network, this is equivalent to requiring that P be positive real.

The definition of positive real matrix is that (a) the continuous-time (discrete-time) linear immittance maxtrix P has no poles in the right half s-plane (outside the unit circle, z-plane), (b) only simple poles on the imaginary axis (unit circle), and (c)

$$P(j\omega) + P^T(-j\omega) \geq 0, \ \forall \omega \geq 0 \tag{3-7}$$

Equation (3-7) also can be refined into another expression such that:

$$\mathrm{Re}(p_{11}) \geq 0 \tag{3-8}$$

$$\mathrm{Re}(p_{22}) \geq 0 \tag{3-9}$$

$$\mathrm{Re}(p_{11})\mathrm{Re}(p_{22}) - \left|\frac{p_{12} + p_{21}^*}{2}\right|^2 \geq 0, \ \forall \omega \geq 0 \tag{3-10}$$

Knowing the definitions of passivity, activity and stability in a two-port network, we may testify passivity and stability for passive loads at the terminal point of a two-port network easily. However, if we would change this passive load into another new one, what would happen to this two-port network? Of course, we can re-examine the stability situation with every new load, but it would be better for us to know in advance its behaviours under any passive load. In general, the relationship between passivity and stability is very worthy for the design of haptic interfaces. As we have known, it is very hard for us to generate all the virtual environments for our haptic interface, furthermore, when haptic interface touches a new virtual environment, it is acceptable not to have a good performance; nevertheless, it should be avoided to make system unstable because this situation would be dangerous to the operators or the haptic interface equipments. As a result, a less conservative way of posing the stability problem for the haptic interface is in terms of "unconditional stability" [95].

A linear two-port network is unconditionally stable if and only if there exists no set of passive terminating one-port for which the system is unstable. But we have to notice that a passive network will always be unconditionally stable, but an unconditionally stable network is not necessary passive. That means the passivity can guarantee stability, while stability couldn't promise passivity in any time. Adma and Hannaford [16] introduces another term "potential instability", which is that a two-port network is potentially unstable if it is not unconditionally stable. Llewellyn's stability criteria provide both necessary and sufficient conditions for unconditional stability [95]

$$\mathrm{Re}(p_{11}) \geq 0 \tag{3-11}$$

$$\mathrm{Re}(p_{22}) \geq 0 \tag{3-12}$$

$$2\,\mathrm{Re}(p_{11})\,\mathrm{Re}(p_{22}) \geq \left|p_{12}p_{21}\right| + \mathrm{Re}(p_{12}p_{21}),\ \forall \omega \geq 0 \qquad (3\text{-}13)$$

Llewellyn's criteria may be equivalently applied to any of the four possible immittance forms (3-2) - (3-5). The satisfaction of (3-11) – (3-13) for one immittance form is necessary and sufficient for the satisfaction of (3-11) – (3-13) for the other three. In the special case of a network for which $h_{21} = -h_{12}$ (or equivalently $z_{12} = z_{21}$), the tests for passivity, (3-8) – (3-10), and for unconditional stability, (3-11) – (3-13), are identical. In this case, a network is said to be reciprocal [96].

The merit of unconditional stability in the design of haptic interface is that human operator doesn't need to worry about the unknown virtual environment which he/she is touching because unconditional stability remains haptic interface completely stable toward any set of passive virtual environments. In the real case, human operator and virtual environment can be nonlinear and time varying, but we can promise stability as long as they are passive because the two-port network is passive as well. Further, two-port structure is a simple case. Generally, most of real cases belong to 2n-ports structure. Even if two-port unconditional stability is extended to the more general concept of 2n-ports "coupled stability" [97], [98], unlike the two-port case, coupled stability criterion for 2n-ports are sufficient, but not necessary. A 2n-port immittance matrix may be tested for coupled stability directly using a Popov-multiplier formulation [99], or by transforming it into scattering form through a bilinear transformation and then applying structured singular value analysis [100], [98].

3.4 Multi-user Haptic Interface

Before we employ two-port network into the design of multi-user haptic interface, we first discuss a single-user haptic interface. In Adma and Hannaford's

work [16], they generalize and extend the concept of virtual coupling network, an artificial link between the haptic display and a virtual world. Their contribution is that they decouple the haptic display control problem from the design of virtual environments.

Their model is shown in Figure 3-3. In conventional designs, such as [45], [90], and [91], virtual coupling, which is also called virtual stiffness, is looked at with virtual environment together. As a result, haptic interface only includes haptic device. This design causes the stability of haptic interface not to be kept by any set of virtual environment because the lower right block in two-port form is zero, thus, the unconditional stability criterion (3-13) becomes $0 \geq |p_{12}p_{21}| + \mathrm{Re}(p_{12}p_{21})$. Apparently, this relationship could not be satisfied for any frequency, which means unconditional stability could not be satisfied. In the proposed design by Adma and Hannafold [16] they combine haptic device and virtual coupling together, and look at them as haptic interface. The remaining structure is not changed any more compared to the conventional design. This change only makes the lower right block in two-port form to be the virtual coupling term, but not zero. The left side of the unconditional stability criterion (3-13) is not a zero any longer; therefore, the criterion for unconditional stability can be easier to satisfy.

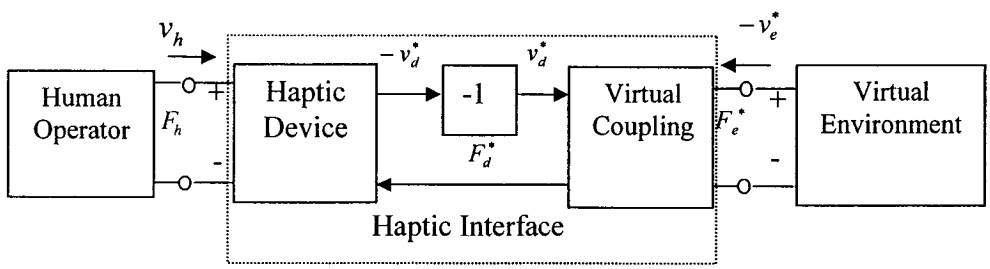

Figure 3-3 Haptic interface for the impedance display case includes both the haptic display and a virtual coupling network

In our multi-user haptic display, we extend this procedure for design. We consider both the haptic device and the virtual coupling together.

As described in chapter 1, time delay is a critical control problem in teleoperation. Similarly, networked haptic display in the shared virtual environment has the above problem as well. In order to solve this control problem, some solutions have been described in chapter 1 already. In this chapter, we hope to use passivity criterion to check the system with time delay stability or not. Our strategy is that the control procedure of the local user not only includes the information of local user, but also has the information of remote user. In this chapter, unit time delay has been used firstly. Further, we use the force/velocity to match the effort/flow in a two-port form. The resulting architecture is shown in Figure 3-4.

Clearly, the haptic devices 1 and 2 are expressed in the continuous-time domain, while the virtual couplings 1 and 2 are expressed in the discrete-time domain. Thus, the complete system is a hybrid system.

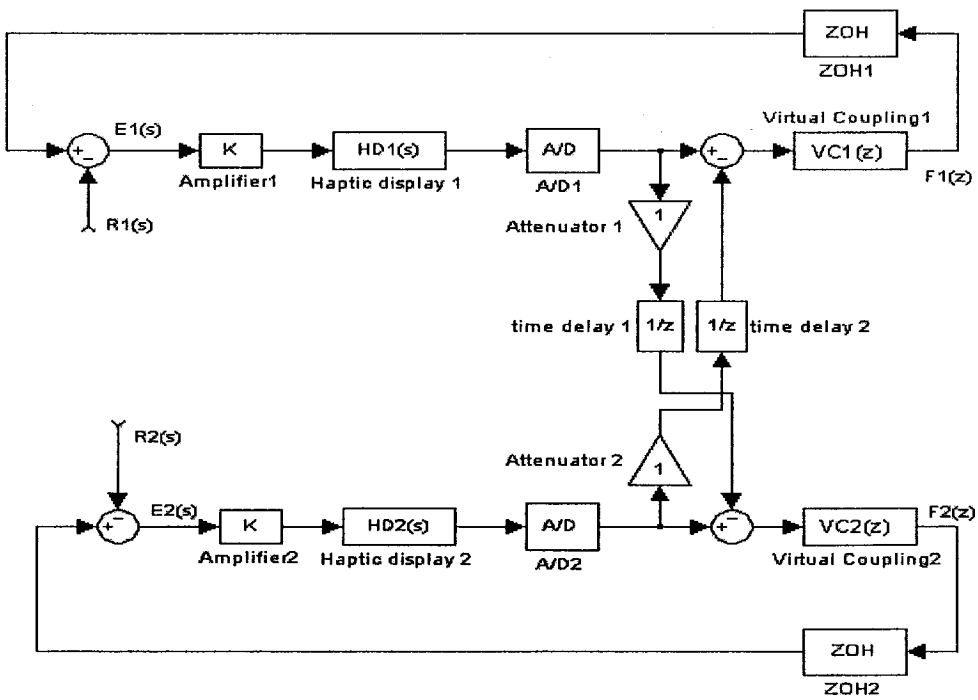

Figure 3-4 Networked haptic feedback system

The signal flow diagram of the networked haptic system is shown in Figure 3-5. The input-output relationship is derived and shown as an immitance matrix given by

$$\begin{bmatrix} V_{h1} \\ V_{h2} \end{bmatrix} = \begin{bmatrix} HD_1 & -z^{-1}(HD_2)(VE_1)(ZOH)(HD_1) \\ -z^{-1}(HD_1)(VE_2)(ZOH)(HD_2) & HD_2 \end{bmatrix} \times \begin{bmatrix} F_{e1} \\ F_{e2} \end{bmatrix} \quad (3\text{-}14)$$

The immitance matrix is of the form $Y = GI$, where Y is the output vector, G is the admittance matrix and I is the input vector and

$G = \begin{bmatrix} g_{11} & g_{12} \\ g_{21} & g_{22} \end{bmatrix}$, where g_{ij}'s are frequency dependent terms and are defined according to (3-14).

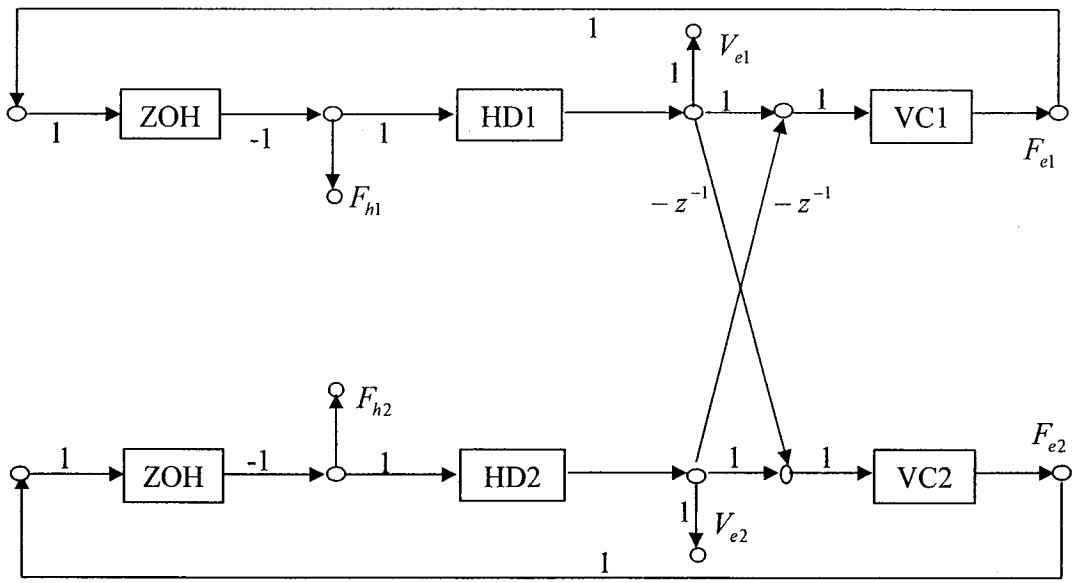

Figure 3-5 Signal flow graph of a networked haptic display

3.5 Benchmark Example

In the previous sections, we have introduced the complete theoretical design procedure for a multi-user haptic interface based on a two-port network and passivity

and stability. Now, we attempt to use a benchmark example to prove our design prcedure.

3.5.1 Haptic Devices

First, we suppose that haptic device is a first order system with a negative pole. It can be expressed in the z -domain using backward rectangular approximation technique as follows.

$$HD_1(s) = \frac{K}{m_1 s + b_1}\bigg|_{s \to \frac{z-1}{Tz}} \Rightarrow HD_1(z) = \frac{TKz}{(m_1 + b_1 T)z - m_1} \quad (3\text{-}15)$$

The relationship between the variable z and the frequency ω is $z = e^{j\omega} = \cos\omega + j\sin\omega$. Thus we also express equivalently

$$HD_1(\omega) = \frac{KTe^{j\omega}}{(m_1 + b_1 T)e^{j\omega} - m_1} \quad (3\text{-}16)$$

Through simple computations, we know that the real part and imaginary part of the haptic device 1 is as following:

$$\mathrm{Re}(HD_1) = \frac{T\,K\,(m_1\cos(\omega) - m_1 - b_1 T)}{(2\,m_1^2\cos(\omega) + 2\,m_1 b_1 T\cos(\omega) - 2m_1^2 - 2m_1 b_1 T - b_1^2 T^2)} \quad (3\text{-}17)$$

$$\mathrm{Im}(HD_1) = \frac{TKm_1\sin(\omega)}{(2\,m_1^2\cos(\omega) + 2\,m_1 b_1 T\cos(\omega) - 2m_1^2 - 2m_1 b_1 T - b_1^2 T^2)} \quad (3\text{-}18)$$

Similarly, we suppose that the haptic device 2 is a first order system with one negative pole. The haptic device system 2 can also be expressed as

$$HD_2(s) = \frac{K}{m_2 s + b_2}\bigg|_{s \to \frac{z-1}{Tz}} \Rightarrow HD_2(z) = \frac{TKz}{(m_2 + b_2 T)z - m_2} \quad (3\text{-}19)$$

$$HD_2(\omega) = \frac{KTe^{j\omega}}{(m_2 + b_2 T)e^{j\omega} - m_2} \quad (3\text{-}20)$$

The real and imaginary part of haptic device 2 are shown below:

$$\mathrm{Re}(HD_2) = \frac{T\,K\,(m_2\cos(\omega) - m_2 - b_2T)}{(2\,m_2^2\cos(\omega) + 2\,m_2b_2T\cos(\omega) - 2m_2^2 - 2m_2b_2T - b_2^2T^2)} \quad (3\text{-}21)$$

$$\mathrm{Im}(HD_2) = \frac{TKm_2\sin(\omega)}{(2\,m_2^2\cos(\omega) + 2\,m_2b_2T\cos(\omega) - 2m_2^2 - 2m_2b_2T - b_2^2T^2)} \quad (3\text{-}22)$$

3.5.2 Zero Order Hold

Our feedback is generated by a discrete-time system and the signal is digital. Zero order hold (ZOH) has to be used to transform the discrete-time system into the continuous-time domain. To maintain simplicity in the analysis, we assume that any aliasing effects due to the sampling are negligible, due to either the low-pass filter effects of the device dynamics or the introduction of an appropriate anti-aliasing filter before sampling. The zero-order hold can then be approximated as a low-pass filter with a steady state gain of T and 90° phase lag at the Nyquist frequency. The sampler can be approximated as a static gain of 1/T. With no loss of generality we can combine the sampler gain with the zero-order hold to get the normalized zero-order hold function

$$ZOH(z) = \frac{1}{2}\frac{(z+1)}{z} \Rightarrow ZOH(\omega) = \frac{1}{2}\frac{(e^{j\omega}+1)}{e^{j\omega}} \quad (3\text{-}23)$$

$$\mathrm{Re}(ZOH) = \frac{1}{2}(1+\cos(\omega)) \quad (3\text{-}24)$$

$$\mathrm{Im}(ZOH) = -\frac{1}{2}\sin(\omega) \quad (3\text{-}25)$$

3.5.3 Virtual Coupling

Discretization of the virtual coupling impedance is performed using a first difference approximation

$$VC_1(s) = be_1 + \left.\frac{Ke_1}{s}\right|_{s\to\frac{z-1}{Tz}} \Rightarrow VC_1(\omega) = be_1 + \frac{Ke_1 Te^{j\omega}}{e^{j\omega}-1} \quad (3\text{-}26)$$

$$\mathrm{Re}(VC_1) = be_1 + \frac{1}{2}Ke_1 T \quad (3\text{-}27)$$

$$\mathrm{Im}(VC_1) = \frac{1}{2}Ke_1 T\frac{\sin(\omega)}{1-\cos(\omega)} \quad (3\text{-}28)$$

Similarly the virtual coupling 2 can also be expressed as following:

$$VC_2(\omega) = be_2 + \frac{Ke_2 Te^{j\omega}}{e^{j\omega}-1} \quad (3\text{-}29)$$

$$\mathrm{Re}(VC_2) = be_2 + \frac{1}{2}Ke_2 T \quad (3\text{-}30)$$

$$\mathrm{Im}(VC_2) = \frac{1}{2}Ke_2 T\frac{\sin(\omega)}{1-\cos(\omega)} \quad (3\text{-}31)$$

3.5.4 Time Delay

The delay is expressed as

$$DELAY(z) = z^n \Rightarrow DELAY(\omega) = e^{jn\omega}\ (n \le 0) \quad (3\text{-}32)$$

We first consider the case with a unit time delay, so we suppose $n = -1$ throughout this chapter, namely we have:

$$\mathrm{Re}(DELAY) = \cos(\omega) \quad (3\text{-}33)$$

$$\mathrm{Im}(DELAY) = -\sin(\omega) \quad (3\text{-}34)$$

3.5.5 Passivity Criterion (3-8) and (3-9)

According to the passivity criterion, (3-17) is the first passivity criterion, and (3-21) is the second one. Let's simplify (3-17) and (3-21) according to:

$$\mathrm{Re}(HD_1) = \frac{TK(m_1 + b_1 T - m_1\cos\omega)}{(1-\cos\omega)(2m_1^2 + 2m_1 b_1 T + b_1^2 T^2)} \quad (3\text{-}35)$$

$$\mathrm{Re}(HD_2)=\frac{TK(m_2+b_2T-m_2\cos\omega)}{(1-\cos\omega)(2m_2^2+2m_2b_2T+b_2^2T^2)} \tag{3-36}$$

Through investigating (3-35) and (3-36), if they satisfy inequality $m_1+b_1T\geq m_1\cos(\omega)$ and $m_2+b_2T\geq m_2\cos(\omega)$, they lead to one of the design criteria for passivity of the system to be satisfied.

3.5.6 Passivity Criterion (3-10)

For (3-13), at first, we simplify this equation. The term g_{12} and g_{21} can be expressed as $g_{12}=\mathrm{Re}(g_{12})+j\,\mathrm{Im}(g_{12})$ and $g_{21}=\mathrm{Re}(g_{21})+j\,\mathrm{Im}(g_{21})$, then we substitute them into (3-13), to get

$$\mathrm{Re}(g_{11})\,\mathrm{Re}(g_{22})-\frac{1}{4}\left\{[\mathrm{Re}(g_{21})+\mathrm{Re}(g_{12})]^2+[\mathrm{Im}(g_{21})-\mathrm{Im}(g_{12})]^2\right\}\geq 0 \tag{3-37}$$

$$\mathrm{Re}(g_{12})=-\frac{1}{2}\frac{(1+\cos\omega)(a_{11}\cos\omega-a_{12})T^2K^2}{(d_{11}\cos\omega-d_{12})(d_{21}\cos\omega-d_{22})} \tag{3-38}$$

$$\mathrm{Re}(g_{21})=-\frac{1}{2}\frac{(1+\cos\omega)(a_{21}\cos\omega-a_{22})T^2K^2}{(d_{11}\cos\omega-d_{12})(d_{21}\cos\omega-d_{22})} \tag{3-39}$$

$$\mathrm{Im}(g_{12})=\frac{1}{2}\frac{T^2K^2(a_{11}\cos^2\omega-a_{13}\cos\omega+a_{14})\sin\omega}{(d_{11}\cos\omega-d_{12})(d_{21}\cos\omega-d_{22})(\cos\omega-1)} \tag{3-40}$$

$$\mathrm{Im}(g_{21})=\frac{1}{2}\frac{T^2K^2(a_{21}\cos^2\omega-a_{23}\cos\omega+a_{24}\sin\omega}{(d_{11}\cos\omega-d_{12})(d_{21}\cos\omega-d_{22})(\cos\omega-1)} \tag{3-41}$$

where the terms a_{11} , a_{12} , a_{13} , a_{14} , a_{21} , a_{22} , a_{23} , a_{24} , d_{11} , d_{12} , d_{21} and d_{22} are expressed as following:

$$\begin{cases}a_{11}=2b_{e1}b_1b_2T^2+2b_{e1}(b_2m_1+b_1m_2)T+2b_{e1}m_1m_2\\ a_{12}=K_{e1}b_1b_2T^3+(b_{e1}b_1b_2+K_{e1}b_1m_2+K_{e1}b_2m_1)T^2+2b_{e1}(b_2m_1+b_1m_2)T+2b_{e1}m_1m_2\end{cases}$$

$$\begin{cases} a_{21} = 2b_{e2}b_1b_2T^2 + 2b_{e2}(b_1m_2 + b_2m_1)T + 2b_{e2}m_1m_2 \\ a_{22} = K_{e2}b_1b_2T^3 + (b_{e2}b_1b_2 + K_{e2}b_1m_2 + K_{e2}b_2m_1) + 2b_{e2}(b_1m_2 + b_2m_1)T + 2b_{e2}m_1m_2 \end{cases}$$

$$\begin{cases} a_{13} = K_{e1}b_1b_2T^3 + (K_{e1}b_1m_2 + K_{e1}b_2m_1 + b_{e1}b_1b_2)T^2 \\ \quad + 2(K_{e1}m_1m_2 + b_{e1}b_1m_2 + b_{e1}b_2m_1)T + 4b_{e1}m_1m_2 \\ a_{14} = (K_{e1}b_1m_2 + K_{e1}b_2m_1 - b_{e1}b_1b_2)T^2 + 2K_{e1}m_1m_2T + 2b_{e1}m_1m_2 \end{cases}$$

$$\begin{cases} a_{23} = K_{e2}b_1b_2T^3 + T^2(K_{e2}b_1m_2 + K_{e2}b_2m_1 + b_{e2}b_1b_2)T^2 \\ \quad + 2Tb_1b_{e2}m_2 + 2m_1(K_{e2}m_2 + b_2b_{e2})T + 4b_{e2}m_1m_2 \\ a_{24} = (K_{e2}b_1m_2 + K_{e2}b_2m_1 - b_{e2}b_1b_2)T^2 + 2TK_{e2}m_1m_2 + 2b_{e2}m_1m_2 \end{cases}$$

$$\begin{cases} d_{11} = 2b_1m_1T + 2m_1^2 \\ d_{12} = b_1^2T^2 + 2b_1m_1T + 2m_1^2 \end{cases}$$

$$\begin{cases} d_{21} = 2m_2b_2T + 2m_2^2 \\ d_{22} = b_2^2T^2 + 2b_2m_2T + 2m_2^2 \end{cases}$$

Up to now, we have derived the passivity criterion with one order haptic device. Investigating (3-37) – (3-41), we found passivity criterion is the functions with frequency ω and the parameters of virtual coupling. Since sine and cosine are the period function with period 2π, the whole systems would be stable if all of passivity criterions are satisfied over the period 2π. Secondly, we also testify which virtual coupling parameters K_e and b_e can make systems passive and stable with some time delay n in all frequency of one period. In our benchmark example, time delay n is set to be –1.

In passivity criterions, another one parameter is sampling period T. A sampling period of T = 0.01 s will be used throughout this paper.

3.6 Passivity for the PHANToM Premium 1.5

Up to now, we have proved the feasibility of passivity criteria to design the parameters of virtual coupling with time delay in the networked haptic display

through the benchmark example as shown in the previous section. In this section, we are going to employ this method to the PHANToM Premium 1.5 device. The structure is shown in Figure 3-4; however, there are some changes as following:

(1) We use the transfer functions of the PHANToM Premium 1.5 instead of a first order system. In chapter 2, we have obtained the stable transfer functions for velocity/force along each axis (x, y and z) as given in (2-98), (2-100) and (2-102). Furthermore it is easy for us to map the above transfer functions from the s-domain into z-domain and write them a function expressed in the frequency ω. The procedure has been shown in the last section 3.5. Therefore, in this section $HD_1(s)$ and $HD_2(s)$ will be expressed by the derived transfer function of the PHANToM Premium 1.5 along each axis.

(2) We assume there are two PHANToM Premium 1.5 devices in our networked haptic display. Because the two devices are the same, they have the same parameters, and we set the same virtual spring $K_{e1} = K_{e2} = K_e$ and virtual damping $b_{e1} = b_{e2} = b_e$ for the virtual coupling as well in order to simplify the computation. This changes lead (3-26), (3-27) and (3-28) to be equal to (3-29), (3-30) and (3-31).

$$VC_1(s) = VC_2(s) = b_e + \frac{K_e}{s}\bigg|_{s\to\frac{z-1}{Tz}} \Rightarrow VC_1(\omega) = VC_2(\omega) = b_e + \frac{K_e T e^{j\omega}}{e^{j\omega}-1} \qquad (3\text{-}42)$$

$$\mathrm{Re}(VC_1) = \mathrm{Re}(VC_2) = b_e + \frac{1}{2}K_e T \qquad (3\text{-}43)$$

$$\mathrm{Im}(VC_1) = \mathrm{Im}(VC_2) = \frac{1}{2}K_e T\frac{\sin\omega}{1-\cos\omega} \qquad (3\text{-}44)$$

(3) In our computation, we set the frequency range from 0 to 2π, the step is 0.1π.

(4) We may use (3-14) as our immitance matrix. Through $HD_1(s)$ and $HD_2(s)$ employed for the PHANToM Premium 1.5 Model, ZOH (3-23), (3-24) and (3-25), virtual coupling 1 and 2 (3-42), (3-43) and (3-44), and time delay (3-32), (3-33) and (3-34), we compute a set of the parameters for the virtual coupling (K_e, b_e) to satisfy the passivity criterions (3-8), (3-9) and (3-37). The detail results are listed below.

For x axis:

(a) Passivity criterion (3-8) and (3-9)

The expressions of haptic devices $HD_1(s)$ and $HD_2(s)$ are replaced by the expression as shown in (2-98).

Table 3-1 Minimum/Maximum $\mathrm{Re}(g_{11})$ **and** $\mathrm{Re}(g_{22})$ **along x axis**

	$\mathrm{Re}(g_{11})$	$\mathrm{Re}(g_{22})$
Minimum/Maximum values over frequency $[0, 2\pi]$	0 / 0.0722	0 / 0.0722

(b) Passivity criterion (3-37)

Through computations, we evaluate $K_e \leq 1400$ and $b_e \leq 25$ to satisfy (3-37) for the frequency over $[0, 2\pi]$. Thus we set $K_e \in [0, 1400]$ with a step 1 and $b_e \in [0, 25]$ with a step 0.1. The results are shown in Figure 3-6.

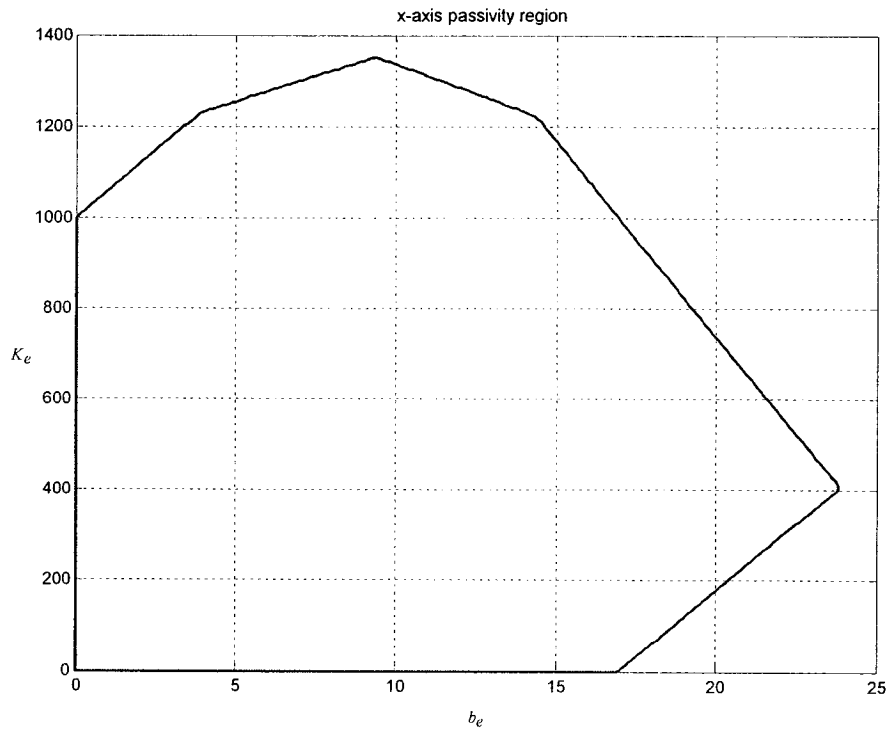

Figure 3-6 Passivity for the x-axis

For y axis:

(a) Passivity criterion (3-8) and (3-9)

The expressions of haptic devices $HD_1(s)$ and $HD_2(s)$ are replaced by the expression as shown in (2-100).

Table 3-2 Minimum/Maximum $\mathrm{Re}(g_{11})$ and $\mathrm{Re}(g_{22})$ along y axis

	$\mathrm{Re}(g_{11})$	$\mathrm{Re}(g_{22})$
Minimum/Maximum values over frequency $[0, 2\pi]$	0 / 0.0454	0 / 0.0454

(b) Passivity criterion (3-37)

Through computations, we evaluate $K_e \leq 2400$ and $b_e \leq 38$ to satisfy (3-37) for the frequency over $[0, 2\pi]$. Thus we set $K_e \in [0, 2400]$ with a step 1 and $be \in [0, 38]$ with a step 0.1. The results are shown in Figure 3-7.

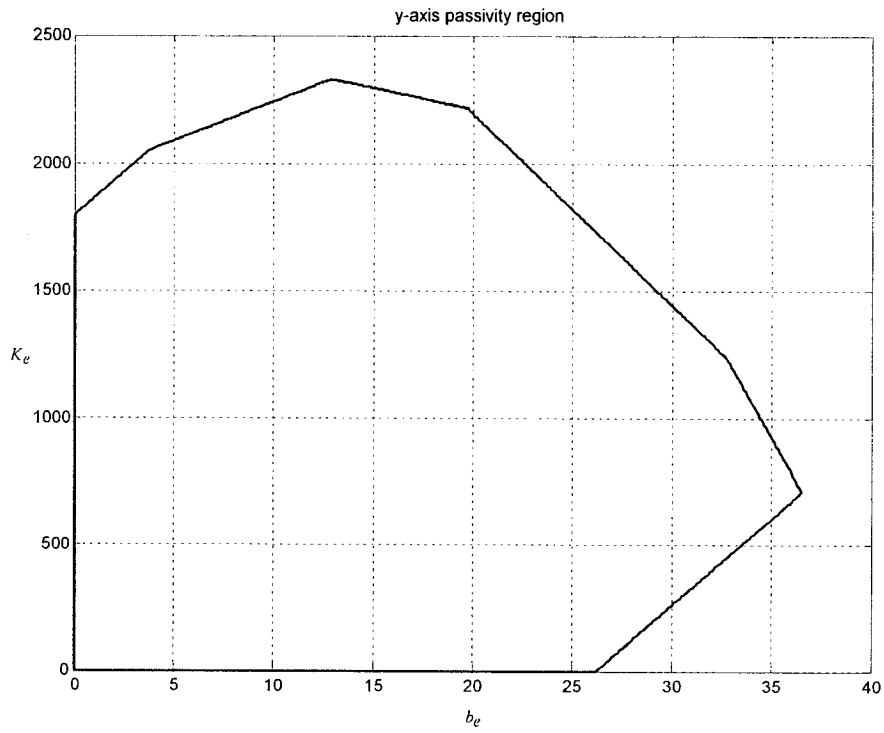

Figure 3-7 Passivity for the y-axis

For z axis:

(a) Passivity criterion (3-8) and (3-9)

The expressions of haptic devices $HD_1(s)$ and $HD_2(s)$ are replaced by the expression as shown in (2-102).

Table 3-3 Minimum/Maximum $\mathrm{Re}(g_{11})$ and $\mathrm{Re}(g_{22})$ along z axis

	$HD_1(s)$	$HD_2(s)$
Minimum/Maximum values over frequency $[0, 2\pi]$	0 / 0.0286	0 / 0.0286

(b) Passivity criterion (3-37)

Through computation, we evaluate $K_e \leq 4300$ and $b_e \leq 56$ to satisfy (3-37) for the frequency over $[0, 2\pi]$. Thus we set $K_e \in [0, 4300]$ with a step 1 and $b_e \in [0, 56]$ with a step 0.1. The results are shown in Figure 3-8.

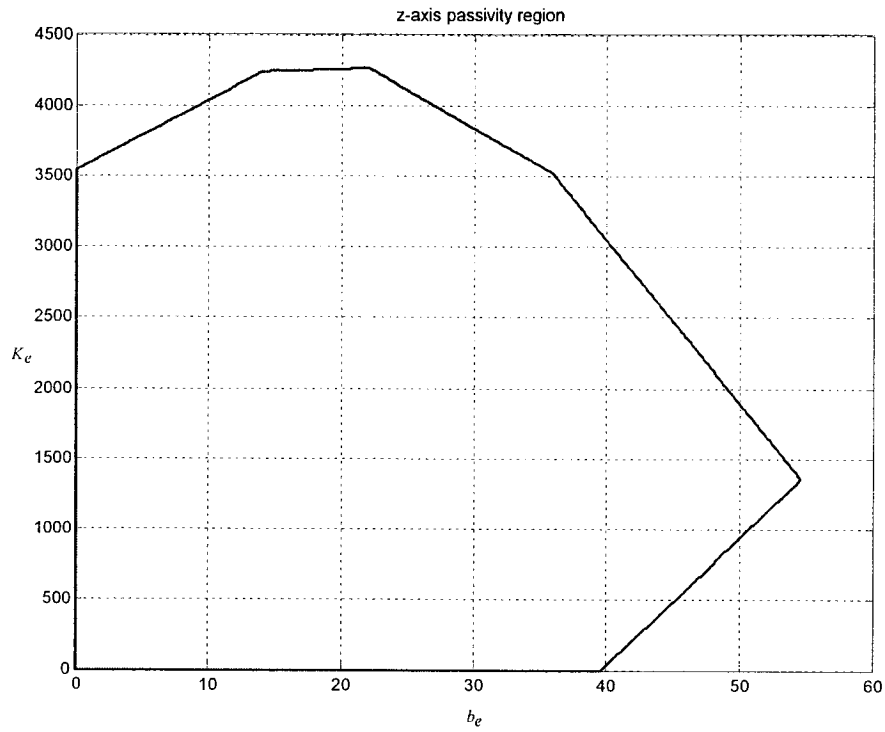

Figure 3-8 Passivity for the z-axis

3.7 Conclusion

Passivity criterion has been employed into the networked haptic display system with PHANToM Premium 1.5 model to satisfy stability. Parameters (K_e, b_e) of the virtual coupling have been computed for three different axes. As described in Adams and Hannaford [16], the introduction of a virtual coupling network between the mechanical device and the virtual environment guarantee the stability of the combined haptic interface for arbitrary passive human operator and environmental impedances. As a result, an unconditionally stable haptic interface will stably interact with any passive virtual environment. Our design procedure is based on a single input and single output (SISO) system without considering the coupling problem among the different axes, and furthermore, since we had built the set of linearized mathematical

models based on dynamic equations of PHANToM Premium 1.5. The equations are linearized at an equilibrium point $(\theta_1,\theta_2,\theta_3) = (0,\frac{\pi}{4},\frac{\pi}{4})$, and the parameters (K_e,b_e) for the virtual coupling are only matched at the neighborhood area of an equilibrium point.

Chapter 4

Stability of A Multi-User Haptic Interface

4.1 Introduction

In chapter 2, we described the model of the PHANToM Premium 1.5. In chapter 3, we discussed the theory of passivity and stability of a two-port network. Furthermore, we proved the feasibility of unconditional stability criterion for the networked haptic interface design through a benchmark example. We also employed the model of the PHANToM Premium 1.5 to our networked haptic interface, and designed a set of (K_e, b_e) for virtual coupling parameters to satisfy the unconditional stability criterions (3-11), (3-12) and (3-37). In the last chapter, our networked haptic display was not concerned with virtual environment only if the virtual environment was passive. Here we will use this model to touch certain virtual environment, and then we will obtain the best value (K_e, b_e) from the result of chapter 2 for different specific virtual environments through the accurate computation and steady state response of the system.

4.2 The Model of Virtual Haptic System with Virtual Environment

In chapter 1, we also reviewed the different current models of virtual environment. In this chapter, we are going to model the virtual environment through a virtual spring, as shown in Figure 4-1. Actually, our objects could be modeled by simplification into this simple mechanical model. We notice the forces F_1 and F_2

acted at each side of the spring. The positive direction is shown in Figure 4-1. As a result, the forces F_1 and F_2 are:

$$F_1 = -k(x_1 - x_2) \tag{4-1}$$

$$F_2 = -k(x_2 - x_1) \tag{4-2}$$

where k is the spring coefficient.

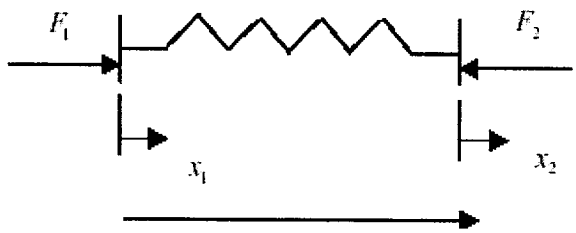

Figure 4-1 Model of the virtual environment

We modify the structure in Figure 3-4. We add the virtual environment into this structure, which is shown in

Figure 4-2

The signal flow diagram of the networked haptic system with virtual environments is shown in Figure 4-3.

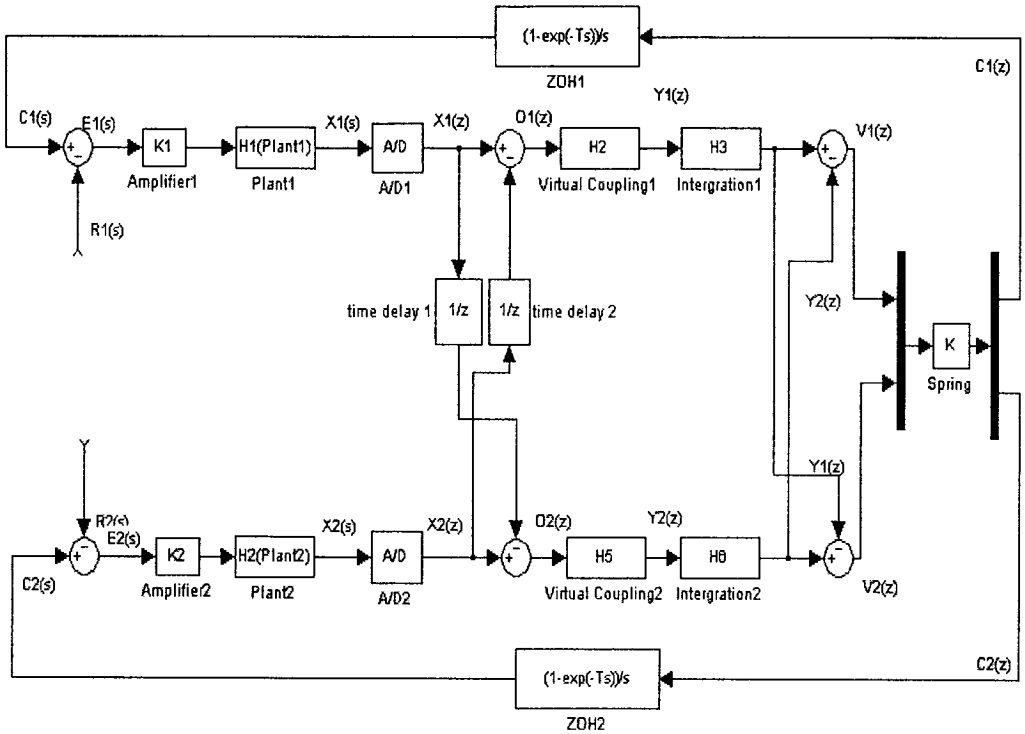

Figure 4-2 Networked haptic display with virtual environments

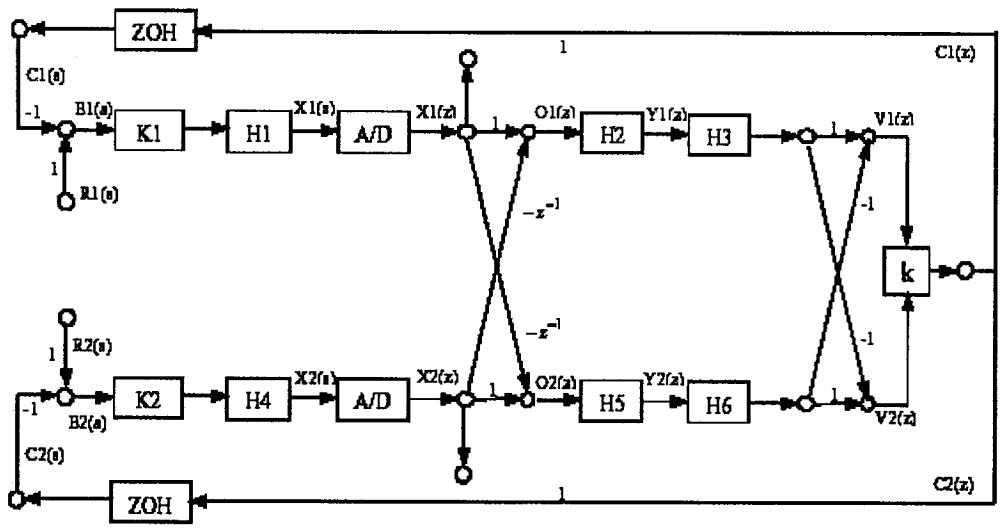

Figure 4-3 Signal flow graph of networked haptic display with VE

4.3 Derivation the Closed-Loop Transfer Functions

We now derive the transfer functions of the closed-loop system in the z-domain based on the Figures 4-2 and 4-3. Because this system is a hybrid system, we may map all of system representation into z-domain or s-domain. In this chapter, we map them into the z-domain.

Firstly, we apply the algebraic method to yield the following equations:

$$E_1(s) = R_1(s) - C_1(s) \tag{4- 3}$$

$$E_2(s) = R_2(s) - C_2(s) \tag{4- 4}$$

$$X_1(s) = K_1 H_1(s) E_1(s) \tag{4- 5}$$

$$X_2(s) = K_2 H_4(s) E_2(s) \tag{4- 6}$$

where $H_1(s)$ and $H_4(s)$ are the transfer function of the plants in the s-domain.

Substituting (4-3) into (4-5) and substituting (4-4) into (4-6) yields:

$$X_1(s) = K_1 H_1(s)(R_1(s) - C_1(s)) \tag{4- 7}$$

$$X_2(s) = K_2 H_4(s)(R_2(s) - C_2(s)) \tag{4- 8}$$

By investigating Figure 4-2, and according to the relationship between $X^*(s)$ and $X(z)$ [101], we found the following expressions:

$$X_1(z) = X_1^*(s)\Big|_{e^{sT}=z} \tag{4- 9}$$

$$X_2(z) = X_2^*(s)\Big|_{e^{sT}=z} \tag{4- 10}$$

At the same time we have:

$$X_1(s) = X_1^*(s) \tag{4- 11}$$

$$X_2(s) = X_2^*(s) \tag{4- 12}$$

Where $C_1(z)$ and $C_2(z)$ are the output of the system, which are the reflected virtual forces by the virtual environment, respectively, we express them as:

$$C_1(s) = ZOH(s) \times C_1^*(s) \tag{4- 13}$$

$$C_2(s) = ZOH(s) \times C_2^*(s) \tag{4- 14}$$

Substituting (4-11) and (4-13) into (4-7) we have:

$$X_1^*(s) = K_1 H_1(s)(R_1(s) - ZOH(s)C_1^*(s)) \tag{4- 15}$$

Substituting (4-12) and (4-14) into (4-8), we get:

$$X_2^*(s) = K_2 H_4(s)(R_2(s) - ZOH(s)C_2^*(s)) \tag{4- 16}$$

Since $H_1(s)$ and $H_4(s)$ are continuous-time systems, hence we take the z-transform for (4-15) and (4-12), and get:

$$X_1(z) = K_1 H_1 R_1(z) - K_1 ZOHH_1(z)C_1(z) \tag{4- 17}$$

$$X_2(z) = K_2 H_4 R_2(z) - K_2 ZOHH_4(z)C_2(z) \tag{4- 18}$$

From Figure 4-3, $O_1(z)$ and $O_2(z)$ are respectively expressed as:

$$O_1(z) = X_1(z) - D_1(z)X_2(z) \tag{4- 19}$$

$$O_2(z) = X_2(z) - D_2(z)X_1(z) \tag{4- 20}$$

where $H_2(z)$ and $H_5(z)$ are the transfer functions of the virtual couples, and the time delay $D_1(z) = \frac{1}{z}$ and $D_2(z) = \frac{1}{z}$, hence

$$Y_1(z) = O_1(z)H_2(z) \tag{4- 21}$$

$$Y_2(z) = O_2(z)H_5(z) \tag{4- 22}$$

Substituting (4-21) into (4-19) and (4-22) into (4-20), we get

$$Y_1(z) = (X_1(z) - D_1(z)X_2(z))H_2(z) \tag{4- 23}$$

$$Y_2(z) = (X_1(z) - D_1(z)X_2(z))H_5(z) \tag{4- 24}$$

For Figure 4-3, $V_1(z)$ and $V_2(z)$ are respectively expressed as:

$$V_1(z) = (Y_1(z) - Y_2(z))H_3(z) \tag{4- 25}$$

$$V_2(z) = (Y_2(z) - Y_1(z))H_6(z) \tag{4- 26}$$

where $H_3(z)$ and $H_6(z)$ are the discrete-time integration. Also,

$$C_1(z) = kV_1(z) \tag{4- 27}$$

$$C_2(z) = kV_2(z) \tag{4- 28}$$

where k is the virtual spring coefficient in the virtual environment.

Finally, by combining (4-17), (4-23), (4-25) and (4-27) to get the output $C_1(z)$, and also combining (4-18), (4-23), (4-25) and (4-27) to get the output $C_2(z)$, we have

$$C_1(z) = \frac{(k(K_1H_2W_1 - K_2H_5W_2)H_3)z + k(-K_2H_2W_2 + K_1H_5W_1)H_3}{(1 + kK_1H_2H_3Z_1 + kK_2H_5H_6Z_2)z + kK_2H_2H_6Z_2 + kK_1H_3H_5Z_1} \tag{4- 29}$$

$$C_2(z) = \frac{(-k(K_1H_2W_1 - K_2H_5W_2)H_6)z - k(-K_2H_2W_2 + K_1H_5W_1)H_6}{(1 + kK_1H_2H_3Z_1 + kK_2H_5H_6Z_2)z + kK_2H_2H_6Z_2 + kK_1H_3H_5Z_1} \tag{4- 30}$$

where $W_1(z) = R_1H_1(z)$, $W_2(z) = R_2H_4(z)$, $Z_1(z) = ZOHH_1(z)$ and $Z_2(z) = ZOHH_4(z)$.

Since $R_1(s)$ and $R_2(s)$ are continuous-time input signals, we can't factor $R_1^*(s)$ and $R_2^*(s)$ from $R_1H_1(s)$ and $R_2H_2(s)$, thus $Z[R_1H_1(s)] \neq Z[R_1(s)]Z[H_1(s)]$ and

$Z[R_2H_4(s)] \neq Z[R_2(s)]Z[H_4(s)]$. Similarly, in $Z_1(z)$ and $Z_2(z)$, we have for the zero order hold:

$$ZOH(s) = \frac{1 - e^{-Ts}}{s} \tag{4-31}$$

$$ZOH(s)H_1(s) = \frac{(1 - e^{-Ts})H_1(s)}{s} \tag{4-32}$$

Therefore we take the z-transform of the above equation, and we get $ZOHH_1(z)$ as following:

$$ZOHH_1(z) = Z[ZOH(s)H_1(s)] = \frac{z-1}{z} Z[\frac{H_1(s)}{s}] \tag{4-33}$$

Similarly, we can also get $ZOHH_4(z)$ as following:

$$ZOHH_4(z) = Z[ZOH(s)H_4(s)] = \frac{z-1}{z} Z[\frac{H_4(s)}{s}] \tag{4-34}$$

According to above description and results, it is impossible for us to get the general expression for the transfer function; however, we can specify the input, and then obtain the transfer function for this specific input. So we assume that the input is:

$$R_1(s) = \frac{1}{s} \Rightarrow R_1(z) = \frac{z}{z-1} \tag{4-35}$$

$$R_2(s) = -\frac{1}{s} \Rightarrow R_2(z) = -\frac{z}{z-1} \tag{4-36}$$

The blocks $H_1(s)$ and $H_4(s)$ are the transfer functions of the plants. We assume that they have the same transfer functions. The transfer functions of the PHANToM Premium 1.5 model from Chapter 2 are given by (2-98), (2-100) and (2-102) along the x, y and z axis. First, we look at the x-axis; thus, we substitute (2-98) into $H_1(s)$ and $H_4(s)$, so that we get

$$H_1(s) = \frac{22.53s}{s^2 + 304s + 304} \tag{4-37}$$

$$H_4(s) = \frac{22.53s}{s^2 + 304s + 304} \tag{4-38}$$

The blocks $H_2(z)$ and $H_5(z)$ are the transfer functions of the virtual coupling. Their expressions are as follows:

$$H_2(z) = \frac{(b_e + TK_e)z - b_e}{z - 1} \tag{4-39}$$

$$H_5(z) = \frac{(b_e + TK_e)z - b_e}{z - 1} \tag{4-40}$$

The blocks $H_3(z)$ and $H_6(z)$ are the transfer functions of the discrete-time integration. Their expressions are as follows:

$$H_3(z) = \frac{T(z+1)}{2(z-1)} \tag{4-41}$$

$$H_6(z) = \frac{T(z+1)}{2(z-1)} \tag{4-42}$$

In order to simplify the calculations, we suppose the system gain K_1 and K_2 have the same value Ks, and the sampling period is $T = 0.01$ s.

By substituting (4-33), (4-35), (4-37), (4-39) and (4-41) into (4-29), we get the output $C_1(z)$. Because $R_1(z)$ cannot be factored from $H_1R_1(z)$ and $ZOHH_1(z)$ separately, have no general transfer function can be found. In order to continue our analysis, we still can obtain its z transform for a specified input $r(t)$. Therefore, we obtain the pseuocontrol ratio $\left[\frac{C_1(z)}{R_1(z)}\right]_p$; that is, we can get

$$[H_1(z)]_p = \left[\frac{C_1(z)}{R_1(z)}\right]_p = \frac{N_1(z)}{D_1(z)} \tag{4-43}$$

where,

$$N_1(z) = 0.1405096\times10^{-2}k\cdot Ks(z^2+2z+1)(b_e z + 0.01K_e z - b_e)$$

$$\begin{aligned} D_1(z) = {} & 2z^4 + (-4.0766686 + .0014050968\ Kskb_e)z^3 \\ & + (.0014050968\ Kskb_e + 2.1723384)z^2 \\ & + (-.095669777 - .0014050968\ Kskb_e)z \\ & - .0014050968\ Kskb_e \end{aligned}$$

By substituting (4-34), (4-36), (4-38), (4-40) and (4-42) into (4-30) we get the output $C_2(z)$. Because $R_2(z)$ cannot be factored from $H_4R_2(z)$ and $ZOHH_4(z)$ separately, hence no general transfer function can be found. In order to continue our analysis, we still can obtain its z-transform for a specified input $r(t)$. Therefore, we obtain the pseuocontrol ratio $\left[\frac{C_2(z)}{R_2(z)}\right]_p$; that is, we can get

$$[H_2(z)]_p = \left[\frac{C_2(z)}{R_2(z)}\right]_p = \frac{N_2(z)}{D_2(z)} \tag{4-44}$$

where,

$$N_2(z) = 0.1405096\times10^{-2}k\cdot Ks(z^2+2z+1)(b_e z + 0.01K_e z - b_e)$$

$$\begin{aligned} D_2(z) = {} & 2z^4 + (-4.0766686 + .0014050968 Kskb_e)z^3 \\ & + (.0014050968 Kskb_e + 2.1723384)z^2 \\ & + (-.095669777 - .0014050968\ Kskb_e)z \\ & - .0014050968 Kskb_e \end{aligned}$$

4.4 Jury Stability Test

In the last section, we have derived pseuocontrol ratios for output versus reference input with specific input signals. Furthermore, in chapter 3, we also

obtained the sets of parameters (K_e, b_e) for the PHANToM Premium 1.5 model to guarantee the stability condition through passivity criteria. In this section, we will find the relationships between parameters (K_e, b_e) gotten in Chapter 3, and different virtual spring coefficient k of the virtual environment model through the Jury's stability test.

As noted in [102], the response transform $C(z)$ has the general form given by the following expressions, where $R(z)$ is the forcing-function transform

$$\begin{aligned} C(z) &= \frac{N(z)}{D(z)} R(z) \\ &= \frac{N(z)}{b_n z^n + b_{n-1} z^{n-1} + b_{n-2} z^{n-2} + \cdots + b_1 z + b_0} R(z) \end{aligned} \tag{4-45}$$

The stability of the response $c(kT)$ ($Z^{-1}[C(z)] = c(kT)$) requires that all roots of $D(z)$ lie inside the UC (unit circle). Since it is usually not necessary to find the exact solution when the response is unstable, a simple procedure to determine the existence of roots that lie outside or on the UC is needed. If such roots of $D(z)$ are found, the system is unstable and must be modified. Jury's stability test, devised by Jury and Blanchard, is a simple method of determining if any roots lie on and/or outside the UC in the z-plane without actually solving for the roots of $D(z)$. It should be noted that the roots of $D(z)$ are poles of $C(z)$. The characteristic equation is

$$D(z) \equiv b_n z^n + b_{n-1} z^{n-1} + b_{n-2} z^{n-2} + \cdots + b_1 z + b_0 = 0 \tag{4-46}$$

where all the coefficients are real, $b_0 \neq 0$ and $b_n > 0$.

The coefficients of the characteristic equation are arranged in the pattern shown in the first two rows of the following Jury-Blanchard (JB) array. These coefficients are then used to evaluate the rest of the constants to complete the array. The constants of the $2j+2$ row consist of the constants of the $2j+1$ row written in reverse order.

The constants c_i, d_i, e_i, etc., where $i = 0,1,...,n-j$, are evaluated from the following determinants:

$$c_i = \begin{vmatrix} b_0 & b_{n-i} \\ b_n & b_i \end{vmatrix}_{j=1}, d_i = \begin{vmatrix} c_0 & c_{n-1-i} \\ c_{n-1} & c_i \end{vmatrix}_{j=2},$$
$$e_i = \begin{vmatrix} d_0 & d_{n-2-i} \\ d_{n-2} & d_i \end{vmatrix}_{j=3}, ..., v_i = \begin{vmatrix} v_0 & v_{3-1} \\ v_3 & v_i \end{vmatrix}_{n-j}, \quad (4\text{-}47)$$

Jury's stability test requires, in order for $D(z) = 0$ not to have any roots on or outside the UC in the z-plane, that the following conditions be both necessary and sufficient:

From (4-46),

$$D(z)\big|_{z=1} > 0 \quad (4\text{-}48)$$

and

$$D(z)\big|_{z=-1} = \begin{cases} > 0 & \text{for } n \text{ even} \\ < 0 & \text{for } n \text{ odd} \end{cases} \quad (4\text{-}49)$$

From (4-47),

$$\left.\begin{array}{l} |b_0| < b_n \\ |c_0| > |c_{n-1}| \\ |d_0| > |d_{n-2}| \\ |e_0| > |e_{n-3}| \\ \vdots \quad \vdots \\ |v_0| > |v_2| \end{array}\right\} n-1 \text{ constrants} \quad (4\text{-}50)$$

We set the spring coefficient for the virtual environment as $k = 1$ and the gain $Ks = 1$. As a result, the characteristic polynomials of the transfer functions are given as following:

$$D_1(z) = 2z^4 + (.0000140509\,68\ KskK_e - 4.0766686 + .0014050968\ Kskb_e)z^3 + (.0014050968\ Kskb_e + 2.1723384 + .0000281019\,36 KskK_e)z^2 + (-.095669777 - .0014050968\ Kskb_e + .0000140509\,68\ KskK_e)z - .0014050968\ Kskb_e \quad (4\text{-}51)$$

$$D_2(z) = 2z^4 + (.0000140509\,68\ KskK_e - 4.0766686 + .0014050968\ Kskb_e)z^3 + (.0014050968\ Kskb_e + 2.1723384 + .0000281019\,36 KskK_e)z^2 + (-.095669777 - .0014050968\ Kskb_e + .0000140509\,68\ KskK_e)z - .0014050968\ Kskb_e \quad (4\text{-}52)$$

We now have

(1) $D(1) > 0$

$D(1) = 0.23\times10^{-3} + .56203872\times10^{2} K_e$

(2) $D(-1) > 0$

$D(-1) = 8.34454$

(3) Jury matrix

$$\begin{bmatrix} -0.14051\times10^{-2} be & a_{12} & a_{13} & a_{14} & 2 \\ 2 & a_{22} & a_{23} & a_{24} & -0.14051\times10^{-2} b_e \\ a_{31} & a_{32} & a_{33} & a_{34} & 0 \\ a_{41} & a_{42} & a_{43} & a_{44} & 0 \\ a_{51} & a_{52} & a_{53} & 0 & 0 \end{bmatrix}$$

where,

$a_{12} = -0.095669777 - .14050968\times10^{-2} b_e + .14050968\times10^{-4} K_e$;

$a_{13} = 2.1723384 + .28101936\times10^{-4} K_e + .14050968\times10^{-2} b_e$;

$a_{14} = .14050968\times10^{-2} b_e - 4.0766686 + .14050968\times10^{-4} K_e$;

$a_{22} = a_{14}$;

$a_{23} = a_{13}$;

$a_{24} = a_{12}$;

$$a_{31} = .19742970\times10^{-5}b_e^{\,2} - 4$$

$$a_{32} = .19742970\times10^{-5}b_e^{\,2} - .26757683\times10^{-2}b_e - .28101936\times10^{-4}K_e + 8.1533372$$

$$a_{33} = -.19742970\times10^{-5}b_e^{\,2} - .58625393\times10^{-2}b_e - .56203872\times10^{-4}K_e - 4.3446768$$

$$a_{34} = -.19742970\times10^{-5}b_e^{\,2} + .85383076\times10^{-2}b_e - .28101936\times10^{-4}K_e + .19133955$$

$$a_{41} = a_{34};$$

$$a_{42} = a_{33};$$

$$a_{43} = a_{32};$$

$$a_{44} = a_{31};$$

$$a_{51} = 0.87940\times10^{-4}b_e^{\,2} - 0.032674318b_e + 15.963389 + 0.10754\times10^{-4}K_e;$$

$$a_{52} = 0.50055\times10^{-4}b_e^{\,2} + (0.31589\times10^{-6}K_e + 0.4892)b_e - 31.782041 + 0.106793\times10^{-5}K_e;$$

$$a_{53} = 0.37885\times10^{-4}b_e^{\,2} + (0.48744\times10^{-6}K_e - 0.045652)b_e + 15.818651 + 0.45931\times10^{-3}K_e;$$

Based on K_e and b_e from the result of the passivity criteria for the x-axis, through computations by the computer, the following result is obtained making the system stable for the virtual spring parameter $k = 1$, as shown in Figure 4-4.

4. 5 Steady State Response

Now we compute the steady state output C_{ss} with the specific input (step input)

$$C_{ss} = \lim_{z\to 1}(1 - z^{-1})C(z) \qquad (4\text{-}53)$$

with

$$C_1(z)=\frac{0.175637z[(K_e+100b_e)z^3+(2K_e+100b_e)z^2+(K_e-100b_e)z-100b_e]}{D_1(z)} \quad (4\text{-}54)$$

where,

$$\begin{aligned}D_1(z) = {} & 0.25\times10^5 z^5+(-0.75948\times10^5+0.175637\ (100\,b_e+K_e)z^4\\ & +(0.781126\times10^5+0.1756371\ K_e)z^3\\ & +(-0.35127\times10^2 b_e-0.1756371\ K_e-0.2835\times10^5)z^2\\ & +(-0.1756371\ K_e+0.119587\times10^4)z+17.563710\ b_e\end{aligned}$$

$$C_2(z)=-\frac{0.175637z[(K_e+100b_e)z^3+(2K_e+100b_e)z^2+(K_e-100b_e)z-100b_e]}{D_2(z)} \quad (4\text{-}55)$$

where,

$$\begin{aligned}D_2(z) = {} & 0.25\times10^5 z^5+(-0.75948\times10^5+0.175637\ (100\,b_e+K_e)z^4\\ & +(0.781126\times10^5+0.1756371\ K_e)z^3\\ & +(-0.35127\times10^2 b_e-0.1756371\ K_e-0.2835\times10^5)z^2\\ & +(-0.1756371\ K_e+0.119587\times10^4)z+17.563710\ b_e\end{aligned}$$

As a result,

$$C_{1ss}=\lim_{z\to1}(1-z^{-1})C_1(z)=1 \quad (4\text{-}56)$$

where the input is $R_1(z)=\frac{z}{(z-1)}$, and

$$C_{2ss}=\lim_{z\to1}(1-z^{-1})C_2(z)=-1 \quad (4\text{-}57)$$

where the input is $R_2(z)=-\frac{z}{(z-1)}$,

From the steady state outputs C_{1ss} and C_{2ss}, we find that the systems are type 1 systems because the steady state error approaches to zero as z approaches to 1.

In order to find the best pair of the variable parameters (K_e, b_e) for spring coefficient k, we have to use the ramp signal as the input signal of our system. Now we set a unit ramp signal $(R_1(s)=1/s^2)$ as the input of the system one, and set minus

unit ramp signal ($R_2(s) = -1/s^2$) as the input of system two. The output is governed through (4-31) and (4-32) as given by

$$C_1(z) = \frac{N_1(z)}{D_1(z)} \tag{4- 58}$$

where,

$$\begin{aligned} N_1(z) = {} & 10^{-2} z[.1015978 \times 10^{-2}(b_e + 10^{-2} K_e) z^4 + 10^{-2}(.14082159 b_e + .24241939 \times 10^{-2} K_e) z^3 \\ & + 10^{-3}(-.62374014 b_e + 1.8004537 \times 10^{-2} K_e) z^2 \\ & + 10^{-3}(-1.4082159 b_e + .39223786 \times 10^{-2} K_e) z - .39223786 \times 10^{-3} b_e] \end{aligned}$$

$$\begin{aligned} D_1(z) = {} & (2 z^4 + (-4.0766686 + .14050968 \times 10^{-2} b_e + .14050968 \times 10^{-4} K_e) z^3 \\ & + (2.1723384 + .14050968 \times 10^{-2} b_e + .28101936 \times 10^{-4} K_e) z^2 \\ & + (-.14050968 \times 10^{-2} b_e + .14050968 \times 10^{-4} K_e - .095669778) z \\ & - .14050968 \times 10^{-2} b_e)(z - 1)^2 \end{aligned}$$

$$C_2(z) = \frac{N_2(z)}{D_2(z)} \tag{4- 59}$$

where,

$$\begin{aligned} N_2(z) = {} & -10^{-2} z[.1015978 \times 10^{-2}(b_e + 10^{-2} K_e) z^4 + 10^{-2}(.14082159 b_e + .24241939 \times 10^{-2} K_e) z^3 \\ & + 10^{-3}(-.62374014 b_e + 1.8004537 \times 10^{-2} K_e) z^2 \\ & + 10^{-3}(-1.4082159 b_e + .39223786 \times 10^{-2} K_e) z - .39223786 \times 10^{-3} b_e] \end{aligned}$$

$$\begin{aligned} D_2(z) = {} & (2 z^4 + (-4.0766686 + .14050968 \times 10^{-2} b_e + .14050968 \times 10^{-4} K_e) z^3 \\ & + (2.1723384 + .14050968 \times 10^{-2} b_e + .28101936 \times 10^{-4} K_e) z^2 \\ & + (-.14050968 \times 10^{-2} b_e + .14050968 \times 10^{-4} K_e - .095669778) z \\ & - .14050968 \times 10^{-2} b_e)(z - 1)^2 \end{aligned}$$

We repeat the Jury's stability criteria to test which K_e and b_e can lead to a haptic interface that is stable. Through numerical computation, the same variable parameters are obtained as in the case of the unit step input, as shown in Figure 4-4.

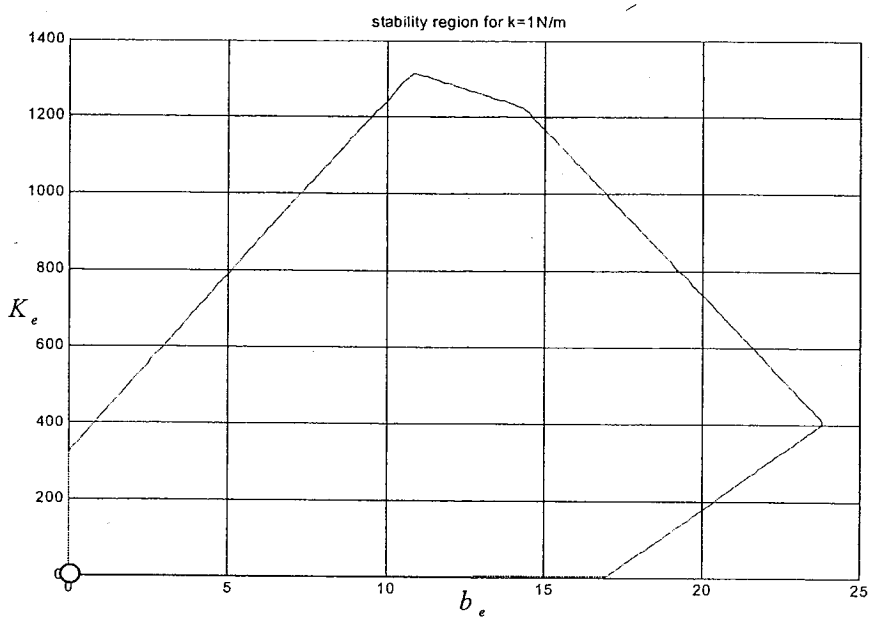

Figure 4-4 Stability of the x-axis for the closed-loop system

Compared to Figures 3-6 and 4-4, we found the acceptable region for parameters (K_e, b_e) that satisfies Jury stability is smaller than the area that satisfies passivity criteria when the spring coefficient of the virtual environment is $k = 1$. Actually, the results of chapter 3 only guarantee haptic interface passivity and stable for the open-loop conditions; however, in this chapter, we are in contact with the virtual environment through haptic interfaces, thus, the results guarantee the stability for the closed-loop system. In control theory, the open-loop stability doesn't necessarily guarantee the closed-loop stability. Passivity criteria are also conservative way. The hardest problem of virtual coupling is that what kind of parameters (K_e, b_e) of the virtual coupling can be selected for any set of passive human operators and virtual environment. The parameters from the passivity criteria define if the virtual coupling selects the (K_e, b_e) values, then the hatpic interface would be passive, which implies unconditional stability, for any set of passive human operators and virtual environment; however, unconditionally stable network is not necessarily passive [16]

Furthermore, Colgate et. al [70] view that when a virtual spring is implemented in discrete-time, the force provided by the spring will not increase smoothly with deflection although an ideal physical spring is a lossless system and it stores energy when pressed and then release it when unpressed. Instead, the force will be repeatedly "held" at a constant value until updated. Because of this, the average force during pressing will be slightly less than for a physical spring of identical stiffness, and the average force during unpressing will be slightly greater. Therefore, the virtual coupling is possible to be an active component.

By further investigation using Jury stability criterion, the region for the parameters (K_e, b_e) will be made smaller with the increase of the spring coefficient. This proves that the requirements of passivity condition for the region of parameters (K_e, b_e) of the virtual coupling become stricter with the increase of stiffness of the virtual environment as shown in

Figure 4-5. Fortunately, those (K_e, b_e) under the worse situation are able to maintain passivity for all the situations, which produces the unconditional stability condition for the closed-loop system. Especially, passivity condition guarantees the passivity of the haptic interface, which means that stability condition of the haptic interface is guaranteed as well.

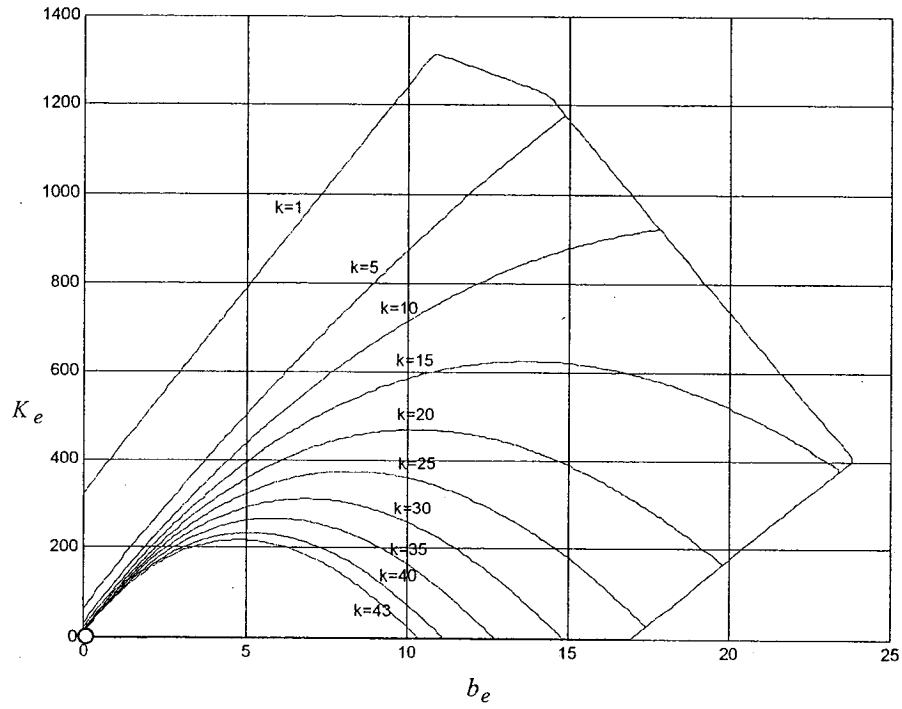

Figure 4-5 The region of parameters (K_e, b_e) for different spring coefficients

$$k \geq 1$$

Using (4-3), (4-4), (4-13) and (4-14), although the feedback loop is not unity in the s-domain, the feedback loop in the z-domain is unity. As a result, the error in the z-domain is given as following:

$$\left.\begin{aligned} E(s) &= R(s) - C(s) \\ C(s) &= ZOH\,(s)C^*(s) \end{aligned}\right\} \overset{z\ \text{transform}}{\Rightarrow} \quad E(z) = R(z) - C(z) \tag{4-60}$$

For the ramp input signal,

$$DC(\infty) = \frac{1}{T}\lim_{z\to 1}\frac{(z-1)^2}{z^2}C(z) \tag{4-61}$$

$$e_{ss}(\infty) = \lim_{z\to 1}\frac{z-1}{z}E(z) = \frac{DC(\infty)}{k_v} \tag{4-62}$$

where k_v is the ramp error coefficient.

Consequently, for the specific virtual spring coefficient $k=1$, the ramp error coefficients k_{1v} and k_{2v}, computed by the above equations, are given as

$$k_{1v}=\frac{(0.02K_e-7b_e)}{-62.381K_e-0.02b_e+11} \tag{4- 63}$$

$$k_{2v}=\frac{(0.02K_e-7b_e)}{-62.281K_e-0.02b_e+11} \tag{4- 64}$$

We notice that the relationship between k_v and $e_{ss}(\infty)$ is inversely proportional. As a result, as k_v becomes larger the steady state error $e_{ss}(\infty)$ gets smaller. Finally, according to the results listed in Figure 4-4, we found that when $K_e=1$ and $b_e=17$, k_v is maximized, and steady state error $e_{ss}(\infty)=0.4355$ is minimized.

According to the results in Appendix A, the workplace of the PHANToM Premium 1.5 model is 19.5 x 27x 37.5cm, and the maximum exertable force is 8.5N. That means the PHANToM Premium 1.5 only reflects a maximum virtual force of 8.5N, and the maximum displacement along an axis is 19.5cm for the virtual spring. As a result, the virtual spring coefficient could not be larger than 43.6N/m. In our design, we choose a maximum k of 43N/m. When k is larger than 43N/m, virtual stiffness will be selected as infinity.

We now change the virtual spring parameter k, and try to find a suitable pair of parameters K_e and b_e to ensure system stability. First, we consider cases of $k>1$, as shown in Table 4-1.

Table 4-1 Steady state error for $k>1$ N/m

k (N/m)	k_v	K_e	b_e	$e_{ss}(\infty)$ (N)
5	$k_v=\frac{-2b_e}{-31.19K_e-0.02b_e+0.9}$	1	17	0.8978

10	$k_v = \frac{0.02K_e - 7b_e}{-62.381K_e - 0.01b_e + 1.1}$	1	17	0.5190
15	$k_v = \frac{0.01K_e - b_e}{-1871.436K_e - 0.02b_e + 2.9}$	1	17	-110.202
20	$k_v = \frac{-0.03K_e + 3b_e}{-249.53K_e - 0.07b_e + 2.2}$	1	17	-4.8866
25	$k_v = \frac{-0.02K_e - 3b_e}{-155.954K_e - 0.08b_e + 1.15}$	1	17	3.0676
30	$k_v = \frac{-0.01K_e + b_e}{-3.743K_e - 0.78}$	1	14.8	-0.3065
35	$k_v = \frac{-0.01K_e + b_e}{-4.3667K_e + 0.78}$	1	12.7	-0.40647
40	$k_v = \frac{b_e}{4.991K_e + 0.01b_e + 0.78}$	1	11.1	0.53109
43	$k_v = \frac{200b_e}{-0.54K_e - 67}$	1	10.3	-0.03286

Next we consider the cases of $k < 1$ N/m, as shown in Table 4-2.

Table 4-2 Steady state error for $k < 1$ N/m

k (N/m)	k_v	K_e	b_e	$e_{ss}(\infty)$ (N)
0.5	$k_v = \frac{0.01K_e + b_e}{-6.238K_e - 0.01b_e - 78}$	1	17	-4.9694
0.1	$k_v = \frac{b_e}{-6.238K_e - 0.01b_e + 110}$	18	17.3	-0.1423
0.05	$k_v = \frac{K_e + 0.01b_e}{-6.238K_e - b_e - 780}$	1	17	-45.9754
0.01	$k_v = \frac{b_e}{-6.238K_e - 0.01b_e + 1100}$	176	19.9	0.09656
0.005	$k_v = \frac{0.01K_e + b_e}{-6.238K_e - 0.01b_e - 7800}$	401	23.8	-371.9792
0.001	$k_v = \frac{b_e}{-6.238K_e - 0.01b_e + 0.11\times10^5}$	1224	14.3	235.86

4.6 Networked Haptic Display with Spring-Damping Virtual Environment

In the previous sections, we have discussed the case of virtual environment modeled by the virtual spring. Actually, in real situations, a spring alone couldn't generate a good model in virtual environment to represent the object. Therefore, we

consider the case of virtual environment that is modeled by a spring and a damper. The spring and the damper configured as a parallel connection is shown in Figure 4-5. The model of the virtual environment now becomes as follow:

$$VE(s) = k + bs\Big|_{s\to\frac{(z-1)}{Tz}} \Rightarrow VE(z) = \frac{(Tk+b)z-b}{Tz} \qquad (4\text{-}65)$$

This model is now substituted into Figure 4-3 instead of the original model of the virtual environment, which is the component k. In (4-65), k is the spring coefficient, and b is the damping coefficient. Furthermore, (4-27) and (4-28) would be now changed into

$$C_1(z) = \frac{(Tk+b)z-b}{Tz}V_1(z) \qquad (4\text{-}66)$$

$$C_2(z) = \frac{(Tk+b)z-b}{Tz}V_2(z) \qquad (4\text{-}67)$$

We now follow the same procedure developed in section 4.3 to derive the new ratio between the input and the output of the system. The first difference is that we use (4-66) and (4-67) instead of (4-27) and (4-28), respectively. The second difference is that we use a unit ramp signal as our reference input, thus (4-35) and (4-36) become respectively

$$R_1(s) = \frac{1}{s^2} \Rightarrow R_1(z) = \frac{Tz}{(z-1)^2} \qquad (4\text{-}68)$$

$$R_2(s) = -\frac{1}{s^2} \Rightarrow R_2(z) = -\frac{Tz}{(z-1)^2} \qquad (4\text{-}69)$$

Consequently, we obtain the new outputs $C_1(z)$ and $C_2(z)$ as follows

$$C_1(z) = \frac{N_1(z)}{D_1(z)} \qquad (4\text{-}70)$$

where

$$
\begin{aligned}
N_1(z) &= 10^{-4} \cdot Ks\{10.16[(K_eT + b_e)(Tk + b)]z^5 \\
&+ [K_eT(14.082b + 24.242Tk) + b_e(14.082Tk + 3.9224b)]z^4 \\
&+ [K_eT(18.005Tk - 6.2374b) - b_e(6.2374Tk + 20.32b)]z^3 \\
&+ [K_eT(3.9224Tk - 14.028) - b_e(14.082Tk + 7.8448b)]z^2 \\
&+ [b_e(-3.9224Tk + 10.16b) - 3.9224K_ebT]z + 3.9224b_eb\}z
\end{aligned}
$$

$$
\begin{aligned}
D_1(z) &= 2z^7 + [0.14051Ks(Tk + b)(K_eT + b_e) - 8.0767]z^6 \\
&+ [-0.14051KsT(b_ek + K_eb) - 0.28102Ksb_eb + 12.326]z^5 \\
&+ [-0.14051Ksb_e(2Tk + b) - 0.28012KsK_eT(Tk + b) - 8.517]z^4 \\
&+ [0.28102KsT(b_ek + K_eb) + 0.56204Ksb_eb + 2.3637]z^3 \\
&+ [0.1405Ks(K_eT(Tk + b) + be(Tk - b)) - 0.9567]z^2 \\
&- 0.14051Ks[K_eTb + be(Tk + 2b)]z + 0.14051Ksb_eb
\end{aligned}
$$

and
$$
C_2(z) = \frac{N_2(z)}{D_2(z)} \tag{4- 71}
$$

where

$$
\begin{aligned}
N_2(z) &= -10^{-4} \cdot Ks\{10.16[(K_eT + b_e)(Tk + b)]z^5 \\
&+ [K_eT(14.082b + 24.242Tk) + b_e(14.082Tk + 3.9224b)]z^4 \\
&+ [K_eT(18.005Tk - 6.2374b) - b_e(6.2374Tk + 20.32b)]z^3 \\
&+ [K_eT(3.9224Tk - 14.028) - b_e(14.082Tk + 7.8448b)]z^2 \\
&+ [b_e(-3.9224Tk + 10.16b) - 3.9224K_ebT]z + 3.9224b_eb\}z
\end{aligned}
$$

$$
\begin{aligned}
D_2(z) &= 2z^7 + [0.14051\,Ks(Tk + b)(K_eT + b_e) - 8.0767]z^6 \\
&+ [-0.14051\,KsT(b_ek + K_eb) - 0.28102\,Ksb_eb + 12.326]z^5 \\
&+ [-0.14051\,Ksb_e(2Tk + b) - 0.28012\,KsK_eT(Tk + b) - 8.517]z^4 \\
&+ [0.28102\,KsT(b_ek + K_eb) + 0.56204\,Ksb_eb + 2.3637]z^3 \\
&+ [0.1405\,Ks(K_eT(Tk + b) + be(Tk - b)) - 0.9567]z^2 \\
&- 0.14051\,Ks[K_eTb + be(Tk + 2b)]z + 0.14051\,Ksb_eb
\end{aligned}
$$

By further analysis, the pseuocontrol ratio $\left[\frac{C_1(z)}{R_1(z)}\right]_p$ and $\left[\frac{C_2(z)}{R_2(z)}\right]_p$ are obtained;

that is, we get

$$
[H_1(z)]_p = \left[\frac{C_1(z)}{R_1(z)}\right]_p = \frac{N_1(z)}{G_1(z)} \tag{4- 72}
$$

where,

$$
\begin{aligned}
N_1(z) &= 10^{-4} \cdot Ks\{10.16[(K_eT + b_e)(Tk + b)]z^5 \\
&+ [K_eT(14.082b + 24.242Tk) + b_e(14.082Tk + 3.9224b)]z^4 \\
&+ [K_eT(18.005Tk - 6.2374b) - b_e(6.2374Tk + 20.32b)]z^3 \\
&+ [K_eT(3.9224Tk - 14.028) - b_e e(14.082Tk + 7.8448b)]z^2 \\
&+ [b_e(-3.9224Tk + 10.16b) - 3.9224K_ebT]z + 3.9224b_eb\}
\end{aligned}
$$

$$
\begin{aligned}
G_1(z) &= T\{2z^5 + [0.14051Ks(Tk + b)(K_eT + b_e) - 4.0767]z^4 \\
&+ [0.14051KsT(b_ek + K_eb) + 0.28102KsK_eT^2k + 2.1723]z^3 \\
&+ [-0.14051Ksb_e(2b + Tk) + 0.14051KsK_eT(Tk - b) - 0.9567]z^2 \\
&- 0.14051KsT(K_eb + b_ek)z + 0.14051Ksb_eb\}
\end{aligned}
$$

$$
[H_2(z)]_p = \left[\frac{C_2(z)}{R_2(z)}\right]_p = \frac{N_2(z)}{G_2(z)} \tag{4- 73}
$$

where,

$$
\begin{aligned}
N_2(z) &= 10^{-4} \cdot Ks\{10.16[(K_eT + b_e)(Tk + b)]z^5 \\
&+ [K_eT(14.082b + 24.242Tk) + b_e(14.082Tk + 3.9224b)]z^4 \\
&+ [K_eT(18.005Tk - 6.2374b) - b_e(6.2374Tk + 20.32b)]z^3 \\
&+ [K_eT(3.9224Tk - 14.028) - b_e(14.082Tk + 7.8448b)]z^2 \\
&+ [b_e(-3.9224Tk + 10.16b) - 3.9224K_ebT]z + 3.9224b_eb\}
\end{aligned}
$$

$$
\begin{aligned}
G_2(z) &= T\{2z^5 + [0.14051Ks(Tk + b)(K_eT + b_e) - 4.0767]z^4 \\
&+ [0.14051KsT(b_ek + K_eb) + 0.28102KsK_eT^2k + 2.1723]z^3 \\
&+ [-0.14051Ksb_e(2b + Tk) + 0.14051KsK_eT(Tk - b) - 0.9567]z^2 \\
&- 0.14051KsT(K_eb + b_ek)z + 0.14051Ksb_eb\}
\end{aligned}
$$

In order to investigate the stability of the closed-loop system, we also follow the Jury stability criteria procedure, as shown in section 4.4 and the steady-state response analysis as shown in section 4.5 to obtain the parameters (K_e, b_e) that are compatible with different spring coefficients k and damping coefficients b in the simulated virtual environment.

We consider the three cases that based on different spring coefficients, namely, $k = 0.05$ N/m, $k = 1$ N/m, and $k = 30$ N/m, which represent a small, medium and large

stiffness properties of the simulated object, respectively. Simultaneously, we choose different damping coefficients to simulate different damping properties of the virtual object, where b is equal to 0.05, 0.5, 1, 5, 20, 30 N·sec/m, respectively. These values of b combined with different spring coefficients k are used to simulate different virtual objects as expressed in (4-65).

Using Jury stability criteria, different stability conditions for the three cases are obtained in Figures 4-6, 4-7 and 4-8. According to the steady state response analysis, the best parameters of (K_e, b_e) for different cases are listed in Tables 4-3, 4-4 and 4-5.

By inspecting Figures 4-6 and 4-7, it follows that the virtual objects with the larger damping coefficients, independent of the virtual spring coefficients, result in stability conditions for the closed-loop system that are much stricter than other cases. This implies that the passivity condition for the haptic interface becomes more difficult. As a result, it is easy to violate the passivity of the haptic interface and cause the closed-system to become unstable. In Tables 4-3 and 4-4, we found that the steady state errors become larger with the increase of the virtual damping coefficient.

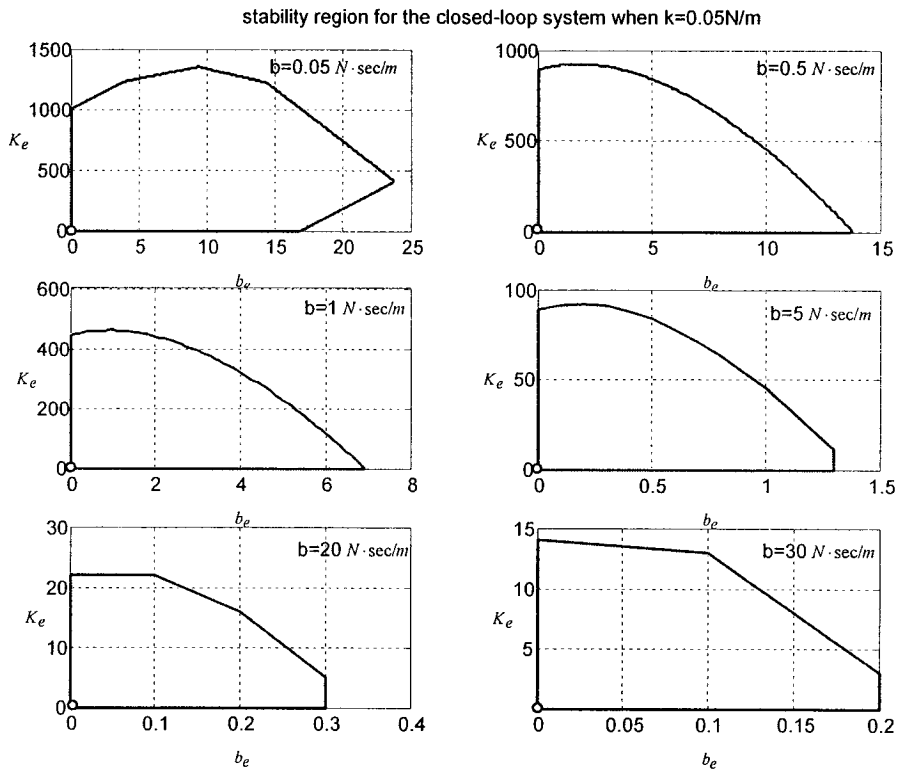

Figure 4-6 The stability condition for the case with $k = 0.05\,\mathrm{N/m}$

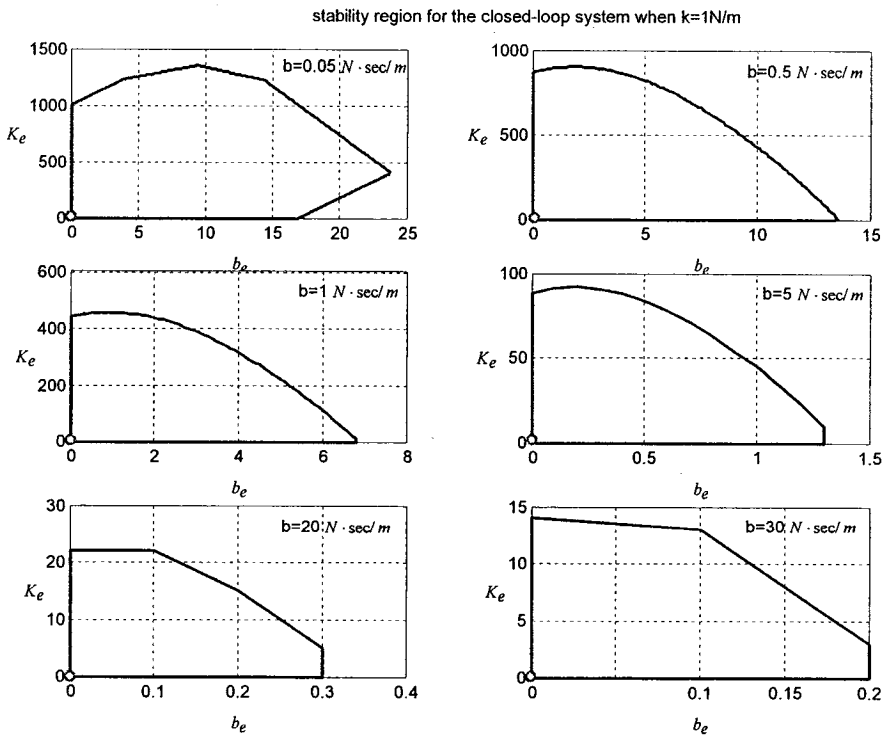

Figure 4-7 The stability condition for the case with $k = 1\,\mathrm{N/m}$

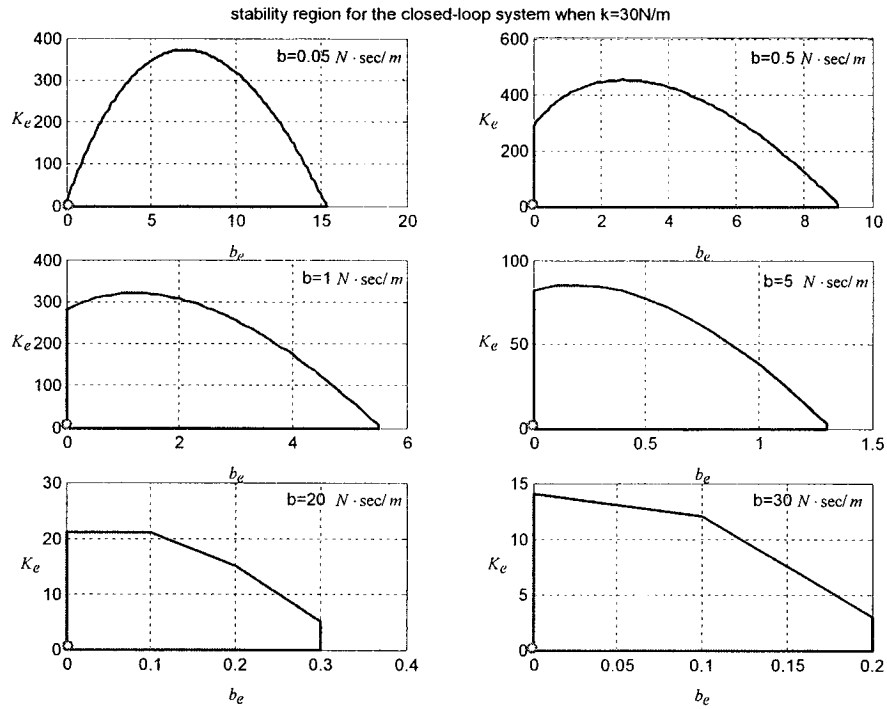

Figure 4-8 The stability condition for the case with $k = 30$ N/m

Table 4-3 The best values for (K_e, b_e) for the case with $k = 0.05$ N/m

k (N/m)	b (N·sec/m)	k_v	K_e	b_e	$e_{ss}(\infty)$ (N)
0.05	0.05	$k_v = \frac{0.5(0.01K_e + b_e)}{-6.235K_e - 3b_e + 220}$	31	8.9	0.00326
	0.5	$k_v = \frac{0.05(0.01K_e + b_e)}{-0.6095K_e - 3b_e + 22}$	11	5.1	-0.0173
	1	$k_v = \frac{0.5(0.01K_e + b_e)}{-5.895K_e - 11.89b_e + 220}$	24	6.6	0.0135
	5	$k_v = \frac{0.5(0.01K_e + b_e)}{-4.795K_e - 599.99b_e + 220}$	46	.0	-2.4833
	20	$k_v = \frac{0.5(0.01K_e + b_e)}{-9.795K_e + 200.01b_e + 220}$	22	0	41.0792
	30	$k_v = \frac{0.5(0.01K_e + b_e)}{-7.795K_e - 11.89b_e + 220}$	13	0.1	1023.25

Table 4-4 The best values for (K_e, b_e) for the case with $k = 1\,\text{N/m}$

k (N/m)	b (N·sec/m)	k_v	K_e	b_e	$e_{ss}(\infty)$ (N)
1	0.05	$k_v = \frac{10(0.01K_e + b_e)}{-124.75K_e + 2.1b_e + 220}$	2	14	-0.0007
	0.5	$k_v = \frac{2(0.01K_e + b_e)}{-24.99K_e - 1.02b_e + 40}$	1	13.6	0.0412
	1	$k_v = \frac{(0.01K_e + b_e)}{-12.4759K_e + 0.01b_e + 22}$	2	6.8	-0.4237
	5	$k_v = \frac{(0.01K_e + b_e)}{-12.4759K_e + 0.01b_e + 22}$	2	1.3	-2.2309
	20	$k_v = \frac{(0.01K_e + b_e)}{-12.4759K_e + 0.01b_e + 22}$	2	0.3	-9.2336
	30	$k_v = \frac{(0.01K_e + b_e)}{-12.4759K_e + 0.01b_e + 22}$	2	0.2	-13.4353

Table 4-5 The best values (K_e, b_e) for the case with $k = 30\,\text{N/m}$

k (N/m)	b (N·sec/m)	k_v	K_e	b_e	$e_{ss}(\infty)$ (N)
30	0.05	$k_v = \frac{6(0.01K_e + b_e)}{-74.862K_e - 0.01b_e + 4}$	0	15.3	0.03497
	0.5	$k_v = \frac{6(0.01K_e + b_e)}{-74.862K_e - 0.3b_e + 4}$	0	9	0.0691
	1	$k_v = \frac{3(0.01K_e + b_e)}{-37.428K_e - 0.03b_e + 2.2}$	0	5.5	0.043
	5	$k_v = \frac{3(0.01K_e + b_e)}{-37.428K_e - 0.03b_e + 2.2}$	0	1.3	0.0407
	20	$k_v = \frac{1.5(0.01K_e + b_e)}{-18.745K_e + 1.05b_e + 1.1}$	0	0.3	0.0515
	30	$k_v = \frac{3(0.01K_e + b_e)}{-37.47K_e + 0.1b_e + 2.2}$	0	0.2	0.0404

4.7 Conclusion

By using jury stability criteria, we obtained the acceptable parameters for (K_e, b_e) to guarantee the stability of the closed-loop system based on the open-loop passivity condition of the haptic interface when the haptic interface interacts with the virtual environment. In this chapter, we consider two mathematical models, namely the spring and the spring-damping models to simulate the virtual environments. The steady state performance of different models based on different parameters have been obtained and listed in this chapter. Based on the results of this chapter, we also conclude that the passivity of the haptic interface guarantees the stability of the closed-loop VR system.

Chapter 5

Simulation Results and Discussion

5.1 Introduction

In the previous chapters we have determined parameters (K_e, b_e) for two mathematical models for simulating the virtual environment. The linearized model for the PHANToM Premium 1.5 along the x-axis is a first order system. Steady state responses of the closed-loop system were obtained in Tables 4-1 and 4-2 for the spring model of the virtual environment, Tables 4-3, 4-4 and 4-5 for the spring-damping model of the virtual environment. Since the model is generally higher, we can't compute the transient response easily. In this chapter, we are going to build a simulation model with two haptic displays to simulate the performance of transient state.

5.2 Simulation and Transient Response

Our simulation model is shown in Figure 4-2. The models of the virtual environment are a simple spring as explained in section 4.2 and a spring-damping model as shown in section 4.6. Using the simulation environment in Matlab Simulink, we will investigate the complete response of the closed-loop VR system for different spring coefficients and damping coefficients.

5.2.1 Simulations with Spring Model of the Virtual Environment

First, we consider the simple case of a virtual environment modeled only by a virtual spring. In the simulations, we implement the two corporative haptic devices to contact a shared virtual environment with different spring coefficients k.

When the two users interact with a shared virtual environment with different spring coefficients k, the reflected virtual forces will be generated by the virtual environment and feedback to the two users. The simulation results for $k \geq 1$ are plotted in Figures 5-1 to 5-6. The simulation results for $k < 1$ are plotted in Figures 5-7 to 5-10. In these plots, system 1 represents the reflected system feedback to user 1, and system 2 represents the reflected system feedback to user 2.

The desired performance characteristics of a tracking system of any order may be specified in terms of the transient response to a unit step-function input. The performance of a system may be evaluated in terms of the following metrics, such as overshoot Mp, the time to maximum overshoot t_p, settling time with 2 or 5 percent of error against the input $t_s(2\%)$ and $t_s(5\%)$, rise time t_r, duplicating time t_d and the delay time to response t_{delay}. Tables 5-1 and 5-2 show the transient performance for different spring coefficients k.

Table 5-1 The complete response of system 1 for different $k \geq 1$

k (N/m)	$e(\infty)$	Mp (N)	t_p (s)	$t_s(5\%)$ (s)	$t_s(2\%)$ (s)	t_d (s)	t_r (s)	t_{delay} (s)
1	0	-	-	23.5	41.1	79.08	10.35	1.01
5	0	-	-	1.0893	11.26	57.25	1.07	1.01
10	0	1.2132	1.05	1.115	1.2089	47.77	1.04	1.01
15	0	1.4689	1.04	1.1665	1.2465	41.47	1.03	1.01
20	0	1.6667	1.04	1.3451	1.4885	1.5	1.02	1.01
25	0	1.8293	1.03	2.8794	3.6277	1.61	1.02	1.01
30	0	1.9098	1.25	25.2648	33.5072	1.54	1.02	1.01
35	0	1.92	1.28	38.395	36.8872	2.43	1.02	1.01
40	0	1.9129	1.28	27.4148	36.8872	12.44	1.02	1.01
43	0	1.8946	1.28	16.4349	21.3554	7.01	1.02	1.01

Table 5-2 The complete response of system 1 for different $k<1$

k (N/m)	$e(\infty)$	Mp (N)	t_p (s)	$t_s(5\%)$ (s)	$t_s(2\%)$ (s)	t_d (s)	t_r (s)	t_{delay} (s)
0.5	0	-	-	39.95	58.94	95.15	24.55	1.01
0.1	0	-	-	6.48	8.03	11.56	5.26	1.01
0.05	0	-	-	219.04	274.56	349.31	169.17	1.02
0.01	0	1.0355	1.3478	5.0888	9.11	5.71	4.67	1.03
0.005	0	1.0599	1.4375	7.3	8.77	4.95	4.24	1.04
0.001	0	1.0097	1.580	6.9156	7.64	8.49	6.15	1.08

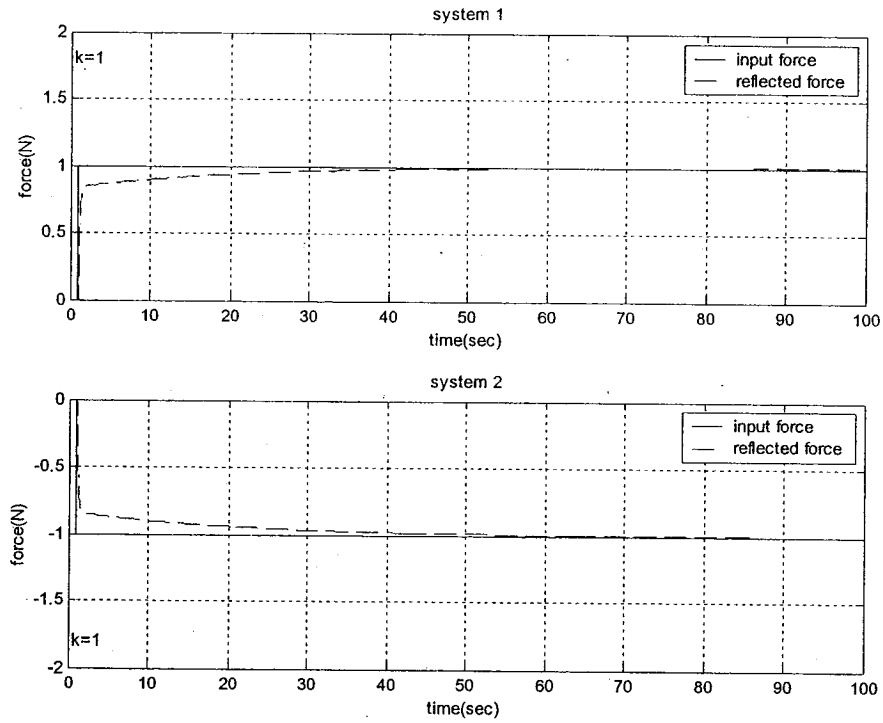

Figure 5-1 The response of spring model with cofficient $k=1$ N/m

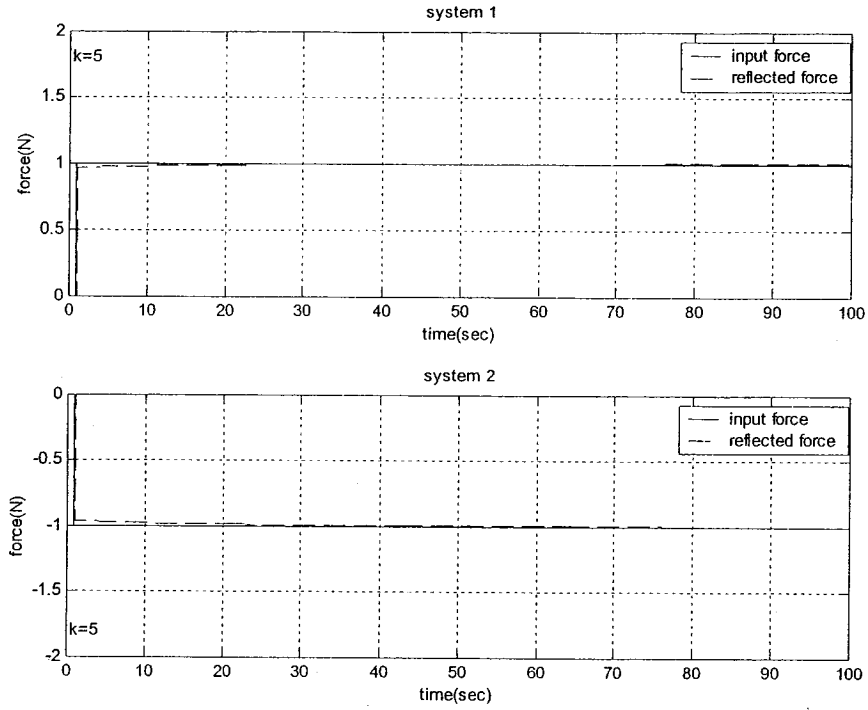

Figure 5-2 The response of spring model with cofficient $k = 5$ N/m

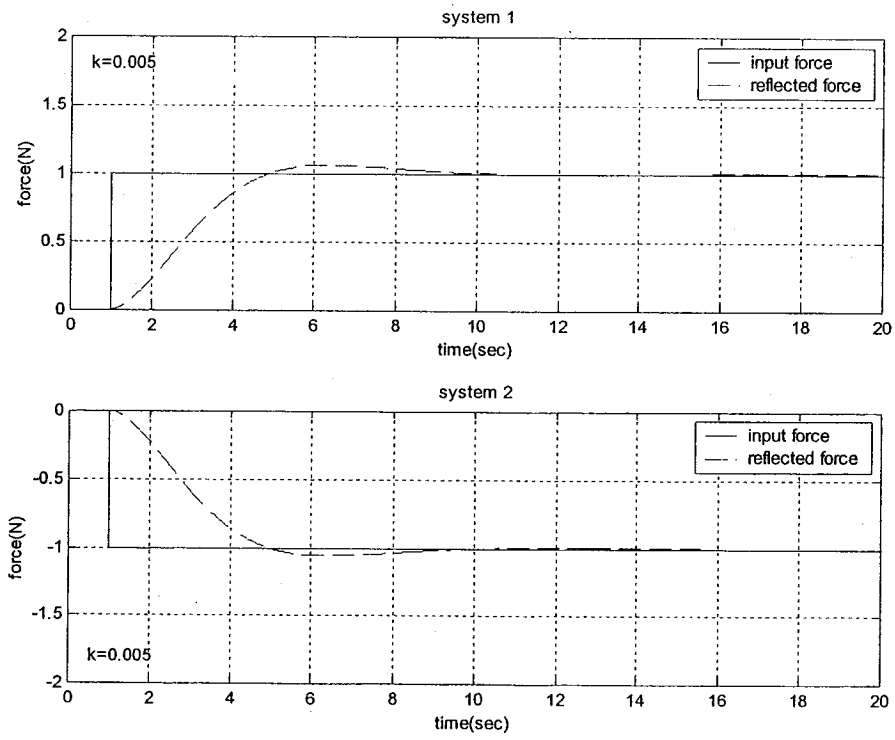

Figure 5-3 The response of spring model with cofficient $k = 10$ N/m

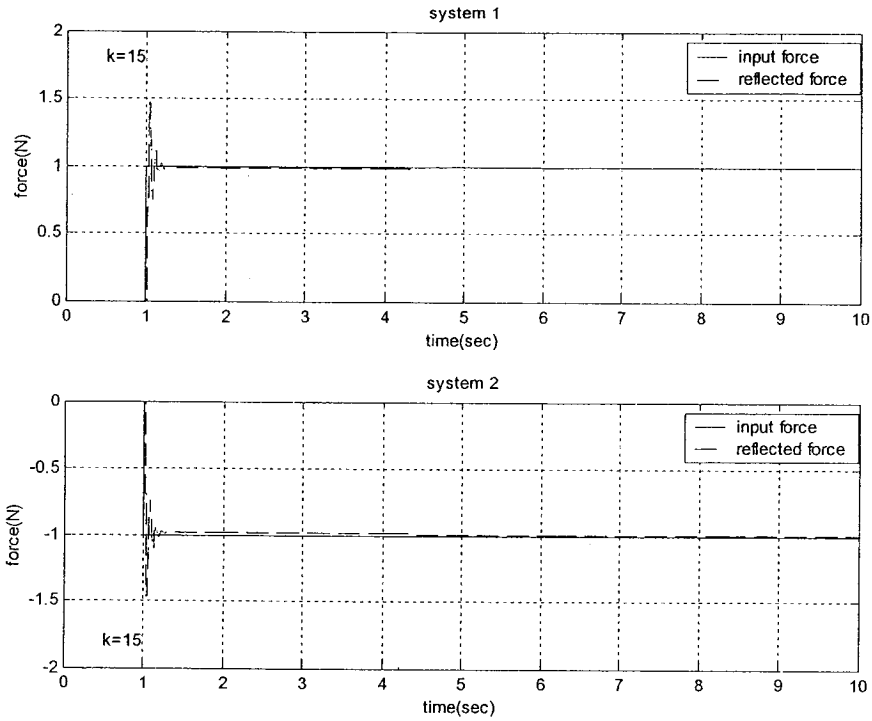

Figure 5-4 The response of spring model with cofficient $k = 15\,\mathrm{N/m}$

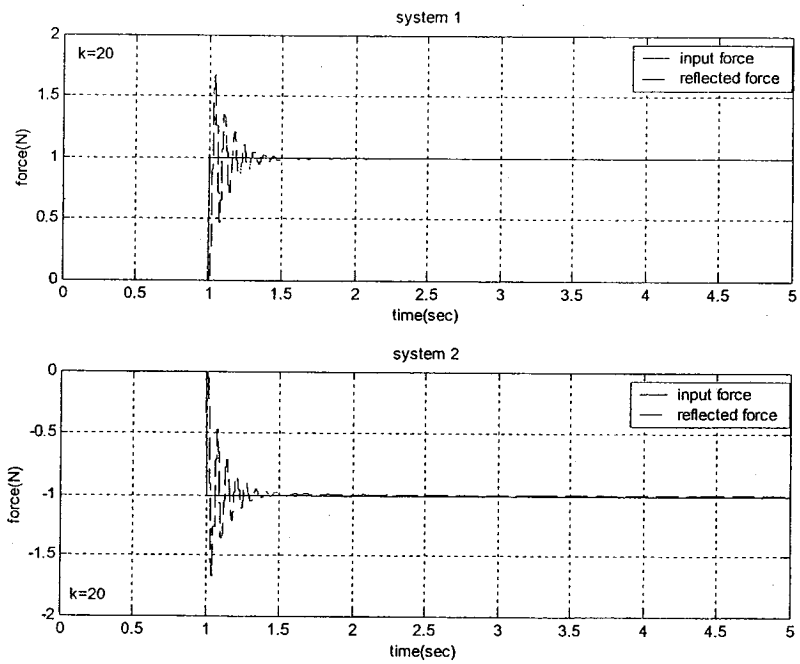

Figure 5-5 The response of spring model with cofficient $k = 20\,\mathrm{N/m}$

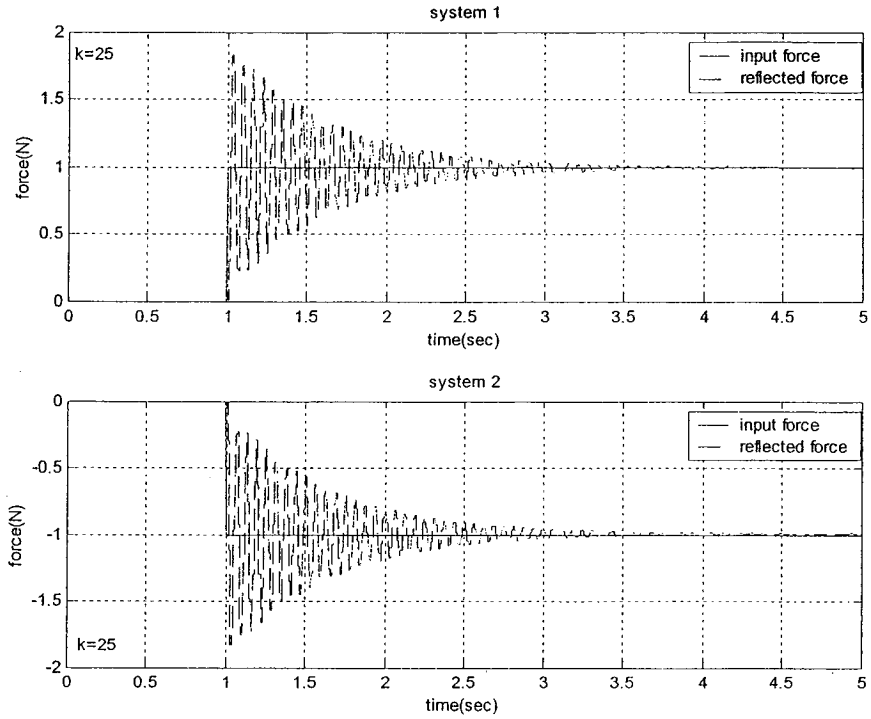

Figure 5-6 The response of spring model with cofficient $k = 25$ N/m

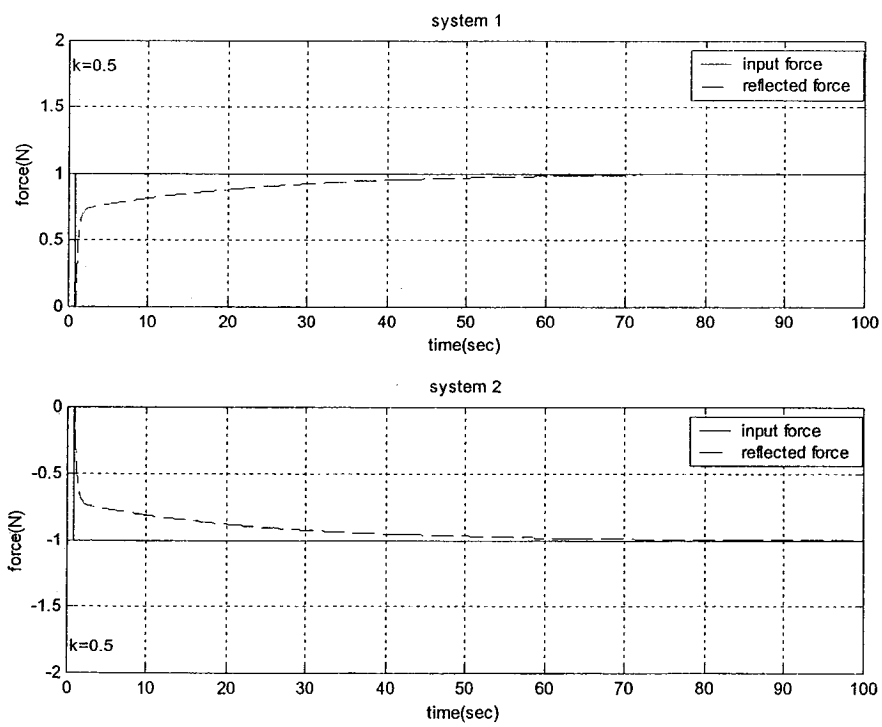

Figure 5-7 The response of spring model with cofficient $k = 0.5$ N/m

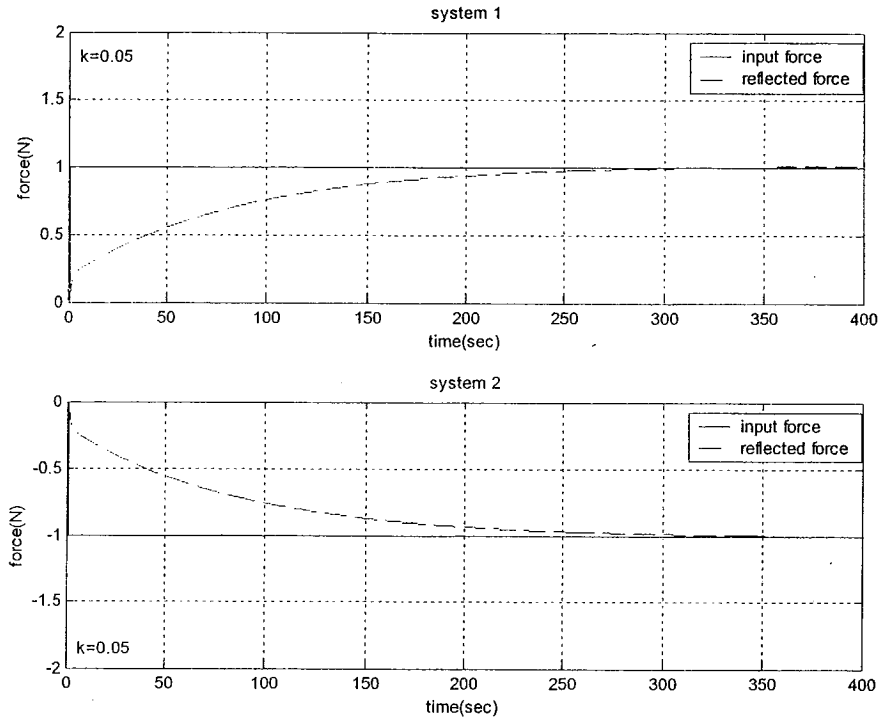

Figure 5-8 The response of spring model with cofficient $k = 0.05\,\mathrm{N/m}$

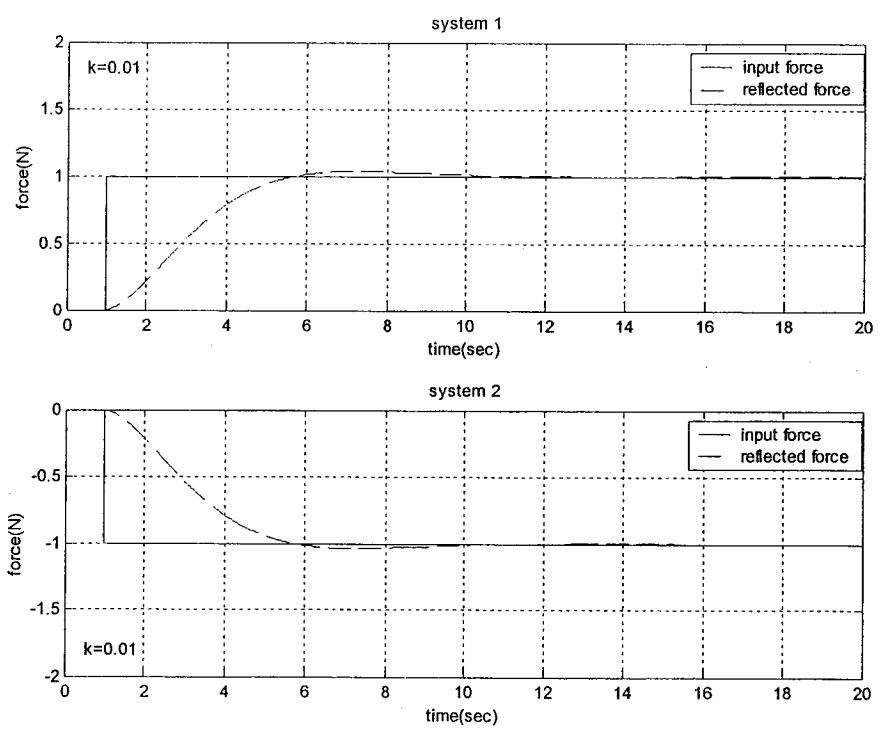

Figure 5-9 The response of spring model with cofficient $k = 0.01\,\mathrm{N/m}$

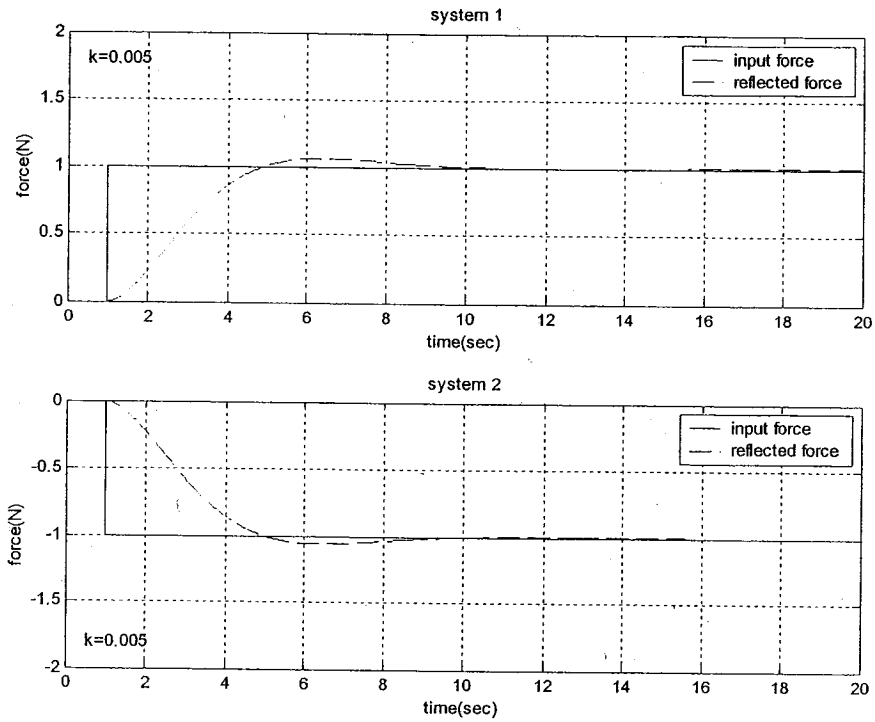

Figure 5-10 The response of spring model with cofficient $k = 0.005\,\mathrm{N/m}$

5.2.2 Simulations with Spring-Damping Model of the Virtual Environment

In the previous section, we have simulated the cases of spring model of the virtual environment; however, the spring alone could not model the virtual objects very well. In order to investigate the complete response of a networked haptic display when they interact with a complex virtual environment, in this section, we use a spring and damping model in parallel connection to represent a complex virtual environment. In order to make our investigations straightforward, we classify the spring coefficient k and the damping coefficient b into three groups, namely small, medium and large. Specifically, $k = 0.05\,\mathrm{N/m}$ and $b = 0.05\,\mathrm{N{\cdot}sec/m}$ correspond to the small case, $k = 1\ \mathrm{N/m}$ and $b = 1\ \mathrm{N{\cdot}sec/m}$ correspond to the medium case, and $k = 30\,\mathrm{N/m}$ and $b = 30\,\mathrm{N{\cdot}sec/m}$ correspond to the large case. Now we simulate the three cases based on three groups of the spring coefficients k with different damping

coefficients b. Case I designates $k = 0.05$ N/m, Case II designates $k = 1$ N/m, and Case III designates $k = 30$ N/m. The complete performance results for these three cases are shown in Tables 5-3 to 5-5. The simulation plots for the three cases are shown in Figures 5-11 to 5-13 for case I, Figures 5-14 to 5-16 for case II and Figures 5-17 to 5-19 for case III.

Table 5-3 The response of system 1 for case I with $k = 0.05$ (N/m)

k (N/m)	b (N·sec/m)	Mp (N)	t_p (s)	t_s(5%) (s)	t_s(2%) (s)	t_d (s)	t_r (s)	t_{delay} (s)
0.05	0.05	-	-	7.99	10.08	14.58	6.34	1.01
	1	1.2806	1.31	20.7	40.68	90.95	1.02	1.01
	30	1.8195	1.17	14.32	19.87	7.26	1.02	1.01

Table 5-4 The response of system 1 for case II with $k = 1$ (N/m)

k (N/m)	b (N·sec/m)	Mp (N)	t_p (s)	t_s(5%) (s)	t_s(2%) (s)	t_d (s)	t_r (s)	t_{delay} (s)
1	0.05	-	-	11.61	18.82	34.55	5.92	1.01
	1	1.2423	1.02	11.478	15.25	2.36	1.02	1.01
	30	1.2591	1.15	3.0183	30.56	109.56	1.02	1.01

Table 5-5 The response of system 1 for case III with $k = 30$ (N/m)

k (N/m)	b (N·sec/m)	Mp (N)	t_p (s)	t_s(5%) (s)	t_s(2%) (s)	t_d (s)	t_r (s)	t_{delay} (s)
30	0.05	1.9394	1.03	19.0352	26.6762	7.91	1.02	1.01
	1	1.6078	1.11	7.5683	12.5	1.95	1.02	1.01
	30	1.117	1.02	-	-	-	1.02	1.01

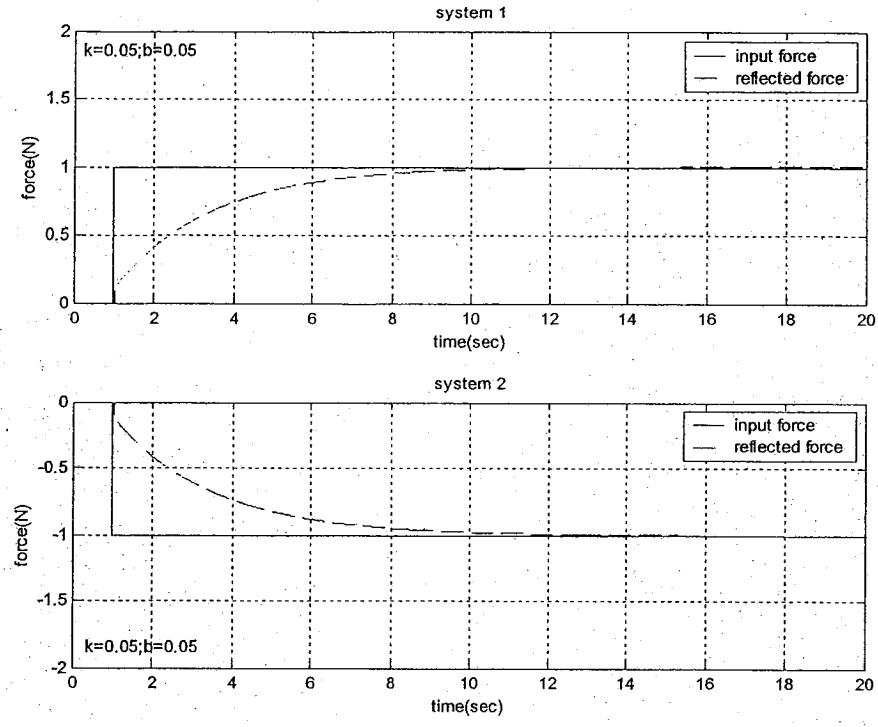

Figure 5-11 The response of case I with $k = 0.05$N/m and $b = 0.05$N·sec/m

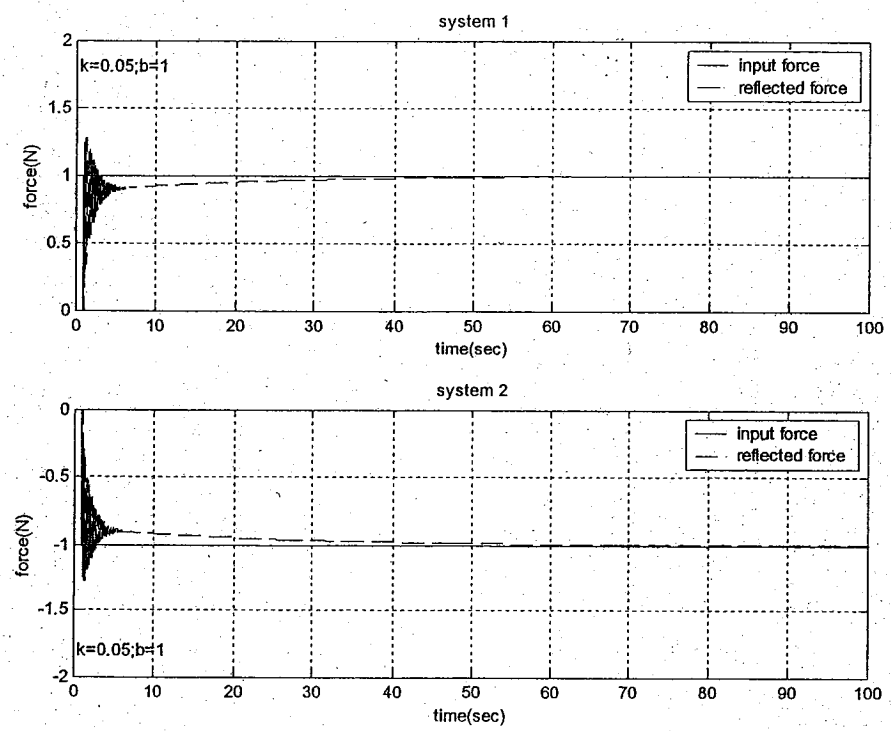

Figure 5-12 The response of case I with $k = 0.05$N/m and $b = 1$N·sec/m

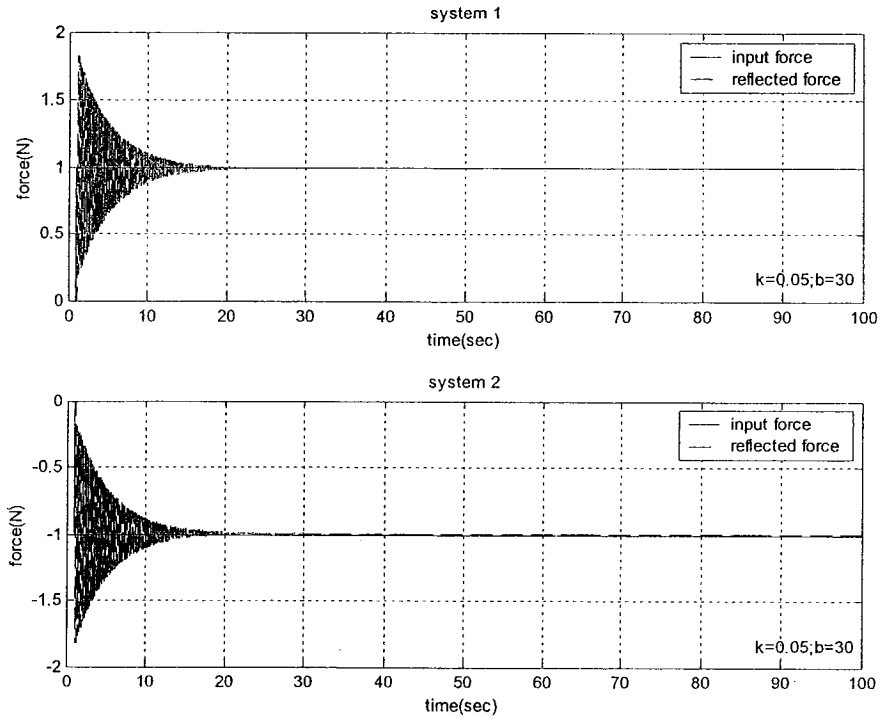

Figure 5-13 The response of case I with $k = 0.05\,\text{N/m}$ and $b = 30\,\text{N·sec/m}$

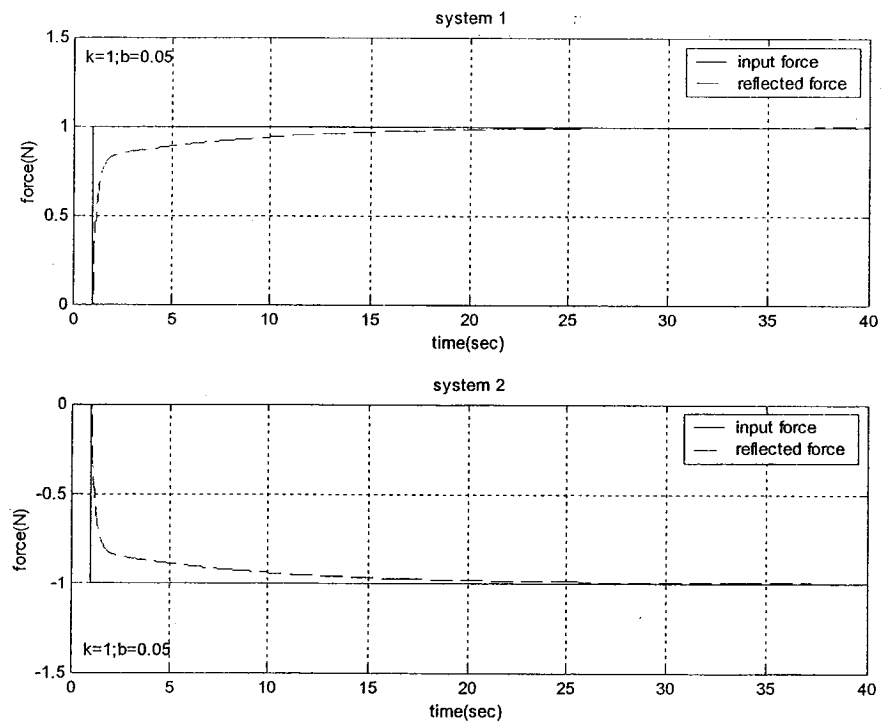

Figure 5-14 The response of case II with $k = 1\,\text{N/m}$ and $b = 0.05\,\text{N·sec/m}$

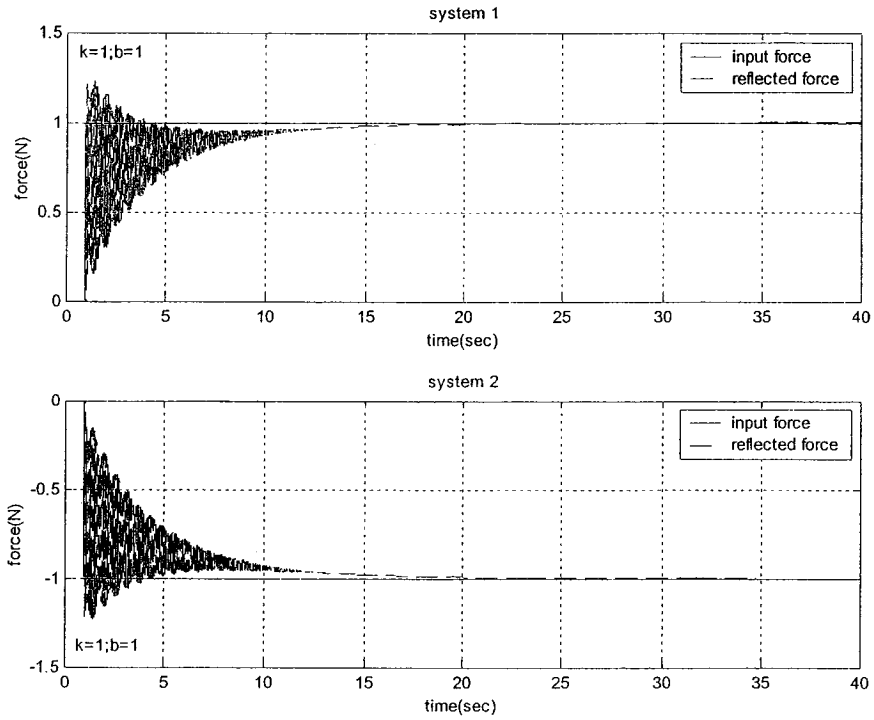

Figure 5-15 The response of case II with $k = 1\,\mathrm{N/m}$ and $b = 1\,\mathrm{N{\cdot}sec/m}$

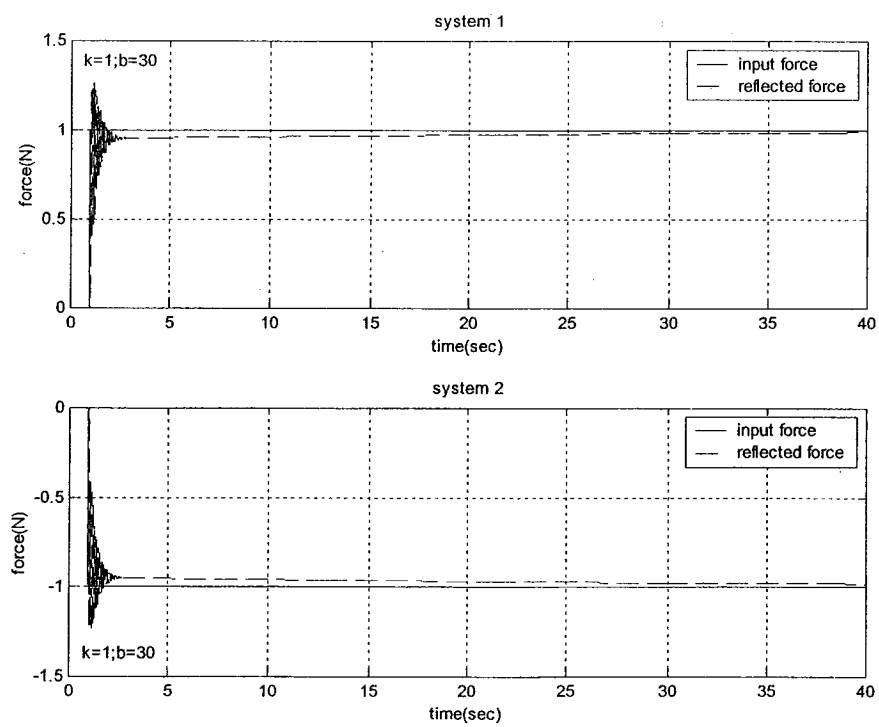

Figure 5-16 The response of case II with $k = 1\,\mathrm{N/m}$ and $b = 30\,\mathrm{N{\cdot}sec/m}$

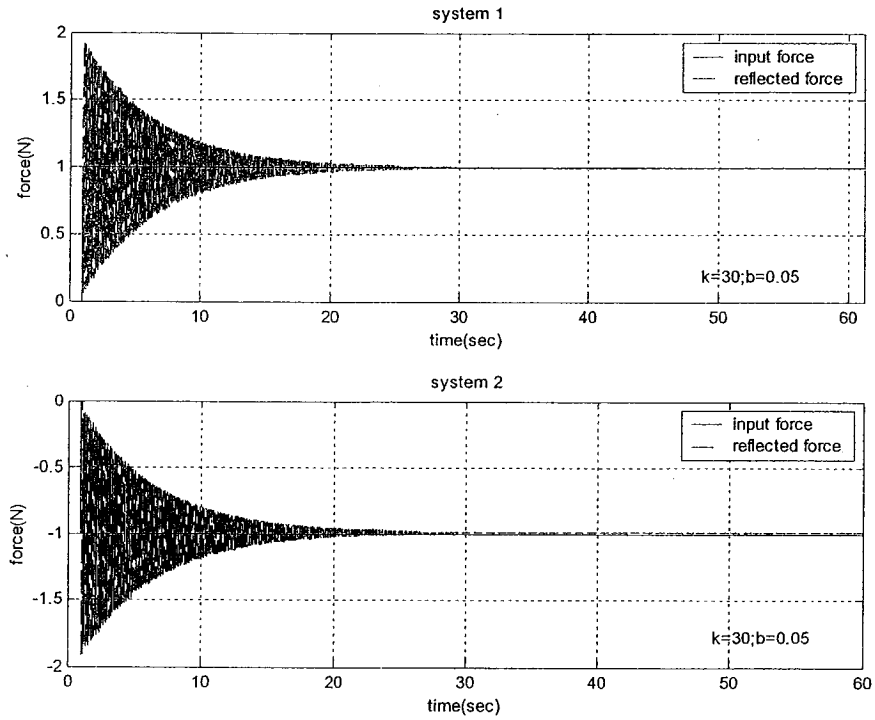

Figure 5-17 The response of case III with $k = 30\,\text{N/m}$ and $b = 0.05\,\text{N·sec/m}$

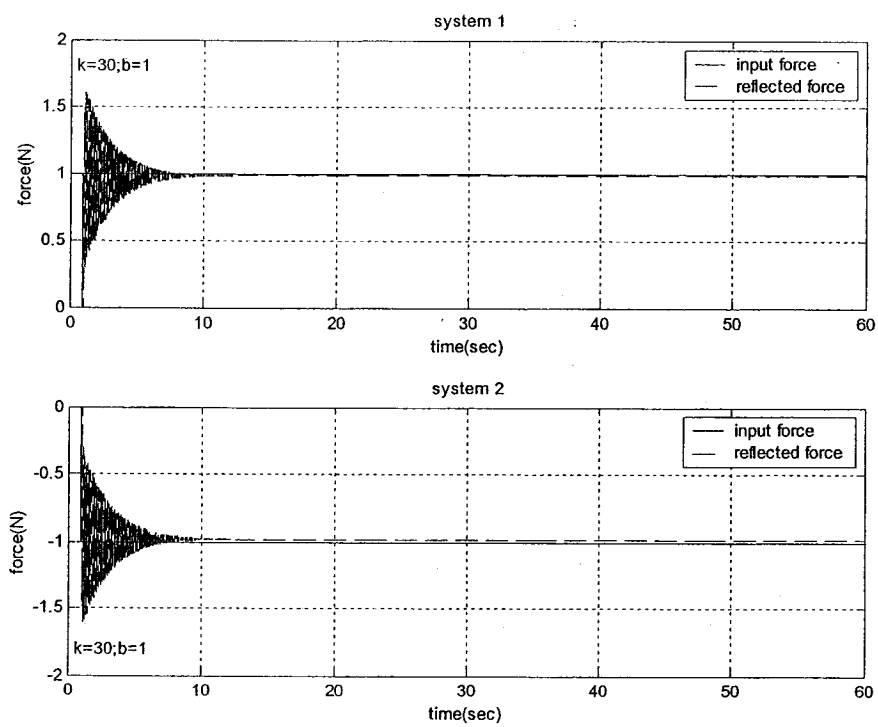

Figure 5-18 The response of case III with $k = 30\,\text{N/m}$ and $b = 1\,\text{N·sec/m}$

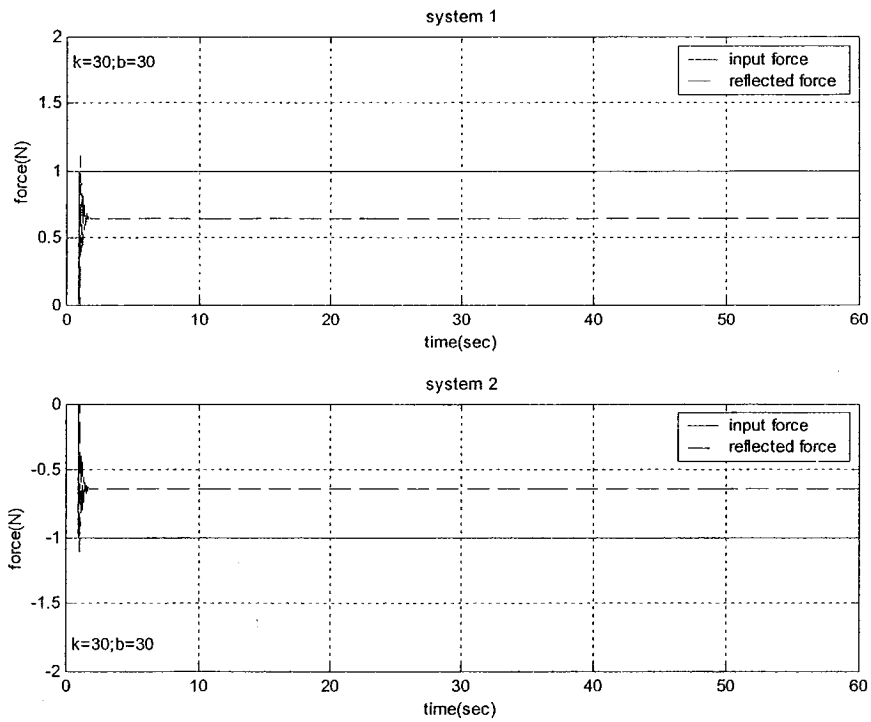

Figure 5-19 The response of case III with $k = 30\,\text{N/m}$ and $b = 30\,\text{N·sec/m}$

5.3 Analysis and Discussion

It follows from Tables 5-1 and 5-2 that the system is under-damped when the spring coefficient is set to $k = 0.05, 0.1, 0.5, 1, 5$ N/m, whereas the system is over-damped when $k = 10, 15, 20, 25, 30, 35, 40, 43\,\text{N/m}$ and $k = 0.01, 0.005, 0.001\,\text{N/m}$.

When the spring coefficient k is continuously increased, the duplicating time t_d becomes shorter; however, the settling time $t_s(5\%)$ and $t_s(2\%)$ becomes larger, which means when the stiffness of the virtual environment becomes harder, the more oscillations would be introduced. Actually, it is necessary to increase b_e to prevent noticeable oscillations when the users interact with the rigid virtual objects; however, increasing b_e too much tends to cause high frequency oscillations that users often reports as a feeling of "rumble"[70].

The overshoot M_p increases with the increase of the spring coefficient k when $k > 1$, and at the same time, t_p also becomes larger. Also for those cases when $k < 1$, the response is over-damped which result in short t_p and small overshoot M_p.

When the spring coefficient k makes the system into under-damped systems, we found that the specific properties, $t_s(5\%)$, $t_s(2\%)$, t_d and t_r become larger with the decrease of the spring coefficient k. Note that when the users contact the soft virtual objects, the VR system takes a longer time to appreciate the property of the virtual object, and furthermore, the steady state errors as shown in Table 4-2 also become larger. As a result, when the spring coefficient k has small values, it is hard to gain better steady state and transient responses from the VR system.

Using equations (3-3) and (3-14), and the fact that we have used admittance matrix in our design, and based on Table 5-2, when the virtual environment simulates free motion or is in contact with soft objects with very small spring coefficient k, the users have a good dynamic performance, but with a large steady state errors, whereas when the virtual environment simulates objects with large stiffness, the users have a good steady state contact feelings, but dynamic performances are worse than the other case. The relationship between stability and performance is contradictory to one another. As a result, the best stability/performance trade-off should be achieved when the coupling impedance is set to a minimum level which makes the combined two-port network unconditionally stable.

For the spring-damping model, when the results are compared to those of the spring model, if follows that the introduction of the parameter damping coefficient in the simulation of the virtual environment generally improves the dynamical

performance, especially as far as $t_s(5\%)$, $t_s(2\%)$, t_d, t_r are concerned behave much better than the cases in which k is equal to that of the spring model.

Chapter 6

Conclusions and Future Work

6.1 Conclusion

In this thesis, the development of a virtual coupling for a networked haptic display system was presented. Lineaization method for the nonlinear PHANToM Premium 1.5 model was applied in this research. A linear spring coefficient was initially used as the virtual environment. The best parameters for (K_e, b_e) of the virtual coupling were computed for different stiffness of the virtual environment. Simulation results for different spring coefficients of the virtual environment model were investigated and performance of the VR system shown experimentally.

The linearized mathematical models for different axes of the PHANToM Premium 1.5 were derived through linearization technique. Furthermore, the closed-loop transfer functions of the VR system were derived through the application of the state feedback compensations for the linearized PHANToM Premium 1.5 models.

The passivity criteria for the two-port network that implies stability conditions were extended to a networked haptic display with a unit of delay and multiple high order PHANToM Premium 1.5 haptic device models. The parameters (K_e, b_e) of the virtual coupling to satisfy passivity conditions were also obtained.

The model of the networked haptic display system with virtual environment was developed in Chapter 4. The ratio of the reflected virtual forces versus reference inputs for the closed-loop system was derived. The parameters (K_e, b_e) of the virtual coupling for the closed-loop system were evaluated and specified through Jury

stability criterion for two kinds of virtual environment models. Although it is generally difficult to consider all the scenarios of virtual environments, we still can define the worst-case scenarios for networked haptic systems depending on the specific limitations of the hardware used. The parameters (K_e, b_e) of the virtual coupling under the worst case can be unconditionally stable for any set of passive human operator and virtual environments.

Simulation results for two kinds of virtual environments and the results for the steady state errors demonstrate the existence of the trade-off between stability and performance. For example, for small spring coefficients, implying that the virtual environment simulates soft objects, the transient responses are much better than those cases of larger spring coefficients while the steady state errors are unsatisfactory for stability of the system; and for large spring coefficients, implying that the virtual environment simulates hard objects, the reflected forces have good performance as far as stability is concerned but the transient response yields more oscillations with the increase of stiffness of the virtual environment.

6.2 Contributions of the Thesis

In this thesis, the analysis of the mathematical models of the PHANToM Premium 1.5 has been done. The parameters of the virtual coupling to guarantee the opened-loop stability of haptic interface have been obtained. The closed-loop pseuocontrol ratios for output versus reference input in a multi-user networked VR system with a unit delay has been derived. The closed-loop stability conditions of the interactions with two kinds of the virtual environment models have been obtained. The complete response results of the closed-loop system with different parameters of the virtual environment model have been simulated.

6.3 Future Work

Networked haptic display system is not a stand-alone field of research interest. 3D graphic technologies, high-speed network and data communication, fast accelerator and processor, software-programming languages, mathematical models for nonlinear physical systems and high efficient controllers affect the future research in this field.

Even though we extended the unconditional stability method to a real physical system, there are a lot of improvements that need to be made further. First, our design is based on a single input and single output (SISO) system; second, we omitted the coupling effects among the different axes. Thirdly, in this thesis we only addressed a simple model for the virtual environment, and it is unknown whether the unconditional stability becomes hard or not for the complex virtual environment. Furthermore, in this thesis, we only considered the case of networked haptic displays having with two identical haptic devices. Actually, having two different kinds of haptic displays will be more general. Finally, although we derived the linearizied mathematical models for the PHANToM Premium 1.5, this derived linearizied model still can not always represent the dynamic specifications of the PHANToM Premium 1.5 completely under arbitrary operating conditions. Consideration of the full nonlinear model of the haptic devices is a major area of research to be involved in.

Appendix A

Phantom Premium 1.5 Technical Specifications

Workspace	7.5 x 10.5 x 15inches 19.5 x 27x 37.5cm
Range of Motion	Lower arm movement pivoting at elbow
Nominal position resolution	860 dpi 0.03 mm
Backdrive friction	0.15 oz. 0.04 N
Maximum exertable force	1.9lbf 8.5N
Continuous exertable force (24 hrs)	0.3 lbf 1.4N
Stiffness	20 lbs/in. 3.5N/mm
Inertia (apparentmass at tip)	< 0.17lbm. < 75 g
Footprint	10 x 13 inches 25 x 33 cm
Force feedback	x, y, z
Position sensing	x, y, z (6DOF optional)
Interface	Via Parallel Port
Supported platforms	Intel-based PCs

Reference

[1] T. A. Funkhouser, "Network Topologies for Scalable Multi-User Virtual Environment", *IEEE Proceedings of VRAIS' 96*, pp. 222-228, 1996.

[2] B. Roehl, "Distributed Virtual Reality – An Overview", *http://ece.uwaterloo.ca /~broehl/distrib.html*, 1995.

[3] C. Greenhalgh, S. Benford, "MASSIVE: a distributed virtual reality system incorporating spatial trading", *Proceedings IEEE 15th International Conference on distributed computing systems (DCS 95)*, Vancouver, Canader, June 1995.

[4] M. R. Stytz, S. B. Banks, "The Distributed Mission Training Integrated Threat Environment System Architecture and Design", *ACM Transactions on Modeling and Computer Simulation*, Vol. 11, No. 1, p106-133, January 2001.

[5] T. Sweeney, "Unreal Networking Architecture", http://unreal.epicgames.com/Network.htm as viewed August 2001.

[6] Q. Shareware, http://www.gamers.org/dEngine/quake/info/techinfo.091, as viewed October 2001.

[7] C. Carlssom, O. Hagsand, "DIVE - A platform for multi-user VE", Computer & Graphics 17(6), pp. 663-669, 1993.

[8] D. Miller, J. A. Thorpe. "SIMNET: The advent of simulator networking", In Proceedings of the IEEE 83(8), pp 1114-1123, August 1995.

[9] Standard for Information Technology, "Protocols for Distributed Interactive Simulation (DIS) Applications", version 2, Institute for simulation and Training report IST-CR-93-15, University of Central Florida, Orlando Florida, May 28 1993.

[10] M.A. Srinivasan "Haptic Interfaces," Virtual Reality: Scientific and Technical Challenges," in *N. Durlach and A. Mavor (Eds.) Report to the Committee on Virtual Reality Research and Development, National Research Council, National Academy Press*, Washington, DC, pp. 161-187, 1994.

[11] G. C. Burdea, "Force and Touch Feedback For Virtual Reality", *John Wiley & Sons, INC.* pp3-4.

[12] G. Burdea and N. Langrana, "Virtual Force Feedback—lessons, Challenges and Future Applications," *Journal of Robotics and Mechatronics*, Vol. 5, No. 2, pp. 178-182, Japan, 1993.

[13] M. Webster, "Webster's Ninth New Collegiate Dictionary," *Merriam-Webster Inc.*, Spring-field, MA.

[14] V. Hayward, J. Choksi, G. Lanvin, and C. Ramstein, "Design and Multi-

Objective Optimization of a Linkage for a Haptic Interface," *Advances in Robot Kinematics and Computational Geometry*, Boston: Kluver Academic, pp. 352-359, 1994.

[15] T.H. Massie and J.K. Salisbury, "The Phantom Haptic Interface: A Device for Probing Virtual Objects," *Proc. ASME International Mechanical Engineering Congress and Exhibition*, Chicago, pp. 295-302, 1994.

[16] R. J. Adams and B. Hannaford, "Stable Haptic Interaction with Virtual Environments." *IEE Transactions on Robotics and Automation* 15(#3), pp465 – 474, 1999.

[17] P. Buttolo and B. Hannaford, "Pen Based Force Display for Precision Manipulation of Virtual Environments," *Proc. IEEE Virtual Reality Annual Int. Symposium*, Raleigh, NC, pp. 217-225, 1995.

[18] Y. Yokokohji, R.L. Hollis, and T. Kanade, "What You See Is What You Can Feel-Development of a Visual/Haptic Interface to Virtual Environment," *Proc. IEEE Virtual Reality Annual Int. Symposium*, Los Alimitos, CA, pp. 46-53, 1996.

[19] C.L. Clover, G.R. Luecke, J.J. Troy, and W.A. McNeely, "Dynamic Simulations of Virtual Mechanisms with Haptic Feedback Using Industrial Robotics Equipment," *Proc. IEEE Int. Conf. Robotics and Automation*, Albuquerque, NM, pp. 3205-10, 1997.

[20] T. Sheridan, "Musings on Telepresence and Virtual Presence," *Prsence-Teleoperators and Virtual Environments,* Vol. 1, No. 1, MIT press, pp120-126, 1992.

[21] R. Goertz and R. Thompson, "Electronically controlled manipulator," *Nucleonics*, pp. 46-47, 1954.

[22] M. Minsky, O. S. Ouh-young, F. Brooks Jr. and M. Behensky, "Feeling and Seeing: Issues in Force Display," *Computer Graphics*, ACM Press, Vol. 24, No.2, pp 235-243, March 1990.

[23] S. E. Salcudean, N. M. Wong, and R. L. Hollis, "A Force-Reflecting Teleoperation System with Magnetically Levitated Master and Wrist," *Proc. IEEE Conf. Robotics Automat.*, Nice, France, pp 1420-1426, 1992.

[24] R. L. Hollis, S.E. Salcdean, and P.A. Allan, "A Six Degre-of-Freedom Magnetically Levitated Variable Compliance Fine Moton Wrist: Design, Modelling and Control," *IEEE Trans. Robotics Automat.*, Vol. 7, pp. 320-332, 1991.

[25] S. E. Salcudean and T. D. Vlaar, "On the Emulation of Stiff Walls and Static Friction With a Magnetically Levitated Input/Output Device," *Journal of Dynamic Systems, Measurement, and Control, Transactions of the ASME*, Vol. 119, pp127-132, March 1997.

[26] P. Buttolo and B. Hannaford, "Pen-Based Force Display for Precision Manipulation in Virtual Environments," *Proceeding IEEE Virtual Reality Annual International Symposium*, North Carolina, pp. 217-224, March 1995.

[27] A. Nahvi, J.M.Hollerback, V.Hayward, "Calibration of a Parallel Robot Using Multiple Kinematic Closed Loops," *Proc. IEEE Robotics and Automation*, , San Diego, CA, vol. 1, pp. 407-413, 1994

[28] P. Buttolo, P.Bratthen, B. Hannaford, "Sliding Control of Force Reflecting Teleoperation: Preliminary Studies," *PRESENCE* Vol3, Num 2, pp. 158-172, Spring 1994.

[29] J. E. Colgate, and N. Hogan. "Robust control of dynamically interacting systems." *International Journal of Control*, vol. 48, no. 1, pp. 65-88, 1988.

[30] N. Hogan "On the Stability of Manipulators Performing Contact Tasks," *IEEE Journal of Robotics and Automation*, vol. 4, no. 6, pp. 677-686, 1988.

[31] R. J. Anderson and M. W. Spong. "Bilateral Control of Teleoperators with a Time Delay," *IEEE Trans. On Automatic Control*, vol. 34, no. 5, pp. 494-501, 1989.

[32] D. E. Whitney, "Historical Perspective and State of the Art in Robot Force Control", *Proceedings of the IEEE Conference on Robotics and Automation*, pp. 262-268, 1985.

[33] N. Hogan, "Controlling Impedance at the Man/Machine Interface", In *Proc. IEEE Int. Conf. Robot. Automat.*, Scottsdale, AZ, pp. 1626–1631, 1989.

[34] J.M. Lanman, "Movement and The Mechanical Properties of The Intact Human Elbow Joint. Ph.D. Thesis", *Department of Psychology, M.I.T.* 1980.

[35] K.C. Hayes and H. Hatze, "Passive Visco-Elastic Properties of The Structures Spanning The Human Elbow Joint", *European J. Applied Physiology*, Vol. 37, pp. 265-274, 1977.

[36] S.C. Cannon and G. I. Zahalak, "The Mechanical Behavior of Active Human Skeletal Muscle in Small Oscillations", *J. Biomechanics*, Vol. 15, pp. 111-121, 1982.

[37] N. Hogan, "Impedance control: An approach to manipulation: Part i - theory, part ii - implementation, part iii - applications," *J. of Dynamic Systems, Measurement, and Control*, pp.1–24, 1985.

[38] I.C. Faye, "An Impedance Controlled Manipulandum for Human Movements Studies. S.M. Thesis", *Department of Mechanical Engineering, M.I.T.* 1983.

[39] Colgate, J. E., P. E. Grafing, M. C. Stanley and G. Schenkel. "Implementation of Stiff Virtual Walls in Force-Reflecting Interfaces," *IEEE Virtual Reality Annual International Symposium*. Seattle, WA. pp. 202-207, 1993.

[40] H. Kazerooni, J. E. Colgate and B. D. Adelstein. "Advances in Robotics, Mechatronics and Haptic Interfaces, 1993". ASME Winter Annual Meeting, vol. DSC-49, 1993.

[41] R. J. Adams, M. R. Moreyra, and B. Hannaford. "Stability and Performance of Haptic Displays: Theory and Experiments." In *Proc. Of the ASME, Dynamic Systems and Control Division*, pp. 227-234, Nov. 1998.

[42] A. Nahvi, D.D. Nelson, J.M. Hollerbach, and D.E. Johnson, "Haptic Manipulation of Virtual Mechanisms from Mechanical CAD Designs." In *Proceedings of the 1998 IEEE International Conference on Robotics and Automation*, Leuven, Belgium, pp. 375-380, May 1998.

[43] T. Yoshikawa and H. Uead. "Construction of Virtual World Using Dynamics Modules and Interaction Modules." In *Proceedings of the 1996 IEEE International Conference on Robotics and Automation*, Minneapolis, Minnesota, pp. 2358-2364, 1996.

[44] J. Edward Colgate and Gerd Schenkel, "Passivity of A Class of Sampled-Data System: Application to Haptic Interfaces," *Proceedings of the 1994 American Control Conference, Baltimore*, MD, pp. 3236-40, 1994.

[45] J. E. Colgate, M. C. Stanley, and J. M. Brown. "Issues in the haptic display of tool use," *In proceedings of the IEEE/RSJ International Conference on Intelligent Robotics and Systems* (IROS'95), pp 140-145, 1995.

[46] B. Hannaford and J. Ryu, "Time-Domain Passivity Control of Haptic Interface", *IEEE Transactions on Robotics and Automation,* vol. 18, No. 1, Feb. 2002.

[47] R. J. Adams, D. Klowden, and B. Hannaford, "Stable Haptic Interaction Using the Excalibur Force Display," in *Proc. IEEE Int. Conf. Robot. Automat.*, San Francisco, CA, pp. 770-775, 2000.

[48] R. J. Adams and B. Hannaford, "Excalibur, A Three-axis Force Display", In *ASME Winter Annu. Meeting Haptics Symp.*, Nashville, TN, Nov. 1999b.

[49] J. Edward Colgate and J. Michael Brown, "Factor Affecting the Z-Width of a Haptic Display", *Proc. IEEE Intl. Conf. on Robotics and Automation*, San Diego, Calif, vol. 4, pp. 3205-3210, May 1994.

[50] L. B. Rosenberg and B. D. Adelstein. "Perceptual Decomposition of Virtual Haptic Surfaces." *IEEE Symposium on Research Frontiers in Virtual Reality.* San Jose, CA. 1993.

[51] B. Hannaford, "A Design Framework for Teleoperators With Kinesthetic Feedback", In *IEEE J. Robot. Automat.*, vol. 5, pp. 426-434, Aug. 1989.

[52] M. Minsky, M. Ouh-Young, O. Steele, F.P. Brooks, and M. Behensky, "Feeling and seeing issues in force display", In *Comput. Graph*, vol. 24, No.2, pp.235-243, 1990.

[53] K. Kim, W.K. Chung and Y. Youm, "On the Design Method of a Haptic Interface Controller with Virtual Coupling", In *International Conference on Control, Automation and Systems*. 2001.

[54] S. Dow, G. Thomas, J.L., "Signal detection performance with a haptic device." In: *1999 Proceedings of the Human Factors and Ergonomics Conference*, Houston, TX, 1999.

[55] H. Kazerooni and M.Her, "The dynamics and control of a haptic interface device." *Trans. On Robotics and Automation*, 10(4), pp. 453-63, 1994.

[56] E. Chen, and B. Marcus, "Force feedback for surgical simulation." *Proc. Of the IEEE*, 86(3), pp.524-530. 1998.

[57] B. Chang, & E.J. Colgate "Real-time Impulse-Based Simulation of Rigid Body Systems for Haptic Display." *Proceedings of the ASME International Mechanical Engineering Congress and Exhibition*, pp.1-8. 1997.

[58] M. C. Cavusoglu, F. Tendick. "Multirate Simulation for High Fidelity Haptic Interaction with Deformable Objects in Virtual Environments." In *Proceedings of the IEEE International Conference on Robotics and Automation (ICRA 2000)*, San Francisco, CA, pp. 2458-2465, April 2000.

[59] K. Zhou, J. C. Doyle, and K. Glover. "Robust and Optimal Control". *Prentice-Hall, Inc.*, New Jersey, USA, 1996.

[60] S. Timoshenko and J. N. Goodier. "Theory of Elasticity. McGraw-Hill Book Company," *Inc., New York, USA*, second edition, 1951.

[61] O. R. Astley and V. Hayward. "Multirate haptic simulation achieved by coupling finite element meshes through norton equivalents." In *Proceedings of the IEEE International Conference on Robotics and Automation (ICRA'98)*, pp. 989-994, May 1998.

[62] L. W. Way. "Development of Virtual Environments for Training Skills and Reducing Errors in Laparoscopic Surgery." In *Proceedings of the SPIE International Symposium on Biological Optics (BIOS'98)*, pp.36-44, January 1998.

[63] H. Arioui, A. Kheddar and S. Mammar, "Stable Shared Virtual Environment Haptic Interaction Under Time-Varying Delay", In *Proc. of the 8th IEEE Intern. Conf Methods and Models in Automation and Robotics*, September 2002.

[64] P. Buttolo, R. Oboe, and B. Hannaford, "Architectures for Shared Haptic Virtual Environments," *Computers and Graphics*, vol. 21, pp. 421–429, July-Aug 1997.

[65] C. Basdogan, "Real-time Simulation of Dynamically Deformable Finite Element Models Using Modal Analysis And Spectral Lanczos Decomposition Methods," *Medicine Meets Virtual Reality*, 2001.

[66] R. J. Anderson and M. W. Spong, "Asymptotic Stability for Force Reflecting Teleoperators With Time Delay," *Int. Journal of Robotics Research*, vol. 11, pp. 135–149, April 1992.

[67] G. Niemeyer and J. J. Slotine, "Stable Adaptive Teleoperation," *IEEE Journal of Oceanic Engineering*, vol. 16, pp. 152–162, 1991.

[68] S. Stramigioli, A. V. der Schaft, and B. Maschke, "Geometric Scattering In Telemanipulation of Port Controlled Hamiltonian Systems," In *Proceedings of the 39th IEEE Conference on Decision and Control*, Sydney, Australia, 2000.

[69] Y. Yokokojhi, T. Imaida, and T. Yoshikawa, "Bilateral Teleoperation Uner Time-varying Communication Delay," *Proc. IEEE/RSJ Int. Conf. Intelligent Robots and Systems (IROS'99)*, pp. 1854–1859, 1999.

[70] J. Edward Colgate, Paul E. Grafing, Michael C. Stanley, and Gerd G. Schenkel, "Implementation of Stiff Virtual Walls in Force-Reflecting Interfaces," *Proceedings of the IEEE Virtual Reality Annual International Symposium*, 202-207, 1993.

[71] K. Kosuge, and al. "Bilateral feedback control of telemanipulators via computer network." *IEEE Conf. on Intelligent Robotics and Systems*, pp. 1380-1385, November 1996.

[72] A. Eusebi and C. Melchiorri, "Force Reflecting Telemanipulators With Time-Delays: Stability analysis and control design," *IEEE Trans. on Robot. And Automat.*, vol. 14, pp. 635–640, August 1998.

[73] R. Oboe and P. Fiorini, "A Design and Control Environment for Internet-Based Telerobotics," *The International Journal of Robotics Research*, vol. 17, pp. 433–449, April 1998.

[74] G. M. H. Leung, B. A. Francis, and J. Apkarian, "Bilateral Controller for Teleoperators With Time Delay Via μ-Synthesis," *IEEE International Conference on Robotics and Automation*, vol. 11, pp. 105–116, February 1995.

[75] G. Niemeyer and J-J. Slotine, "Using Wave Variables for System Analysis and Robot Control". *IEEE Conf. Robot. And Automat.* , pp. 1619-1625, April 1997.

[76] N. A. Tanner and G. Niemeyer, "Practical Limitations of Wave Variable Controllers in Teleoperation," *IEEE International Conference on Robotics and Automation*, New Orleans, Louisiana, April 26 - May 1, 2004.

[77] H. Arioui, M. Mana, A.Kheddar and S. Mammar, "Master-Model Based Time-delayed Force Feedback Interaction: Experimental Results", *Proceedings of the 2002 IEEE International Symposium on Intelligent Control*, Vancouver, Canada, October 27-30, 2002.

[78] G. Niemeyer and J.-J. E. Slotine, "Telemanipulation with time delays," *International Journal of Robotics Research*, vol. 23, no. 9, pp. 873–890, Sept.

2004.

[79] J.-J. E. Slotine and W. Li, *Applied Nonlinear Control.* Prentice Hall, Englewood Cliffs, NJ, 1991.

[80] H. Arioui, S. Mammar, and T. Hamel, "A smith-prediction Based Haptic Feedback Controller For Time Delayed Virtual Environments Systems", *Proc. of the American Control Conference (2002)*, Anchorage, Alaska, USA, pp. 4303-4308, 2002.

[81] O.J.M.Smith, "A Controller To Overcome Dead Time", *ISA J.6 (1959)*, No. 2, 28-33, 1959.

[82] W.S. Levine, The Control Handbook. CRC Press, ISBN: 0849385709,1996.

[83] K.L. Koay and G. Bugmann, "Compensating Intermittent Delayed Visual Feedback in Robot Navigation", *Proceeding of Taros'04*, 6-8 Colchester, UK, Sept 2004.

[84] H. Arioui, A. Kheddar et S, Mammar, "A model-based Controller for interactive force reflecting virtual environment under time delay", *Journal of Intelligent and Robotic Systems - Theory and Applications* -, volume 37, number 2, pp. 193-207, June 2003.

[85] M. Otsuka, K. Kosuge, and Al., "Bilateral Telemanipulation System with Communication Time Delay Based on Force-sum Driven Virtual Internal Models," *IEEE Int. Conf. on Robotics and Automation*, pp. 343–350, 1995.

[86] R. M., Murray, Z. Li, & S.S. Sastry, "A Mathematical Introduction To Robotic Manipulation," *CRC Press, Inc. Boca Raton, FL*, 1994.

[87] J.J. Craig "Introduction to robotics (Second ed.)," *Addison-Wesley. Reading, MA*, 1989.

[88] M. Cavusoglu, D. Feygin, and F. Tendick, "A critical study of the mechanical and electrical properties of the phantom*TM* haptic interface and improvements for high performance control," *PRESENCE Rev.*, Vol. 11, pp. 555-568, 2002.

[89] M.C. Cavusoglu, & D. Feygin "Kinematics and dynamics of PHANToM(TM) model 1.5 haptic interface (Tech. Rep.)". *University of California at Berkeley, Electronics Research Laboratory Memo M01/15*, 2001.

[90] C.B. Zilles and J.K. Salisbury, "A Constraint-based God-object Method for Haptic Display," *Proc. IEEE/RSJ Int. Conf. on Intelligent Robots and Systems*, Pittsburgh, PA, pp. 146-151,1995.

[91] D.C. Ruspini, K. Kolarov, and O. Khatib, "The Haptic Display of Complex Graphical Environments," *Computer Graphics Proceedings, SIGGRAPH' 97,* Ls Angeles, 345-352, 1997.

[92] R. J. Adams, and B. Hannaford, "Control Law Design for Haptic Interface to

Virtual Reality", *IEEE Trans. Control Systems Technology,* vol. 10, pp. 3-13, Jan 2002.

[93] E. S. Kuh and R. A. Rohrer, "Theory of Linear Active Networks," San Francisc, CA: Holden-Day, 1967.

[94] L. D. Pian, "Linear Active Network Theory", *Prentice-Hall, Inc.*, pp. 310-313, 1962.

[95] F. B. Llewellyn, "Some Fundamental Properties of Transmission Systems," *Proc. IRE,* vol. 40, pp. 271-283,1952.

[96] S. S. Haykin, "Active Network Theory," London, U.K.: Addison-Wesley, 1970.

[97] J.E. Colgate, "Coupled Stability of Multiport Systems-Theory and Experiments," *Trans. ASME, Journal of Dynamic Systems, Measurement, and Control*, vol. 116, no. 3, pp. 419-28, 1994.

[98] J.E. Colgate, "Robust Impedance Shaping Telemanipulation," *IEEE Trans. Robotics and Automation*, vol. 9, no. 4, pp. 374-384, 1993.

[99] J.H. Ly, M.G. Safonov, and R.Y. Chiang, "Real/Complex Multivarible Stability Margin Computation via Generalized Popov Multiplier-LMI Approach," *Proc. of the ACC*, Baltimore, MD, pp. 425-9, 1994.

[100] J.C. Doyle, "Analysis of Feedback Systems with Structured Uncertainty," *IEE Proc.*, vol. 129, pt. D, no. 6, pp. 242-250, 1982.

[101] C. L. Phillips and H. Troy Nagle, "Digital Control System Analysis and Design (Second Edition)", Prentice Hall, Englewood Cliffs, New Jersey 07632, pp. 121-122, 1990.

[102] C. H. Houpis and Gary B. Lamont, "Digital Control Systems Theory, Hardware, Software", McGraw-Hill Inc., 1993.

[103] H. Kazerooni and M.Her. "The dynamics and control of a haptic interface device", *Trans. on Robotics and Automation*, Vol.10 (4), pp. 453-63, 1994.